

## Department of Precision and Microsystems Engineering

Investigation of the relation between repeatability and preload for linear guides based on a position controlled input

Laurens van Driessen

Report no : 2022.067  
Coach : Giuseppe Radaelli  
Professor : Just Herder  
Specialisation : MSD  
Type of report : Master Thesis  
Date : November 2, 2022



# Investigation of the relation between repeatability and preload for linear guides based on a position controlled input

by

Laurens van Driessen

to obtain the degree of Master of Science  
at the Delft University of Technology,  
to be defended publicly on Wednesday November 2, 2022 at 14:30 PM.

Student number: 4484495  
Project duration: September 1, 2021 – November 2, 2022  
Thesis committee: Prof. dr. ir. J. L. Herder, TU Delft, chair  
Dr. ir. G. Radaelli, TU Delft, daily supervisor  
Ing. A. Geelkerken, Hittech Multin, daily supervisor

An electronic version of this thesis is available at <http://repository.tudelft.nl/>.



# Preface

This thesis marks the end of my study High-Tech Engineering at the TU Delft. During this thesis, I learned a lot about the high-tech industry and about myself.

I would like to thank my supervisors Giuseppe and Ard for the meetings we had throughout this year. Also, I would like to thank my colleagues at Hittech for the support they gave. I had a good time coming to the office and I always got the feeling that people wanted to help me. Furthermore, I want to thank the other students from the research group for the inspiring group meetings and the informal conversations.

After this thesis, I will continue with my second master program before I officially end my study period.

*Laurens van Driessen  
Delft, November 2022*



# Contents

<b>1</b>	<b>Introduction</b>	<b>1</b>
1.1	Thesis objective . . . . .	2
1.2	Thesis outline . . . . .	2
<b>2</b>	<b>Literature Review</b>	<b>3</b>
<b>3</b>	<b>Research paper</b>	<b>19</b>
<b>4</b>	<b>Discussion</b>	<b>33</b>
<b>5</b>	<b>Conclusion</b>	<b>37</b>
<b>A</b>	<b>Concept generation</b>	<b>41</b>
A.1	Selection of Linear guides . . . . .	41
A.2	Morphological table. . . . .	41
A.3	Trade off . . . . .	42
A.3.1	Concept 1 . . . . .	42
A.3.2	Concept 2 . . . . .	42
A.3.3	Concept 3 . . . . .	42
A.3.4	Concept 4 . . . . .	43
A.3.5	Selection . . . . .	43
A.4	Final Design . . . . .	43
A.4.1	Actuation . . . . .	43
A.4.2	Rotational mechanism . . . . .	44
A.4.3	Spring mechanism . . . . .	44
A.4.4	End stop . . . . .	44
A.4.5	Linear guide system . . . . .	44
<b>B</b>	<b>Additional results</b>	<b>45</b>
B.1	Results external preload rail 1 and rail 2 . . . . .	45
B.1.1	V1 . . . . .	45
B.1.2	V3 . . . . .	46
B.1.3	Longitudinal repeatability position and preload class . . . . .	47
B.1.4	Rotational repeatability position and preload class . . . . .	48
B.1.5	All preload classes combined . . . . .	49
B.2	Forces & Moments in system . . . . .	50
B.2.1	Forces. . . . .	50
B.2.2	Moments . . . . .	51
B.3	Resolution lasers . . . . .	52
B.4	Drift linear guides . . . . .	53
B.5	Parallelism rails. . . . .	54
<b>C</b>	<b>Kinematic coupling</b>	<b>55</b>
<b>D</b>	<b>Glue process kinematic coupling</b>	<b>57</b>
<b>E</b>	<b>SAM analysis</b>	<b>59</b>
<b>F</b>	<b>Data processing</b>	<b>61</b>
F.1	Data analyses experiments . . . . .	61
F.2	Calculations resolution . . . . .	62
F.3	Calculations drift . . . . .	63
F.4	Calculations kinematic coupling . . . . .	65
F.5	Calculations dimensions . . . . .	65





# Introduction

High precision machines are becoming more important in many high-tech industry. In a number of machines, linear guides are used to establish this highly accurate and highly repeatable movement. Examples are CNC machines [1, 11, 19], microscopes [3, 6, 12, 17], 3D printers [5, 9, 13], and pick and place machines [2, 4, 10]. Different types of linear guides are available on the market including rolling-element guides, sliding guides, magnetic bearing guides, and air-bearing guides. Each type is again divided into different versions, with its own characteristics and (dis)advantages. Besides their performance, also cost plays a more significant role in the industry. Often, high performance for linear guides goes together with high prices. Therefore, when designing a high precision machine the requirements of the machine should match the requirements of the linear guide to avoid additional high costs.

The performances of high precision machines that are using linear guides are not only dependent on the performances of that linear guide but also on the total system. Overconstraints in systems will cause internal stresses which could affect performance. Besides that, the way of manufacturing and assembling could have a large effect on the performance. Contamination that occurs over time together and wear that takes place during the use of the system have effects as well. Therefore, when improving the performance of a system an analysis of the whole system with all the external effects should be made.



Figure 1.1: Linear motion stage example [15]

This thesis started with the question of whether it was possible to improve the current concept of a 5-axis stage. Although the basic requirements are already met, the accuracy and repeatability could be further improved. To come up with ideas to improve the current concept the total system has been analyzed. Costs play a role in the final decision of whether to improve the concept or not. A trade-off between costs and improved performance should be made.

Accuracy is defined as the degree to which the result of the measurements conforms to the correct value. Repeatability is defined as the variation in consecutive measurements of one variable with the same conditions [8].

The system we are interested in has multiple linear guides that move simultaneously along the same axis to accurately move multiple times to a position and have a predefined preload. The system is powered by a motor that rotates the spindle in order to move the stage. This system with linear

guides is overconstrained due to the two linear guides that make the same movement. The system is therefore sensitive to misalignment. The accuracy and repeatability could be improved by using other types of linear guides, improving the alignment of the system, and using more or other types of preload.

Two types of linear guides are selected for further investigation. These are the non-recirculating ball linear guide and the non-recirculating cross roller linear guide. Both guides have relatively high stiffness and high dynamic load capacity. The ball guide has four contact points with the rails while the cross roller has two times two lines contacts. Ball guides tend to deform more and as a consequence have more friction compared to roller guides.

Alignment of the system is of importance for the performances of the linear guides. Since the system is overconstrained a small misalignment could cause an increase in the internal stresses, resulting in lower performances. A position change to one of the rails could be applied to improve the parallelism of the two rails. This could also be seen as a specifically applied preload.

The amount and variation in preload play an important role in the total motion errors [14]. Increasing the preload could improve the repeatability of linear guides since it will eliminate large deflection due to external loads, decrease noise and vibrations, enhance fatigue life, reduce rattle due to clearance, and prevent skidding [7, 16]. However, the drawbacks of this are more friction, reduction of moment loads and maximum loads, increased displacement resistance, and reduces service life [18].

### **1.1. Thesis objective**

The relation between the amount of preload and repeatability is lacking in literature as well as the effects of additional applied mass on repeatability. The results could be used to improve high precision machines even further by preloading the linear guides with the right amount. Also, the decision of how to preload a specific linear guide to achieve the best performance could be of interest to companies.

The objective of this thesis is to investigate the relation between repeatability and preload for the non-recirculating ball guide and the non-recirculating cross roller guide.

### **1.2. Thesis outline**

This thesis starts with a literature review into the different kinds of linear guides. It gives an overview of the available rolling element linear guides, categorizes these guides based on the technique that is used for movement and type of contact and evaluates them by our performance criteria. Two linear guides are selected to be used in the research paper; the ball linear guide and the cross roller linear guide. The research paper investigates the relation between preload and repeatability for both the cross roller guide and the ball guide by performing experimental tests. The preload will be applied uniformly at one side by an adjusting screw, by adjusting only one screw so that the rail is set on a defined angle, and by adding mass on top of the system. Both the longitudinal repeatability and rotational repeatability are measured for these situations at three positions on each guide. Finally, a general discussion and conclusion are given about the two papers.

# 2

## Literature Review

# Literature Review: Rolling Element Linear Guides

Laurens van Driessen (4484495)  
TU Delft, 18-03-2022

**Abstract—** Rolling element linear guides are used in various applications with all kinds of requirements. To give insight into the diversity of concepts and performances of the rolling element linear guides, this paper aims to give an overview of the available rolling element linear guides, provide a categorization, and evaluate them based on a set of performance criteria. These criteria are cross-sectional area, length, degree of freedom, dynamic load capacity, deformations, speed, and friction. The classification consists of the techniques used for the movement of the rolling elements in linear guides and the type of contact of these rolling elements. Models found from cross-categories are discussed and evaluated. Differences in load capacity, deformation, and friction between the models can be seen and are discussed.

**Index term —** Rolling Element Linear Guides - Recirculating - Non-Recirculating - Point-contact - Line-contact

## I. INTRODUCTION

Linear guides are being used in multiple applications with the aim to support a linear motion of a system [1]. They play a key role in applications where high accuracy is required, such as pick and place machines [2]–[4], 3D printers [5]–[7], CNC machines [8]–[10], and microscopes [11]–[14]. Linear guides consist of two parts, a moving object that is connected to the moving part of the system and a rail part that is connected to the fixed part of the system. In some applications, multiple linear guides are placed in parallel or in series. Linear guides can be categorized into different categories, a few of them include sliding contact-based, air contact-based, magnetic-based, and rolling element-based guides. In this paper, we will focus on the rolling element linear guides.

High accuracy and repeatability are often desired in the aforementioned applications [1], [15]. Accuracy is defined as "the degree to which displacements executed by a positioning system match agreed upon standards of length" [1]. Repeatability is defined as the extent to which multiple attempts to travel to a defined location vary in position [1].

Several things could hamper a system to achieve the desired level of accuracy and repeatability. The level of repeatability of a rolling element linear guide heavily depends on the complete system and the surrounding. Examples are external noise, way of assembly, and contamination. Data about the repeatability of rolling element linear guides is, therefore, neither reported in papers nor in product catalogs. In this paper, the parameters that play a crucial role in the level of repeatability are discussed in more detail.

Motion errors caused by multiple sources occur quite often. One of the most predominant factors for motion

accuracy is the rail form errors of guide rails [1], [16]. Rahmani and Bleicher (2016) address the straightness error and joint stiffness of different types of guides [17]. He et al. (2020) proposes an adjustment algorithm to improve motion accuracy [18]. A linear transfer function based on the Hertzian contact theory is designed, which includes the relationship between the error of the moving part and the straightness error of the guide rail [18].

Furthermore, the amount and variation in preload play an important role in the total motion errors [1]. Applying preload to a bearing will eliminate large deflection due to external loads, decrease noise and vibrations, enhance fatigue life, reduce rattle due to clearance, and prevent skidding [19] [20]. At higher preloads the nonlinear effects in bearings are negligible [21].

Also, contaminants between the rolling element and the guide rail as well as external forces affect the motion error. When the external forces on the rolling element exceed the friction forces in the load-bearing contacts, sliding could occur [1].

Moreover, heat that is generated by friction processes at the contact areas affects the motion accuracy. More friction means more heat generation. Friction increases with the preload, normal load, and velocity [16]. At high velocities, it is beneficial to use guides with low friction grease that has low viscous friction [22]. Materials like Stellite offers good wear and friction performances compared to other materials and Si<sub>3</sub>N<sub>4</sub> was found to operate well under sliding conditions [23]. The use of hardened balls and raceways offer the highest load capacities and longest lifetime [24].

Researchers have done quite some research into the effects on motion accuracy of several linear guides [1], [16]–[20], [23]. Also, instruction books about several linear guides are published [25], [26]. An overview of several linear guides evaluated on key performance criteria like cross-sectional area, load capacity, deformations, speed, degree of freedom, and friction is lacking in the literature.

Therefore, the objective of this literature review is to give an overview of the available rolling element linear guides, categorize these guides based on the technique that is used for movement and type of contact, and evaluate them by our performance criteria.

## II. METHOD

### A. Literature search

In order to find relevant literature, multiple search terms have been used that are connected to linear guides. The use of the working principles of the guides in combination with

	AND		
OR	Circular arch	Cam rollers	Accuracy
	Gothic arch	Profiled rails	Friction
	Point contact	Ball cage	Preload
	Line contact	Flat rollers	Vibrations
	2,3,4 contact	Ball spline	Deformations
	Recirculating	Cross roller	Speed
	Non-recirculating	Linear guide	Creep
		Roller bearing	Rigidity
			Load capacity

TABLE I: Used search terms

the type of contact resulted in valuable papers. In Table I, the used terms are shown. Horizontally with 'AND' and vertically with 'OR' between the terms in the search string.

Another technique that has been used to find additional relevant papers was to look at the references of papers that were already obtained. In that way, we found more in-depth information about a specific phenomenon. Furthermore, the company catalogs of THK, Schneeberger, and SKF have been used to find the dimensions and performance results of the different models. The search engines used for this literature review are Scopus, Google (Scholar), and Web of Science.

### B. Classification

The classification consists of two main categories. First, the techniques that are used for the movement of the rolling elements in linear guides, and second the type of contact of these rolling elements. This has been done to make a clear distinction between technique on the one side and contact points on the other side. For every technique the same variation in contact points exists, so a matrix of 5x3 solutions arises. The overview can be found in Figure 1. Note that the character in the top left of every cell refers to the subsection that discusses that model in more detail.

1) *Techniques for movement of rolling elements in linear guides*: In general there are three ways in which the rolling elements could move in a linear guide, being *recirculating*, *non-recirculating*, and *both recirculating and non-recirculating*. The former is based on the concept that a rolling element within a bearing moves continuously through a circuit, or path and keeps repeating that. This allows the bearing to have unlimited travel, regardless of the bearing length and will be constrained only by the shaft guideway or the length of the rail [41]. The second method has rolling elements that are contained in a housing and rotate about their axes, without translation with respect to the housing. The load is directly supported and the stroke is limited by the number of rolling elements and the length of the bearing. The latter method is a combination of the two previously explained phenomena, in which one part can be seen as recirculating and another part as non-recirculating with their corresponding characteristics [41]. The recirculating parts are often located in the wheels, while the non-recirculating part consists of the chassis of the guide. Together they form a working linear guide.

*a. Recirculating*: In recirculating bearings, the rolling elements move from a load-carrying zone to a non-load-

carrying zone and vice-versa. Moreover, this transition is not completely linear and smooth and causes pulsations that affect the travel accuracy and could result in pronounced rotational movements of the carriage. [1], [41]–[43]. High forces are required to force the rolling element from the unloaded zone back into the loaded zone, which could cause pilling and sliding of the balls in the return tube [23].

To reduce these dynamic motions, one could dampen the forces by using an insert that leads the rolling element from the loaded to the unloaded zone. Another solution is to make the transition from loaded to unloaded more gradual by using a longer entry zone of the rolling element. These methods reduce both the friction forces in the carriage and the variations of the friction forces which reduces the overshoot or undershoot position in the system [23], [42], [44]. This transition from loaded to unloaded zone induces undesired vibrations. Another method to reduce this vibration is by using a carriage with crowned raceways as suggested by Otha et al. [43], [45].

However, there are also disadvantages of using recirculating bearings. The maximum speed is limited in recirculating bearing due to the forces exerted on the end caps during the transition from the loaded to the unloaded stage. Since the speed has a direct relation with the deceleration and therefore with the force on the end cap, a higher speed will result in higher forces. Nonetheless, to achieve a higher speed one could either design an end cap that could resist higher forces or reduce the mass of the rolling element so that the force will decrease. The former solution could result in a maximum speed of 5 m/s. For the latter, ceramic is often chosen because of its material properties (low mass-to-strength ratio) which results in a maximum speed of up to 10 m/s. Note that the dynamic load capacities can be reduced by up to 30 percent compared to the traditional rolling elements made of steel [41], [46].

Another negative effect that occurs in recirculating bearings is the collision of balls. Surfaces of contiguous balls rotate in opposite direction causing noise, sliding friction, and change in the ball pitch. In a lot of applications, this has been solved by introducing smaller diameter spacer balls between the balls or using a ball cage that eliminates these effects [23], [44], [47].

Moreover, an error in the alignment of the rails causes uneven loading of the bearing, premature wear, and affects the preload of the bearing [48].

*b. Non-Recirculating*: In non-recirculating bearings, the speed is not limited as described for the recirculating bearing. Furthermore, there are no pulsations, noise, and sliding friction due to rolling elements that collide or recirculate. Therefore, the non-recirculating bearing can achieve a higher position accuracy [22]. However, angular errors and torque moments could occur if the table overhangs the base. Possible solutions are a set of rolling elements that are equal or greater in length than the table and base. A higher degree of support could be achieved, but force and angular perturbations are introduced when balls enter and exit the railways [1].

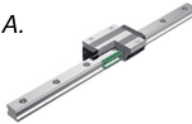
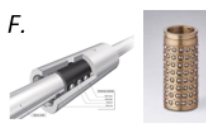

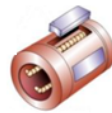







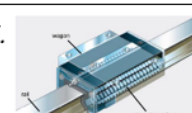
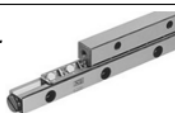

Techniques used for movement of rolling elements				
Recirculating	Non-recirculating	Both Recirculating & Non-recirculating		
A. 	F. 	K. 	2 points	Type of contact of rolling elements
B. 		L. 	3 points	
C. 	G. 	M. 	4 points	
D. 	H. 	N. 	2 lines	
E. 	I. 	O. 	2 x 2 lines	

Fig. 1: Overview of linear guide systems. [27]–[40]

Non-recirculating bearings often suffer from cage creep. Cage creep is a phenomenon where the cage shifts to one end of the bearing and therefore does not remain in its intended centered position. This could occur when accelerations and speeds are high, load distribution is uneven, different heat expansion coefficients are present, lacking rigidity and/or accuracy of connecting structure, and protruding cage. In vertical application, the chance of cage creep is often higher than in horizontally positioned cages, because of the gravity force [29], [49].

The stroke of the bearing is shortened when cage creep occurs or the cage could bump into an end stop if that is provided. The latter causes both the cage and the rolling element to slide, which increases friction and thus generates heat. Also, more rapid wear occurs and one of the guide elements or the cage could be damaged by this. Furthermore, it reduces the optimal load distribution and a large expense of energy is required to correct the stroke to its centered position. Controlling the speed of the cage could ensure the correct cage to ball speed ratio to prevent cage creep [29], [49], [50]. Moreover, a cage control system could be used to prevent cage creep and avoid correction strokes. It regulates the displacements of the cage and keeps it in the right position. Thus, no additional action is needed to reset the cage to its centered position [29].

*c. Both Recirculating and Non-Recirculating:* Linear guides that are both recirculating and non-recirculating are a combination of the two principles described above. The

recirculating parts are often located in the wheels, while the non-recirculating part consists of the chassis of the guide. This guide has therefore advantages and disadvantages of both techniques. The stroke of the guide is often not limited by the cage or bearing, only by the length of the rails which is also the case for recirculating bearing. Furthermore, the speed is not limited and there are no effects of rolling elements that move from a loaded stage to a non-loaded stage [31], [48]. In contrast, this technique is less applicable for a compact and ultra-high accurate solution. The size is larger since it has both a recirculating part and a non-recirculating part. Also, the accuracy suffers from the combination of the two techniques since misalignment between parts occurs. Besides that, friction between parts increases and effects of contamination occurs [51].

2) *Type of contact of rolling elements:* In this paper, we distinguish three categories of rolling elements; balls, rollers, and needles. These rolling elements are exposed to a variety of contact surfaces, such as circular arc, gothic arc, and flat surfaces. These are categorized by differentiating point contacts (2,3, and 4 points contact) and line contacts (2, 2x2 lines contact).

*a. 2 points contact:* When using circular arc grooves (Figure 3a), balls will have two-point contacts. This means that there are only 2 contact areas with the groove (Figure 2a). The curvature radius of the grooves is in general about 52% of the ball diameter, which results in larger rated load and higher rigidity than grooves with larger radii (Figure 4) [52].

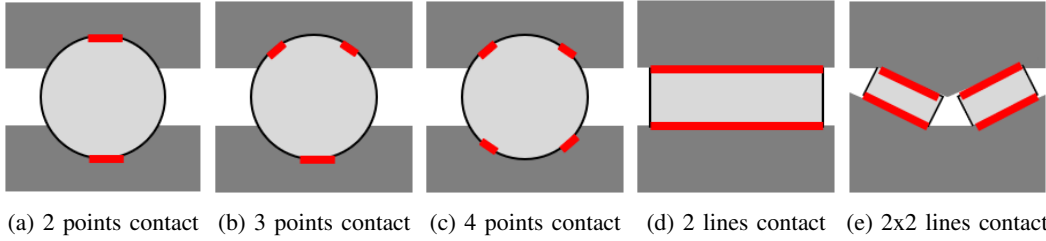


Fig. 2: Types of contact of rolling elements. Red lines indicate the contact points [32], [52]

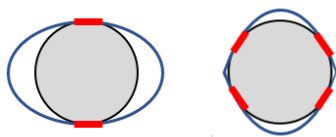
Due to the circular arc grooves, it is possible to increase the preload, and obtain higher rigidity, while only getting a slight increase in rolling resistance [52].

When loaded, the rolling elements and raceway slightly deform due to their small elasticity, which transforms the contact point into an elliptical contact area. Additional Hertzian contact stresses are created in this area that leads to more differential slip [53]. The Hertzian contact stress can be calculated by using Equation 1, in which  $p_0$  is the maximum contact stress,  $r$  is the distance from the center of the circle,  $a$  the radius of the contact area,  $F$  the applied force,  $E$  the E-modulus,  $R$  the radius of the ball, and  $d$  the total deformation [54].

$$\begin{aligned} p(r) &= P_0 \left(1 - \frac{r^2}{a^2}\right)^{\frac{1}{2}} \\ p_0 &= \frac{1}{\pi} \left(\frac{6FE^2}{R^2}\right)^{\frac{1}{3}} \\ a &= \sqrt{Rd} \end{aligned} \quad (1)$$

The differential slip is caused by the fact that the velocities (calculated by multiplying the radius from one point to the center axis with the bearing angular velocity) at numerous points vary across the contact area. Thus, part of the contact of the rolling element slides or slips across the rails instead of rolling. This variance in velocities is due to the variance in radius to the center axis because of the elliptical shape [53].

Although differential slip happens, it is relatively small compared to configurations with more contact points since both the curvature rate of the circular arc grooves and the contact area are smaller. Differential slip decreases with the decrease of the contact area as well as a smaller difference between the circumference of the outer contact diameter and the diameter of the inner surface [52].



(a) Circular Arch (b) Gothic Arch

Fig. 3: Two types of grooves (contact points shown in red)

Comparison of rigidity by curvature (per ball)

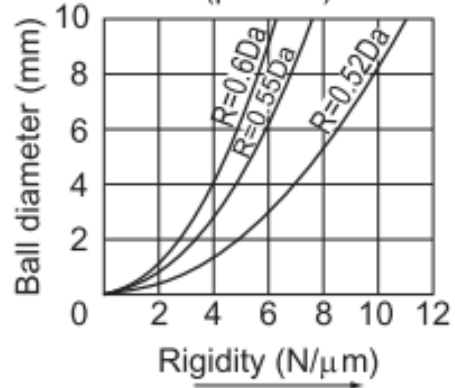


Fig. 4: Curvature radius vs rigidity [52]

**b. 3 points contact:** Three point contact systems are often a combination of a system with circular arc grooves on one side and gothic arch grooves on the other side of the ball (Figure 2b). Using circular arc grooves instead of a flat surface allows the balls to bear a load that is 13 times greater. The service life is proportional to the cube of the permissible load and therefore leads to a service life that is approximately 2200 times longer [52]. Using Equation 1, the Hertzian contact stress per contact point is smaller than for the 2point contact since the total contact area has been increased due to the additional contact point [54].

**c. 4 points contact:** When using gothic arch grooves (Figure 3b) in linear guides, each ball in the load zone has contact with the raceways at four points (Figure 2c). This prevents the contact points from moving and the balls from being highly elastically deformed [32]. This configuration allows no self-adjusting capabilities and therefore an accuracy error of the rail or a slight distortion of the mounting surface leads to an inconsistent motion. Hence, should be combined with a high precision rail and a highly rigid mounting base should be used [52], [55].

The gothic arch curvature radius has to be between 55 to 60% of the ball diameter and therefore the rated load is reduced to approximately 50% of that of the circular arc groove. Hence, the service life decreases to 87.5% [52].

The performances of linear bearings are affected by differential slip since there is an increase in friction and heat generation. Also, the preload that can be applied is affected, which increases the area of contact and therefore increase

the friction and heat generation even more [53]. Since the preload cannot be sufficiently applied a high rigidity could also not be obtained [52].

Compared to the circular arc geometries the differential slip in gothic arch raceways is higher since the contact area is larger as well as the difference between the circumference of the inner and outer diameter. Because of this larger difference, the friction coefficient increases with more than 10 times and the friction resistance also largely increases [52], [53].

Using Equation 1, the Hertzian contact stress per contact point is even smaller than for the 2 and 3 points contact since the total contact area has been increased due to the additional contact point [54].

The maximum speed rating is approximately 70 % higher for the four-point contact ball bearing (Figure 5) than the two points contact bearing. One of the reasons for that is the lower contact angle ( $35^\circ$  versus  $40^\circ$ ) [56].

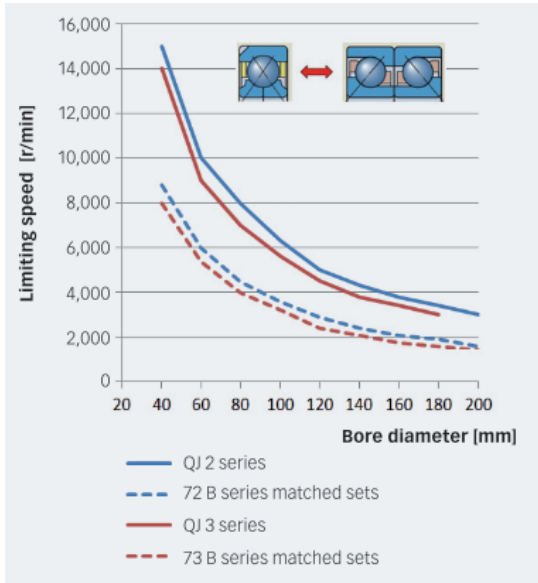


Fig. 5: Maximum speed of 4 points contact bearing (full lines) compared to 2 points (dashed lines). [56]

**d. 2 lines contact:** Using cylinders instead of balls means that we now consider line contacts instead of point contacts (Figure 2d). Since the contact area of line contacts is greater than those of point contacts the performances in terms of load capacity and rigidity are better. The load is distributed among a greater area, which reduces the pressure on one point and allows the bearing to carry higher loads. Different Hertzian contact stress equations (Equation 2) are used to determine this pressure [54], [57]. In this equation,  $p_0$  is the maximum contact stress,  $r$  is the distance from the center of the circle,  $R$  is the radius of the roller, and  $d$  is the total deformation. Since the pressure on rollers is lower than the pressure on ball contacts (Equation 1), less deformation of the roller will occur so the rigidity is higher [18], [58], [59].

$$p(r) = P_0 \left(1 - \frac{r^2}{R^2}\right)^{-\frac{1}{2}} \quad (2)$$

$$p_0 = \frac{1}{\pi} E \frac{d}{R}$$

Needle rollers could also be used and offer even better performance in load capacities since the load is distributed among more and smaller rollers. The ratio of length-to-diameter of needles is between 3 and 10, while the ratio for cylindrical rollers is around 3 [60]. The rigidity of needles is higher as well since less load per roller means fewer deflections under the load. The rigidity could be up to 50% higher than the cylindrical rollers [58], [60]. The smaller diameter also results in less vertical pulsations (Figure 6). Note that the dynamic running friction (due to their larger contact area) is higher in needle rollers which in the case of high-load, high-rigidity applications can be beneficial for the damping of vibrations due to external forces [60]. Differential slip does occur in roller-based bearings but it is less significant than in balls [53].

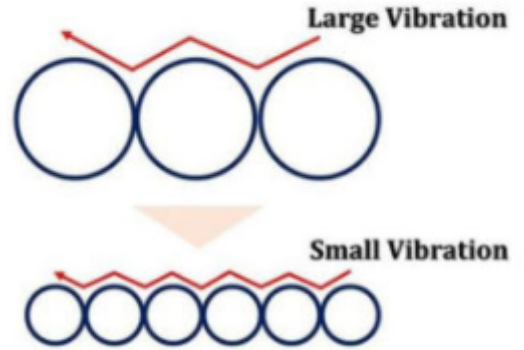


Fig. 6: Vibrations of needles compared to rollers [60]

**e. 2x2 lines contact:** The principles behind this type are the same as for the 2 lines contact. However, the configuration is different, since here two line contacts are used instead of one (Figure 2e). By using two line contacts the bearing can bear forces in all directions, increase the rigidity in those directions and increase the load capacity [61].

### C. Performance criteria

In order to evaluate the identified principles, we composed a list of relevant criteria. The models found in the classification will be evaluated by these criteria. As mentioned in the introduction, repeatability is not being considered since it heavily depends on the complete system, and so no data is available. However, the deformation and friction coefficient are important for the repeatability and thus will be evaluated. There exists a positive relation between the volume of the guide and the maximum load capacity and rigidity. Since some models are restricted to a larger volume because of their design, it would not be fair to compare these models



on those criteria. Therefore, we compare the larger segments' linear guides and the smaller segments separately with each other. Some models are available in both segments and will thus be considered in both comparisons. Most of the data about the different models are based on the information found in product catalogs of Schneeberger, THK and SKF [29], [35], [62]–[65].

1) *Cross Sectional Area*: The size of the guideway is relevant since the available space in some applications is limited. The dynamic load capacity and rigidity increase with the volume. A constant height has been chosen to compare the concepts for the same application in which space is limited.

2) *Length*: The length of the moving part (guide). To compare the different models for the same application. The rail length will not be considered.

3) *Degrees of Freedom (DOF)*: The allowable motion of the system in different directions.

4) *Dynamic load capacity*: The dynamic load capacity is the load at which a nominal service life of travel distance is achieved. This is commonly the L10 life, which is the life that 90% of the bearings are expected to achieve under the set conditions [62]. High dynamic load capacity is in some applications favorable.

5) *Deformation*: Deformations occur due to an applied load on the system. Highly rigid systems have less deformation than systems with low rigidity. In order to compare these systems on rigidity, the deformation that occurs under a load of 50N is determined. High rigidity is wanted to achieve higher accuracy.

6) *Speed*: The maximum allowable speed that could be achieved without malfunctioning.

7) *Friction*: The friction coefficient of a system provided by the companies.

### III. RESULTS

#### A. Recirculating - Ball 2 points contact

As described in the method, recirculating guides have rolling elements that move continuously through a circuit. In this category, these rolling elements are balls that have 2 contact points with the rails, which have a circular arc shaped groove Figure 7.



Fig. 7: Recirculating, 2 point contact, profiled rail bearing [27]

Angular error could be caused by diverse problems, which include curvature of the rails, entry and exit of balls, variation or insufficient preload. Contaminants between the rolling element or torsional compliance due to external forces or overhang torques [1].

Due to the possibility of the elastic deformation of the balls a light distortion of the mounting surface could be absorbed. It eliminates the need for a robust mounting base and allows the system to have unforced, smooth motion. The curvature radii, and so the contact angle, together with the ball diameter are important parameters that could alter the dynamics and the overall stiffness of linear ball guides [59].

Angular misalignment errors of the inner ring highly influence the contact load distribution which causes uneven load distribution inside the bearing. Larger angular misalignment will lead to an increase in maximum and average contact loads and an increase in translation and tilting stiffness coefficients. The magnitude and the direction of the angular misalignment also influence the number of contacted rolling elements, the position of the maximum contact load, and the stiffness coefficient. These change in stiffness has a significant influence on the performance. [17], [66].

While moving back and forth to the same position, micro-mechanics causes a variation of the subset of recirculating balls contacting the guideway since the entire ball loop has shifted relative to the truck. The arrangement and number of loaded balls change with every ball passage period. This causes changes in tilting stiffness and normal stiffness in a plane, which produces ball passage vibrations [45]. Also, the error motion at any position is influenced by the combination of active balls/guideways due to the local imperfections of both the active balls and the guideways. Moreover, the usage causes a change in error motion since abrasion and adhesion between the rolling elements cause wear due to sliding, corrosion, material fatigue, pitting, and cracking [23], [67].

Four different configurations could be identified in this category; back-to-back (O-arrangement), face-to-face (X-arrangement), tandem (Figure 8), and ball splines (Figure 10). The principal difference between the former, the second, and the third arrangement are associated with the positions of the effective load centers which is the point where the load lines intersect. The moment arm, defined as the distance between the center of the bearing and the effective load center, of the O-arrangement is larger (roughly double the length) than the moment arm of the X-arrangement. Therefore, the moment stiffness/rigidity and the moment load capacities of the O-arrangement are significantly higher than those of the X-arrangement. The shorter moment arm allows the X-arrangement design to compensate for misalignment. This could be useful in applications where there may be height deviations between for example two rails that are mounted in parallel [68] [69]. The moment arms for the tandem arrangement are both on one side, which makes them stiff on that side but less capable of bearing loads on the other side [19]. These three configurations can also be seen in angular contact ball bearings and the working principle is similar.

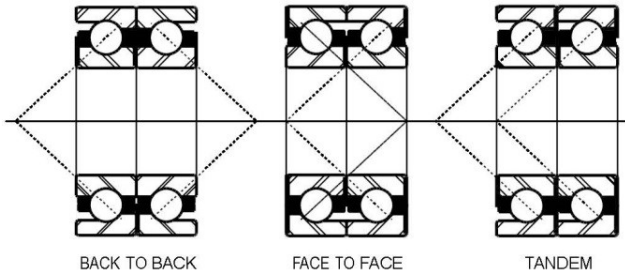


Fig. 8: Back to Back, Face to Face and Tandem configuration [70]

The stiffness element in axial and radial directions are, on the other hand, higher for the X-arrangement than those of the O-arrangement. The load capacities are equal in all directions for the X-arrangement [69]. The range of effective preload of the X-arrangement is clearly larger than that of the O-arrangement [68], [69]. All the stiffnesses of the two arrangements can be seen in Figure 9.

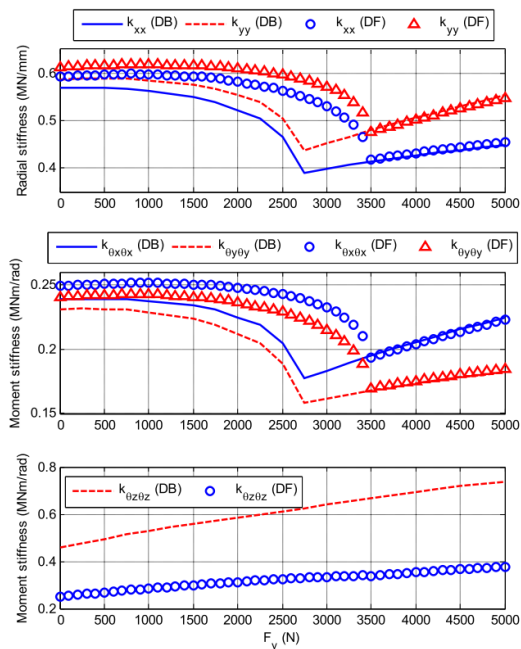


Fig. 9: Stiffness of Face to Face (DF) and Back to Back (DB) configuration.  $x$  in the radial direction,  $z$  in the axial direction, and  $y$  in the downwards direction. [68]

1) *Back-to-back configuration*: The moment arm is larger and therefore the moment stiffness/rigidity and moment load capacities higher. However, the allowable tilt angle is smaller for this configuration and therefore it requires a high mounting precision [52]. The natural frequencies that are related to the radial and tilting motion occur at higher frequencies due to the higher moment stiffness [19]. Under misalignment operating conditions this configuration can still provide higher stiffness and higher load-carrying capacity compared to the X-arrangement [66].

If there is a deflection in the table or an error in the flatness, the internal load applied to the block is approximately 6 times greater than the X-arrangement which results in shorter service life. Also the fluctuation in sliding resistance is larger with this configuration [52].

2) *Face-to-Face configuration*: The moment arm for this configuration is smaller so the moment stiffness/rigidity and moment load capacities are lower. Furthermore, it allows larger angular misalignment under angular misalignment operating conditions. The allowable tilt angle is larger, which makes the system highly self-adjustable. Therefore, the internal structure will not be easily affected by inconsistencies of the mounting surface [52], [66].

3) *Tandem configuration*: For tandem configurations, the moment load on one side is much higher than that of the other configurations. Therefore, the axial stiffness on that side is much higher. It can accommodate heavy axial loads and radial loads. The other side of the bearing is not able to tolerate high moment loads [19].

4) *Ball spline*: Circular-arch grooves in ball splines excel in applications that are having fairly consistent torque requirements, low inertial moments, and are somewhat tolerant of slight backlash [32]. Ball spline sound happens as a result of the collision between the balls and the spline shaft, and between the balls and the spline nut at the entrance of the load zone [47].

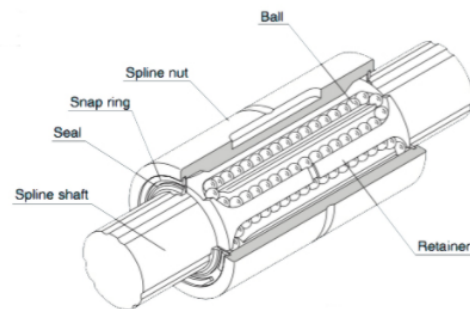


Fig. 10: Linear ball spline [30]

### B. Recirculating - 3 points ball contact

Some ball splines have 3 points contact and are recirculating. They mostly have gothic arc grooves on the outer nut and circular arc grooves on the shaft. The bearing has lower rigidity than both the 2 point contact and the 4 points contact since it is not fully constrained [28], [32]. The investigated companies are not providing any information about this type of linear guide and did not include them in their catalogs.

### C. Recirculating - 4 points ball contact

In this category, gothic arc groove rails are used which provide 4 points contacts for each load-carrying ball that recirculates. This combination provides a highly rigid system, with relatively high friction and low self-alignment capacity. They can withstand load from more directions, although they

can handle less load compared to circular arc designs, and have a relatively high moment load capacity. Differential slip together with increased sliding friction are two of the main drawbacks in this system, which also negatively affects the allowable preload [32], [71].

Ball splines using gothic arch groove profiles have lower backlash than ball splines having other raceways. Besides that, they excel on axes that require dynamic torque transmission [32].

#### D. Recirculating - roller 2-line contact

An example of this group is a bearing that uses rollers that are being held by a retainer and move infinite circulations. Due to the use of rollers the load carrying capacity is higher compared to the previous designs, also the friction coefficient is lower and the design is free from stick-slip [72], [73].

#### E. Recirculating - roller 2x2-line contact

Designs in this group consist of rollers oriented in multiple directions that recirculate and therefore allow unlimited movement. One of the applications has profiled rails and wagons (Figure 11). Due to the circulating rollers inside the wagon and the profiled rail, this roller bearing could achieve infinite motion. The inner preload that has been applied results in no guide clearance between the rail and the wagon and allows the bearing to bear tractive and compressive loads [31]. Roller guides are often offered in larger sizes and are therefore less applicable if a small solution is required [58].

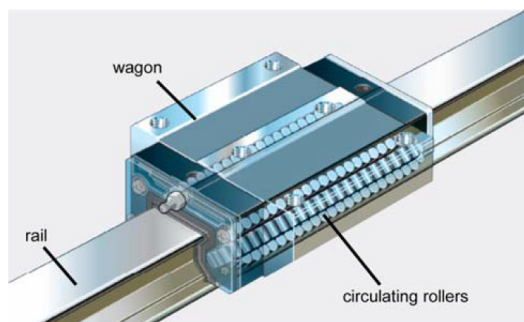


Fig. 11: Profiled roller rail bearing [31]

The ultimate loading can be larger than that of a ball guideway due to the increased contact area. The abrasion of the roller bearings is less compared to other guides since the increased contact area makes the lubrication more efficient [73].

Elastic deformation occurs between the roller and the raceway when the roller is subjected to a load. The Palgém formula (Equation 3) could be used to calculate the contact force of the roller with the assumption that the deformation at the two contact lines occurs at the same time and that the roller and guide are made of the same material [18].

$$F_{ki} = C \left( \frac{\Delta d_{Ki}}{2} \right)^{\frac{10}{9}} 1001 [18] \quad (3)$$

Fatigue life can be calculated by using the Hertzian contact pressure and the contact width (Equation 2). Due to the

circulation, the carriages of preloaded roller bearings were moved periodically with the roller passing frequency [73].

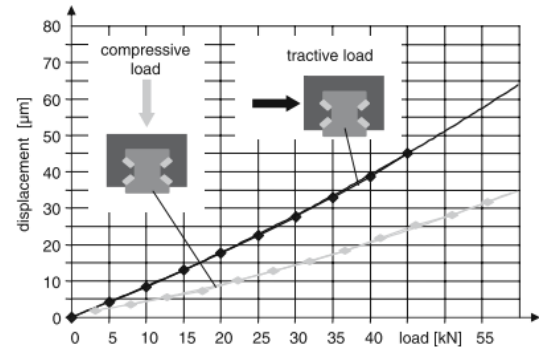


Fig. 12: Displacement at different loads [31]

Another application is the usage of cross rollers in the wagons. Each roller in this bearing is positioned in an angle of 90 degrees relative to the roller before and after that one [61]. Hence, there are fewer rollers used than in the previously mentioned design. Even higher loads could be carried and higher rigidity could be achieved. Effects of recirculating bearings like vibrations and speed limitation due to the movement from a loaded to an unloaded zone still play a role. However, the collision of the rollers does not happen since the rollers are placed inside a cage [61].

Needles could be used instead of rollers as well. As explained in the method, this will increase the rigidity and the load capacity since more needles could be used due to the smaller diameter. This model does exist in theory, however, all the investigated companies do not offer them in their catalogs.

#### F. Non-Recirculating 2 points contact

An example design of this group has a ball cage with balls incorporated into a cylindrical nut. The retainer holds the balls in the right position and guarantees enough space between the balls. Friction will remarkably reduce and stay constant along the stroke by eliminating the ball collision [30], [74]. The balls and the ball raceway are in a 2 points contact configuration and the balls are arranged in a zigzag position to evenly receive a load. The structure allows rotational as well as reciprocal motion. Cage creep could take place and the stroke is limited to twice the range in which the ball cage can travel. Overshooting is prevented by a thrust ring and a snap ring on both sides of the inner surface of the nut [74]. Compared to a recirculating ball spline this model could be made much smaller and has a lower friction coefficient [30].

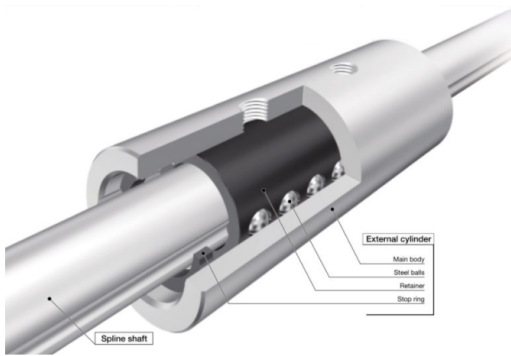


Fig. 13: Stroke ball spline [30]

Especially in vertical applications or under high-speed operation creep could occur and therefore the retainer need occasionally be re-centered by incorporating full-length strokes. Because of their size, it does not allow the use of an anti-creep mechanism. The dynamic friction is around 4 times less compared to the recirculating ball splines [30], [49].

#### G. Non-Recirculating 4 points contact

An example design consists of precision balls that are arranged in short pitches in a ball cage that moves in a dedicated rail. The stroke is limited due to the non-recirculating nature and cage creep could lead to higher friction force and more rapid wear [50]. The balls are fixed in the retainer and therefore could not collide with each other. This design also has an extended version which is the telescopic bearing. That bearing could retract to move away from the process [24].

#### H. Non-Recirculating 2 lines contact

Designs in this category have a flat roller that is sandwiched between two raceways. It moves half the distance of the table and has a relatively large load capacity. Since it uses rollers the deflections are small and therefore the rigidity is high. The rollers are held in a rigid cage so friction between the rollers is eliminated and skewing and stick-slip of the rollers are minimized. The rollers are only constrained by friction from moving toward the radial direction. Therefore, the load capacity and rigidity are only high in the axial directions and not in the radial ones [75].

#### I. Non-Recirculating 2x2 lines contact

A clear example of this group is the cross roller bearing. The rollers that are fixed inside a roller cage are orthogonally aligned one after another and move along a rail that has a V-shape groove. Mounting two cross roller guides in parallel allows the guide system to receive loads in all directions. Preload could be applied to obtain a highly rigid, clearance-free, and smooth slide mechanism [76].

Vibrations and oscillations are less, due to their non-recirculating property. Also, the fluctuations in frictional resistance are reduced so that the dynamic and static friction are almost equal. This minimizes the effects of stiction, which is the total static friction that must be overcome in

order to cause motion in a body at rest. Resulting in smooth motion and lower noise [61], [77].

Furthermore, load capacities and rigidity are high due to the larger contact area of the line contact compared to the point contact. Drawbacks are that the travel of crossed roller slides is mostly limited to around 1 meter. The total system should be double the length of the stroke because the guides proceed in opposite direction [58].

Creep is a common problem in this kind of guides. However, some solutions are already found to combat this problem, see Figure 14. This method uses a center roller that engages with the indentations in the rail to keep the cage centered. Another method is to use a pinion and a rack, in which the rack is mounted on one of the rails and the pinion gear is integrated into the cage [49].

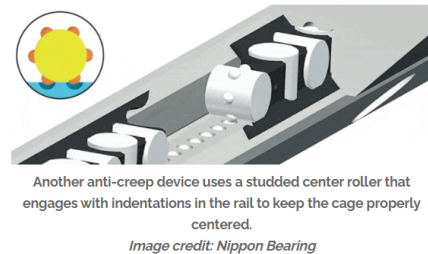


Fig. 14: Creep cross-roller [49]

In line with the recirculating 2x2 lines contact, the cross roller concept does also exist for the non-recirculating 2x2 line contact. To eliminate clearance in the guides and rollers a preload is mostly applied in these bearings. Cross roller slides are produced on a flat and rigid surface to achieve high parallelism and flatness [61].



Fig. 15: Crossed-roller bearing [27]

Another concept in this category is the needle type non-recirculating bearing. Since needles are used, the load is divided among more needles and thus a large contact area. This leads not only to a better load distribution but also to less deformation and higher rigidity.

### J. Both Recirculating and Non-recirculating - general



Fig. 16: Cam roller bearing [37]

One of the few applications in which both the recirculating and non-recirculating technique is used is cam rollers. Cam rollers consist of multiple wheels that rotate around their axes and move along a rail. Inside these wheels, rolling elements recirculate. The same as for the recirculating and non-recirculating techniques the division is made between 2point contact, 3 points contact, 4 points contact, and 2 lines contact.

In general, cam rollers can achieve relatively high speeds and accelerations, of respectively 10 m/s and 50 m/s<sup>2</sup>. Increasing the preload will result in even higher performances because less slipping occurs. This preload can be regulated and adjusted by the user itself by pressing the roller bodies against the frame. Higher preload will increase the rigidity and speed, but will also increase deformations and wear and so reduces lifetime [31], [48]. Mounting of the cam roller is much less stringent compared to for example recirculating guides since the preload is adjustable and thus a reference edge is in most cases not required. Because of this adjustable preload, also replacement of the block is simplified [48], [51].

The weight of cam rollers is relatively low compared to other linear guides since most parts are made of aluminum which is lighter than steel which is used in a lot of other guides. Other guides have to use steel to achieve the desired load capacity, which will not be reached when using aluminum. Because of the lower weight, the acceleration could be higher and the forces are reduced of which highly dynamic applications benefit the most. Contamination is less detrimental to cam rollers than to other linear guides. The radial bearing that supports the cam roller is completely sealed and lubricated while recirculating bearings are highly dependent on lubrication. Cam rollers could therefore be used in more harsh environments [48]. In general, cam rollers are less applicable for a compact and ultra-high accurate solution but are a good choice when ruggedness, speed, forgiving installations, and long lifetime are important factors [51]. Lower accuracy could be achieved since misalignment between the parts is larger. Also, the application of preload is done manually which introduces human errors.

### K. Both Recirculating and Non-recirculating - 2 points contact

Cam rollers that are using wheels with 2 points of contact can achieve higher rigidity than bearings with more contact points. Under large loads, the contact angle could significantly increase which results in a disadvantageous displacement of the contact zone. This will lead to contact fatigue. The same could happen if axial clearance becomes higher [78].

### L. Both Recirculating and Non-recirculating - 3 points contact

Wheels that are using 3 points contacts have both a gothic arc and a circular arc. One of them is in the outer ring and the other one in the inner ring [28]. The investigated companies are not providing any information about this type of linear guide and did not include them in their catalogs.

### M. Both Recirculating and Non-recirculating - 4 points contact

Four points contact bearings could withstand axial loads in the horizontal and vertical direction and could accommodate radial loads only limited. The bearing saves space compared to the double row angular bearing [56]. Four points contact bearings in cam rollers have a lower rated load due to the gothic arc shape of the outer ring [32].

### N. Both Recirculating and Non-Recirculating - 2 lines contact

Cam rollers with 2 lines contact could only function as cam followers since they could only bear radial forces. In this category, we distinguish two types: bearings using rollers and bearings that are using needles. The main reason to choose needles rollers is their compact size and the increased load capacities [60].

### O. Both Recirculating and Non-Recirculating - 2x2 lines contact

The same bearings as discussed in the previous section with 2 lines contact are used but now the configuration of the wheels is different. The wheels are configured in a cross roller configuration, meaning that the rollers have a 90-degree angle relative to the adjacent rollers. This will allow the cam roller to bear forces in all directions. The rigidity and load capacities of this type are the highest among all the cam rollers due to the combination of using rollers instead of balls and using a cross roller configuration [51], [58].

### P. Overview of concepts

For all working principles, concepts are selected based on their cross-sectional area. They will be compared based on the performance criteria mentioned in subsection II-C. The results can be found in Figure 17. In Figure 17a, the comparison is based on a constant cross-sectional area with a height of around 15mm. The second comparison, Figure 17b, is based on a height of around 35mm. The models in bold are new models that are not included in the first comparison because they were not available in the small height.

	Model - (Company)	Cross Sectional Area (Height x Width [mm])	Length [mm]	DOF	Dynamic Load Capacity [N]	Deformation [ $\mu$ m]	Speed [m/s]	Friction coefficient
Recirc. - 4-point	MNN15 - (S)	16 x 32	43,7	1	3680	1,5	5	0,005
Recirc. - 2-line	NRT19077 - (S)	19 x 27	77	2	43000	<0,1	1	0,005
Recirc. - 2x2-line	SR6 100 - (S)	15 X 25,7	100	1	2150	<0,1	2	0,005
Non-Recirc. - 2-point	ST8 - (T)	$\emptyset$ 15	24	2	980			
Non-Recirc. - 4-point	R6 - AK6 - (S)	15 x 31	200	1	910	0,4	1	0,0005 - 0,0030
Non-Recirc. - 2-line	FT5038250 - (T)	5 x 38	250	2	109000			
Non-Recirc. - 2x2-line	R6 - AC6 - (S)	15 x 31	200	1	7420	0,3	1	0,0005 - 0,0030
Non-Recirc. - 2x2-line	N/O-62015 - (S)	15 X 31	200	1	169600	<0,1	1	0,0005 - 0,0030

(a) Small segment comparison

	Model - (Company)	Cross Sectional Area (Height x Width [mm])	Length [mm]	DOF	Dynamic Load Capacity [N]	Deformation [ $\mu$ m]	Speed [m/s]	Friction coefficient
<b>Recirc. - 2-point</b>	<i>BMW25F - (S)</i>	<i>36 x 48</i>	<i>84,9</i>	<i>1</i>	<i>21100</i>	<i>0,1</i>		<i>0,005</i>
<b>Recirc. - 2-point</b>	<i>SLS25 - (T)</i>	<i><math>\emptyset</math> 37</i>	<i>60</i>	<i>2</i>	<i>18200</i>			
Recirc. - 2-line	NRT38144 - (S)	38 x 52	144	2	181000	<0,1	1	0,005
<b>Recirc. - 2x2-line</b>	<i>MRW25F - (S)</i>	<i>36 x 48</i>	<i>88</i>	<i>1</i>	<i>27700</i>	<i>0,1</i>		<i>0,005</i>
Recirc. - 2x2-line	SR12 200 - (S)	28 x 51,5	200	1	10000	<0,1	2	0,005
Non-Recirc. - 2-point	ST25 - (T)	$\emptyset$ 37	45	2	4120			
Non-Recirc. - 4-point	R12 - AK12 - (S)	28 x 58	200	1	1820	0,8	1	0,0005 - 0,0030
Non-Recirc. - 2-line	FT 10080-500 - (T)	10 x 80	500	2	459000			
Non-Recirc. - 2x2-line	R12 - AC12 - (S)	28 x 58	200	1	17500	0,5	1	0,0005 - 0,0030
Non-Recirc. - 2x2-line	N/O 3045 - (S)	35 x 78	500	1	64800	0,1	1	0,0005 - 0,0030
<b>Recirc. &amp; non-Recirc. 2 point</b>	<i>305801 C-2Z - (SK)</i>	<i><math>\emptyset</math> 35</i>			<i>9040</i>		<i>17,4</i>	
<b>Recirc. &amp; non-Recirc. 4 point</b>	<i>361201 R - (SK)</i>	<i><math>\emptyset</math> 35</i>			<i>6240</i>		<i>20,1</i>	
<b>Recirc. &amp; non-Recirc. 2 line</b>	<i>NA 2202,2RS - (SK)</i>	<i><math>\emptyset</math> 35</i>			<i>7480</i>		<i>9,16</i>	
<b>Recirc. &amp; non-Recirc. 2x2 line</b>	<i>STO15 - (SK)</i>	<i><math>\emptyset</math> 35</i>			<i>9130</i>		<i>9,16</i>	

(b) Large segment comparison

Fig. 17: Comparisons of models. Recirculating (recirc.) and Non-recirculating (non.recirc.) models from catalogs from Schneeberger (S), THK (T), and SKF (SK). [29], [35], [62]–[65]

#### IV. DISCUSSION

Several linear guides have been analyzed throughout this report, each with its advantages and limitations. As described earlier, there exists a positive relation between the volume of the guide and the maximum load capacity and rigidity. Since some models are restricted to a larger volume because of their design, it would not be fair to compare these models on those criteria. Therefore, we compare the larger segments' linear guides and the smaller segments separately with each other. Some models are available in both segments and will thus be considered in both comparisons.

Some concepts have 2 DOF, which means that they could also make another motion apart from the full linear motion. Examples are the 2 lines contact category which could also move in the radial direction, and the non-recirculating 2 points contact that also could rotate around the axis of rotation. For both construction hold that a second linear guide is necessary to perform a complete linear motion.

In the smaller segment linear guides, the recirculating 2 lines contact cart and the non-recirculating 2-line contact got by far the highest values for the dynamic load rating. Also, the rigidity in the vertical direction is quite high (almost no displacement when applying 50N). However, as just explained they are not constrained in the radial direction. Only friction force could prevent the bearing from moving

to that direction. They are thus not rigid in the radial direction, and so not applicable for applications that require a constrained linear motion.

A concept of the smaller segment that is rigid in all directions and has a relatively high dynamic load rating is the non-recirculating 2x2 line contact bearing. Both the cross-roller and needle show good results on this. Due to the use of needles, the contact area increases even more and therefore reduces the pressure on one point. The Hertzian contact stresses become less and as a result, fewer deformations occur.

The speed of the 4 points recirculating bearing is the highest among the concepts. From theory, we could however conclude that the speed of non-recirculating guides should be higher than recirculating guides. Differences between the table and theory could be explained by the fact that companies are using a standard safety margin that keeps the speed lower than the actual speed that could be achieved. Also, due to the stroke limitation, it is practically difficult to achieve high speeds, as they are limited by accelerations.

The different techniques do differ in total friction, the friction of recirculating guides is in general around 2-10 times larger than non-recirculating. This can be explained by the friction that is generated by the collision of the balls and at the transition from a loaded to an unloaded zone.

For the larger segment, we see comparable results. The highest load rating and best rigidity are achieved with concepts that are using line contacts. Furthermore, the 2-line concepts that allow another motion have higher dynamic loads and rigidity. However, in the unconstrained direction, these concepts will have significantly lower values. The 2x2 line contacts have high scores on the load capacity and rigidity as well. Similarly to the smaller segment comparison, these higher scores for line contacts compared to point contacts are due to the larger contact area of the line contacts resulting in less Hertzian contact stress, so fewer deformations. The speed of the cam-rollers, in the category of both recirculating and non-recirculating, is significantly higher than the speed of the other concepts. The bearings used in this concept are in a closed circuit, fewer contaminants are present and smoother motion could be achieved. This results in less friction and higher speeds. The friction coefficient for non-recirculating is in this case also lower than the friction coefficient of the recirculating guides.

A system using cross roller guides needs to be mounted with two guides in parallel to enable a fully constrained linear motion. This is due to the fact that the cross roller on its own does not have a horizontal constraint. Using two cross rollers will increase the load capacity and the total stiffness of the system. This higher total stiffness will lead to fewer deformations. Assuming that a constant load is applied and that the cross rollers behave like springs in parallel, there can be concluded that the deformations will be decreased by a factor of two. It is important to take this into account when designing a system that uses cross rollers.

Three points contact bearings do exist in theory, however, bearing manufacturers are not fabricating them since it does not have significant advantages compared to the two points contact bearings and the four points contact bearings.

For the comparison of the models, standard guides are used for each working principle. However, the companies have improved models or are improving existing models and therefore can achieve better performances than displayed in the results. Also, not all guides are available in all sizes, and since the size does have a significant influence on the load capacity and rigidity a completely fair comparison could not be made. This introduces a variation in the results that makes the comparison in a way subjective. This subjectivity is also the case for the classification. The cam rollers are defined as a combination of both recirculating and not recirculating but could also be designated to one of the categories by other researchers.

The performances that are provided by suppliers of linear guides are however sometimes different than the performances measured by a customer. This could, for example, be caused by the way the construction is assembled, the alignment procedure, the temperature and pressure during assembly, the applied torque on the bolts, and the applied preload. It is therefore interesting to know in what way the assembly procedure will influence the performances of a linear guide and to what extent that differs for various linear guides. Furthermore, the influence of the amount of preload

on the specific models could be investigated to illustrate the effect on the final performances.

## V. CONCLUSION

The goals of this paper are to provide a classification of the types of linear guides and to compare them by using some performance criteria. The classification consists of the techniques used for the movement of the rolling elements in linear guides and the type of contact of these rolling elements. The former is divided into recirculating, non-recirculating and a combination of both and the latter includes 2 points contact, 3 points contact, 4 points contact, 2 lines contact, and 2x2 lines contact. Designs of linear guides belonging to cross-categories are discussed. For every design, a model has been chosen based on the height of the model to make a good comparison between the designs. They are compared based on the performance criteria to give an impression of how well they perform as a linear guide.

This overview supports researchers and businesses in making a decision on what model to choose for their application based on their main criteria. It illustrates the working principle and the effects that occur for every concept.

## REFERENCES

- [1] K. McCarthy, "Accuracy in positioning systems," *Proc. The Motion Control Technology Conf*, 1991. [Online]. Available: <http://fp.optics.arizona.edu/optomech/studentreports/2007/JasonRuhl.doc>
- [2] H. H. Huang and J. Wey, "Research on the high-speed pick and place device for die bonders," *2010 8th IEEE International Conference on Control and Automation, ICCA 2010*, pp. 1683–1687, 2010.
- [3] S. Briot and I. A. Bonev, "Pantopteron-4: A new 3T1R decoupled parallel manipulator for pick-and-place applications," *Mechanism and Machine Theory*, vol. 45, no. 5, pp. 707–721, 2010. [Online]. Available: <http://dx.doi.org/10.1016/j.mechmachtheory.2009.07.007>
- [4] E. Amann, "Modeling and motion control of a pick and place machine with air bearings," 2012.
- [5] L. G. Marques, R. A. Williams, and W. Zhou, "A mobile 3D printer for cooperative 3D printing," *Solid Freeform Fabrication 2017: Proceedings of the 28th Annual International Solid Freeform Fabrication Symposium - An Additive Manufacturing Conference, SFF 2017*, pp. 1645–1660, 2020.
- [6] C. T. Hsieh, "Investigation of Delta Robot 3D Printer for a Good Quality of Printing," *Applied Mechanics and Materials*, vol. 870, pp. 164–169, 2017.
- [7] C. Cajal, J. Santolaria, J. Velazquez, S. Aguado, and J. Albajez, "Volumetric error compensation technique for 3D printers," *Procedia Engineering*, vol. 63, pp. 642–649, 2013. [Online]. Available: <http://dx.doi.org/10.1016/j.proeng.2013.08.276>
- [8] X. Y. Wang, H. T. Feng, C. G. Zhou, and K. Q. Ye, "A thermal model for real-time temperature forecast of rolling linear guide considering loading working conditions," *International Journal of Advanced Manufacturing Technology*, vol. 109, no. 7-8, pp. 2249–2271, 2020.
- [9] Z. T. Abdullah, G. S. Sheng, and S. B. Yun, "Conventional Milling Machine into CNC Machine Tool Remanufacturing, Eco-comparison Ratio Based Analysis," *Current Journal of Applied Science and Technology*, vol. 28, no. 6, pp. 1–18, 2018.
- [10] W. Kwintarini, A. Wibowo, B. M. Arthaya, and Y. Y. Martawirya, "Modeling of Geometric Error in Linear Guide Way to Improved the vertical three-axis CNC Milling machine's accuracy," *IOP Conference Series: Materials Science and Engineering*, vol. 319, no. 1, pp. 0–6, 2018.
- [11] M. Figl, C. Ede, J. Hummel, F. Wanschitz, R. Ewers, H. Bergmann, and W. Birkfellner, "A fully automated calibration method for an optical see-through head-mounted operating microscope with variable zoom and focus," *IEEE Transactions on Medical Imaging*, vol. 24, no. 11, pp. 1492–1499, 2005.
- [12] H. Sadeghian, B. Dekker, R. Herfst, J. Winters, A. Eigenraam, R. Rijnbeek, and N. Nulkes, "Demonstration of parallel scanning probe microscope for high throughput metrology and inspection," *Metrology, Inspection, and Process Control for Microlithography XXIX*, vol. 9424, no. March 2015, p. 942400, 2015.
- [13] D. Y. Lee, D. M. Kim, D. G. Gweon, and J. Park, "A calibrated atomic force microscope using an orthogonal scanner and a calibrated laser interferometer," *Applied Surface Science*, vol. 253, no. 8, pp. 3945–3951, 2007.
- [14] D. S. Biggs, "A Practical Guide to Deconvolution of Fluorescence Microscope Imagery," *Microscopy Today*, vol. 18, no. 1, pp. 10–14, 2010.
- [15] Y. J. Oh, C. H. Park, J. Hwang, and D. W. Lee, "Measurement of Five DOF Motion Errors in the Ultra Precision Feed Tables," *Materials Science Forum*, vol. 505-507, pp. 187–192, 2006.
- [16] S. H. Jang, G. Khim, and C. H. Park, "Estimation of friction heat in a linear motion bearing using Box-Behnken design," *International Journal of Advanced Manufacturing Technology*, vol. 89, no. 5-8, pp. 2021–2029, 2017.
- [17] M. Rahmani and F. Bleicher, "Experimental and analytical investigations on normal and angular stiffness of linear guides in manufacturing systems," *Procedia CIRP*, vol. 41, pp. 795–800, 2016. [Online]. Available: <http://dx.doi.org/10.1016/j.procir.2015.12.033>
- [18] G. He, P. Shi, L. Guo, and B. Ding, "A linear model for the machine tool assembly error prediction considering roller guide error and gravity-induced deformation," *Proceedings of the Institution of Mechanical Engineers, Part C: Journal of Mechanical Engineering Science*, vol. 234, no. 15, pp. 2939–2950, 2020.
- [19] A. Gunduz, J. T. Dreyer, and R. Singh, "Effect of bearing preloads on the modal characteristics of a shaft-bearing assembly: Experiments on double row angular contact ball bearings," *Mechanical Systems and Signal Processing*, vol. 31, pp. 176–195, 2012.
- [20] P. Pawełko, S. Berczyński, and Z. Grzadziel, "Modeling roller guides with preload," *Archives of Civil and Mechanical Engineering*, vol. 14, no. 4, pp. 691–699, 2014.
- [21] T. J. Royston and I. Basdogan, "Vibration transmission through self-aligning (spherical) rolling element bearings: Theory and experiment," *Journal of Sound and Vibration*, vol. 215, no. 5, pp. 997–1014, 1998.
- [22] T. Groothuijsen, D. Laro, and T. Ruijl, "Recirculating linear ball bearings and their effect on the accuracy of positioning systems," *European Society for Precision Engineering and Nanotechnology, Conference Proceedings - 19th International Conference and Exhibition, EUSPEN 2019*, no. June, pp. 142–145, 2019.
- [23] P. E. Dale and R. Tristani, "Wear performance of materials for ball screw and spline applications in Candu reactor fuelling machines," no. 6, pp. 365–370.
- [24] D. Collins. Tips for selecting and applying telescoping linear bearings. [Online]. Available: <https://www.linearmotiontips.com/tips-for-selecting-and-applying-telescoping-linear-bearings/>
- [25] M. D. Guide, "Linear guides," *Design Engineering (London)*, no. DEC., p. 26, 2001.
- [26] NSK Ltd, "Chapter 1 What Is A Linear Guide ?" 2010.
- [27] M. Solutions. Linear motion. [Online]. Available: <https://www.motionsolutions.com/products/linear-motion/linear-bearings-guides/>
- [28] A. Leblanc and D. Nelias, "Analysis of ball bearings with 2, 3 or 4 contact points," *Tribology Transactions*, vol. 51, no. 3, pp. 372–380, 2008.
- [29] Schneeberger, "Linear Bearings - Product Catalog," 2021. [Online]. Available: <https://www.schneeberger.com/en/products/linear-bearings-linear-roller-guideways/recirculating-unit-with-long-stroke/recirculating-unit-with-ball/recirculating-unit-with-ball-type-sk/#downloadscatalogue>
- [30] D. Collins. What are stroke ball splines and how do they differ from standard ball splines? [Online]. Available: <https://www.linearmotiontips.com/what-are-stroke-ball-splines-and-how-do-they-differ-from-standard-ball-splines/>
- [31] B.-A. Behrens and M. Ahrens, "Determination of the load on profiled roller guide rails used as ram guides for metal-forming machines," *Production Engineering*, vol. 1, no. 1, pp. 45–49, 2007.
- [32] L. Eitel. Gothic arches, tracks, and roller bearings in the context of linear motion. [Online]. Available: <https://www.linearmotiontips.com/gothic-arches-tracks-and-roller-bearings-in-the-context-of-linear-motion/>
- [33] Schaeffler. Miniaturkogelomloopenheden. [Online]. Available: [https://www.schaeffler.nl/content/schaeffler.nl/nl/products-and-solutions/industry/product-portfolio/linear\\_guidance\\_systems/miniature\\_ball\\_monorail\\_guidance\\_systems/index.jsp](https://www.schaeffler.nl/content/schaeffler.nl/nl/products-and-solutions/industry/product-portfolio/linear_guidance_systems/miniature_ball_monorail_guidance_systems/index.jsp)
- [34] Rodavigo. Ball cage ref. fibro 206.71.040.120. [Online]. Available: <https://rodavigo.net/en/p/ball-cage-ref-fibro-20671040120/58820671040120>
- [35] THK, "FT Product Information," 2021. [Online]. Available: <https://tech.thk.com/en/products/thklinks.php?id=346>
- [36] D. 360. Franke linear guides. [Online]. Available: <https://www.dynamic360.it/wp-content/uploads/2021/07/19-Schede-tecniche-di-tutti-i-modelli-di-guide-lineari-Franke.jpg>
- [37] I. Companies. Pbc linear – actuators, linear bearings, linear guides, and shafting. [Online]. Available: <https://isccompanies.com/parts-distribution/parts-by-manufacturer/pbc-linear/>
- [38] Schaeffler. Track roller guidance systems. [Online]. Available: [https://www.schaeffler.nl/content/schaeffler.nl/en/products-and-solutions/industrial/product-portfolio/linear\\_guidance\\_systems/track\\_roller\\_guidance\\_systems/index.jsp](https://www.schaeffler.nl/content/schaeffler.nl/en/products-and-solutions/industrial/product-portfolio/linear_guidance_systems/track_roller_guidance_systems/index.jsp)
- [39] i4mart. Nsk vbt20z-1. [Online]. Available: <https://www.i4mart.com/nsk-vbt20z-1-angular-contact-thrust-ball-bearings-single-direction-cbi>
- [40] SKF. Nup 204 ecml. [Online]. Available: <https://www.skf.com/it/products/rolling-bearings/roller-bearings/cylindrical-roller-bearings/single-row-cylindrical-roller-bearings/productid-NUP%20204%20ECML>
- [41] D. Collins. What are recirculating bearings. [Online]. Available: <https://www.linearmotiontips.com/faq-what-are-recirculating-linear-bearings/>
- [42] ——. Profiled rail accuracy: When accuracy class doesn't tell the whole story. [Online]. Available: <https://www.linearmotiontips.com/when-profiled-rail-accuracy-class-doesnt-tell-whole-story/>
- [43] H. Ohta, Y. Kitajima, S. Kato, and Y. Igarashi, "Effects of ball groupings on ball passage vibrations of a linear guideway type ball bearing (pitching and yawing ball passage vibrations)," *Journal of Tribology*, vol. 129, no. 1, pp. 188–193, 2007.



- [44] S. Shimizu, C. S. Sharma, and T. Shirai, "Life prediction for linear rolling element bearings: A new approach to reliable life assessment," *Journal of Tribology*, vol. 124, no. 1, pp. 121–128, 2002.
- [45] H. Ohta, S. Kato, J. Matsumoto, and K. Nakano, "A design of crowning to reduce ball passage vibrations of a linear guideway type recirculating linear ball bearing," *Journal of Tribology*, vol. 127, no. 2, pp. 257–262, 2005.
- [46] D. Collins. What limits linear bearing speed? (part 1). [Online]. Available: <https://www.linearmotiontips.com/what-limits-linear-bearing-speed-part-1/>
- [47] H. Ohta, S. Iwasaki, T. Kazama, and K. Hoshino, "Sound of a ball spline operated at a certain linear velocity," vol. 223, pp. 17–25, 2009.
- [48] D. Collins. When to use cam roller guides. (hint: it's more often than you think.). [Online]. Available: <https://www.linearmotiontips.com/when-to-use-cam-roller-guides-hint-its-more-often-than-you-think/>
- [49] ——. What is cage creep and why does it matter? [Online]. Available: <https://www.linearmotiontips.com/what-is-cage-creep-and-why-does-it-matter/>
- [50] W. Shapiro, F. Murray, R. Howarth, N. York, and R. Fusaro, "Learned Study," 2019.
- [51] L. Eitel. Basics of cam followers (including those for linear motion). [Online]. Available: <https://www.linearmotiontips.com/basics-of-cam-followers-including-those-for-linear-motion/>
- [52] THK, "Features of the LM Guide."
- [53] D. Collins. Motion basics: What is differential slip and how does it affect linear bearings? [Online]. Available: <https://www.linearmotiontips.com/motion-basics-what-is-differential-slip-and-how-does-it-affect-linear-bearings/>
- [54] A. C. Fischer-Cripps, "The Hertzian contact surface," *Journal of Materials Science*, vol. 34, no. 1, pp. 129–137, 1999.
- [55] H. Ohta, G. Hanaoka, and Y. Ueki, "Sticking of a Linear-Guideway Type Recirculating Ball Bearing," *Journal of Tribology*, vol. 139, no. 3, pp. 1–6, 2017.
- [56] Skf, "Four-point contact ball bearings – two in one | Evolution Online," pp. 25–28, 2015. [Online]. Available: <http://evolution.skf.com/four-point-contact-ball-bearings-two-in-one/>
- [57] I. N. Sneddon, "The relation between load and penetration in the axisymmetric boussinesq problem for a punch of arbitrary profile," *International Journal of Engineering Science*, vol. 3, no. 1, pp. 47–57, 1965.
- [58] D. Collins. When to consider crossed roller slides. [Online]. Available: <https://www.linearmotiontips.com/when-to-consider-crossed-roller-slides>
- [59] V. C. Tong, G. Khim, C. H. Park, and S. W. Hong, "Linear ball guide design optimization considering stiffness, friction force, and basic dynamic load rating using particle swarm optimization," *Journal of Mechanical Science and Technology*, vol. 34, no. 3, pp. 1313–1323, 2020.
- [60] D. Collins. What are needle roller linear bearings? [Online]. Available: <https://www.linearmotiontips.com/what-are-needle-roller-linear-bearings/>
- [61] ——. What is a crossed roller slide? [Online]. Available: <https://www.linearmotiontips.com/what-is-a-crossed-roller-slide/>
- [62] Schneeburger, "Mini-X - Product Catalog," 2019. [Online]. Available: <https://www.schneeburger.com/en/products/linear-bearings-linear-roller-guideways/linear-guidance-with-long-stroke/linear-bearings-with-balls/linear-bearing-miniature-minirail-2-row-with-and-without-integrated-cage-assist/#downloadscatalogue>
- [63] —, "Monorail and AMS - Product catalog," 2021. [Online]. Available: <https://www.schneeburger.com/en/products/linear-bearings-linear-roller-guideways/linear-guidance-with-long-stroke/linear-bearings-with-balls/linear-ball-bearing-monorail-4-row/#downloadscatalogue>
- [64] THK, "ST Product Information," 2021. [Online]. Available: <https://tech.thk.com/en/products/thklinks.php?id=327>
- [65] —, "Caged Ball Spline - Model SLS," 2021. [Online]. Available: [https://tech.thk.com/en/products/thklinks.php?id=20019&\\_ga=2.127566606.260722863.1638785928-183241580.1632742197](https://tech.thk.com/en/products/thklinks.php?id=20019&_ga=2.127566606.260722863.1638785928-183241580.1632742197)
- [66] T. Xu, L. Yang, W. Wu, and K. Wang, "Effect of angular misalignment of inner ring on the contact characteristics and stiffness coefficients of duplex angular contact ball bearings," *Mechanism and Machine Theory*, vol. 157, 2021.
- [67] G. W. Vogl, K. F. Shreve, and M. A. Donmez, "Influence of bearing ball recirculation on error motions of linear axes," *CIRP Annals*, vol. 70, no. 1, pp. 345–348, 2021.
- [68] V.-c. Tong, G. Khim, S.-w. Hong, and C.-h. Park, "Construction and validation of a theoretical model of the stiffness matrix of a linear ball guide with consideration of carriage flexibility," *Mechanism and Machine Theory*, vol. 140, pp. 123–143, 2019. [Online]. Available: <https://doi.org/10.1016/j.mechmachtheory.2019.05.021>
- [69] D. Collins. When should you use dual guide rails? [Online]. Available: <https://www.linearmotiontips.com/use-dual-guide-rails/>
- [70] A. R. B. C. Solutions. Duplex pair ball bearings. [Online]. Available: <https://www.amroll.com/angular-contact.html>
- [71] D. Collins. How raceway geometry affects profiled rail guide performance. [Online]. Available: <https://www.linearmotiontips.com/how-raceway-geometry-affects-recirculating-profiled-rail-guide-performance/>
- [72] THK, "Features of the LM Roller," pp. 10.2–10.3, 2015. [Online]. Available: [https://tech.thk.com/en/products/pdf/en\\_a10\\_002.pdf#1](https://tech.thk.com/en/products/pdf/en_a10_002.pdf#1)
- [73] T.-L. Horng, "The Study of Contact Pressure Analyses and Prediction of Dynamic Fatigue Life for Linear Guideways System," *Modern Mechanical Engineering*, vol. 03, no. 02, pp. 69–76, 2013.
- [74] THK, "LM Stroke Models ST, ST-B and STI."
- [75] —, "Features of the Flat Roller," pp. 11.2–11.3, 2015. [Online]. Available: [https://tech.thk.com/en/products/pdf/en\\_a11\\_002.pdf#1](https://tech.thk.com/en/products/pdf/en_a11_002.pdf#1)
- [76] —, "Features of the Cross Roller Guide/Ball Guide," pp. 7.2–7.3, 2015. [Online]. Available: [https://tech.thk.com/en/products/pdf/en\\_a07\\_002.pdf#1](https://tech.thk.com/en/products/pdf/en_a07_002.pdf#1)
- [77] E. Haug, "Simulation of friction and stiction in multibody dynamics model problems," *Mechanics Based Design of Structures and Machines*, vol. 46, no. 3, pp. 296–317, 2018. [Online]. Available: <https://doi.org/10.1080/15397734.2017.1341840>
- [78] L. Kania, S. Śpiewak, and R. Pytlarz, "the Modification of the Raceway Profile in the Double Row Slewing Bearing," *Journal of KONES. Powertrain and Transport*, vol. 23, no. 1, pp. 139–146, 2016.



3

Research paper

# Investigation of the relation between repeatability and preload for linear guides based on a position controlled input

Laurens van Driessen (4484495)  
TU Delft, 19-10-2022

**Abstract**— Increasing demand for higher precision machines is arising in the high-tech industry. Linear guides are often used to establish this highly accurate and highly repeatable motion. The amount and variation in preload play an important role in the total motion errors. The objective of this paper is to investigate the relation between preload and repeatability for both the ball linear guide and the cross-roller linear guide by performing experimental tests. Three preload cases at three positions are investigated and both longitudinal repeatability and rotational repeatability are measured. In the first case, the preload will be applied uniformly by adjusting two adjustment screws on one side. In the second case, only one screw will be adjusted and therefore generates an angular preload. In the third case, an additional mass is added resulting in external preload. The experiments are performed at  $0 - 25\text{mm}$ ,  $25 - 50\text{mm}$ , and  $50 - 75\text{mm}$ , in which zero represents the position both rails are in one line. Performances of the roller guide have a smaller spread at different positions compared to the ball guide. Also, after averaging the different positions for both rails, the repeatability of the roller guide tends to be generally lower than the ball guide, suggesting that the performances of the roller guide are better than those of the ball guide. For the ball guide, the longitudinal repeatability has an optimal point for uniform applied preload, while for the roller guide the performances slightly improves as the preload increases. The longitudinal repeatability generally increases for both the ball and roller guide with the angular applied preload, with the exception of an adjustment of 10 degrees for the ball guide. The longitudinal repeatability stays constant with the external preload. The rotational repeatability decreases for both the ball and roller guide with both uniform and angular applied preload. The rotational repeatability remains constant for both the ball and roller guide with external preload.

**Index term** — Linear guide - Repeatability - Preload - Position controlled

## I. INTRODUCTION

High precision machines are becoming more important in many high-tech markets. In a number of machines, linear guides are used to establish this highly accurate and highly repeatable movement. Examples are CNC machines [1]–[3], microscopes [4]–[7], 3D printers [8]–[10], and pick and place machines [11]–[13]. Different types of linear guides are available on the market including rolling-element guides, sliding guides, magnetic bearing guides, and air-bearing guides. Each type is again divided into different versions, each with its own characteristics and (dis)advantages. In this paper, we focus on the rolling element-based guides and more specifically the non-recirculating cross roller guide and the non-recirculating ball guide.

Rolling-element linear guides have a lower friction coefficient, have higher load capacities, and tend to run with

better position repeatability compared to sliding contact-based guides [14]. Repeatability is defined as the variation in consecutive measurements of one variable with the same conditions [14], [15].

The speed of the non-recirculating bearing is not limited, unlike the recirculating bearing. There is no additional noise, sliding friction, and pulsations due to rolling elements that recirculate or collide. Therefore, the non-recirculating bearing can achieve a higher position accuracy compared to recirculating bearings [16].

Multiple things could impede a system to achieve the desired level of repeatability. The repeatability depends not only on the selection of a linear guide but also on the complete system and its surrounding. Examples of such effects are external noise, contamination, and way of assembly [17]. Results of repeatability are therefore not mentioned in the product catalogs of linear guide manufacturers.

Cho [18] did research into the effect of yaw rotation on repeatability. Yaw rotation is defined as the rotation around a vertical axis that changes the direction of motion to the right or left. He found that this rotation has a dominant effect on the repeatability that could be reduced by adding balancing weight and adjusting the stiffness of the platform.

He also found that the damping coefficient and friction forces vary depending on driving conditions, maintenance, and operating environment. The yaw angle increases as the friction coefficient increases, which causes a decrease in repeatability. Furthermore, he found that the yaw motion is most dominant affected by parallelism [18].

Schneeberger [19] stated that the repeatability could be improved by increasing the preload. Drawbacks of this are more friction, reduction of moment loads and maximum loads, increased displacement resistance, and reduces service life.

Furthermore, the amount and variation in preload play an important role in the total motion errors [14]. Applying preload to a bearing will eliminate large deflection due to external loads, decrease noise and vibrations, enhance fatigue life, reduce rattle due to clearance, and prevent skidding [20] [21]. At higher preloads the nonlinear effects in bearings are negligible [22].

However, the relation between preload and repeatability is lacking in the literature, as well as the effects of additional applied mass on repeatability.

The objective of this paper is to investigate the relation between preload and repeatability for both the cross roller guide and the ball guide by performing experimental tests.

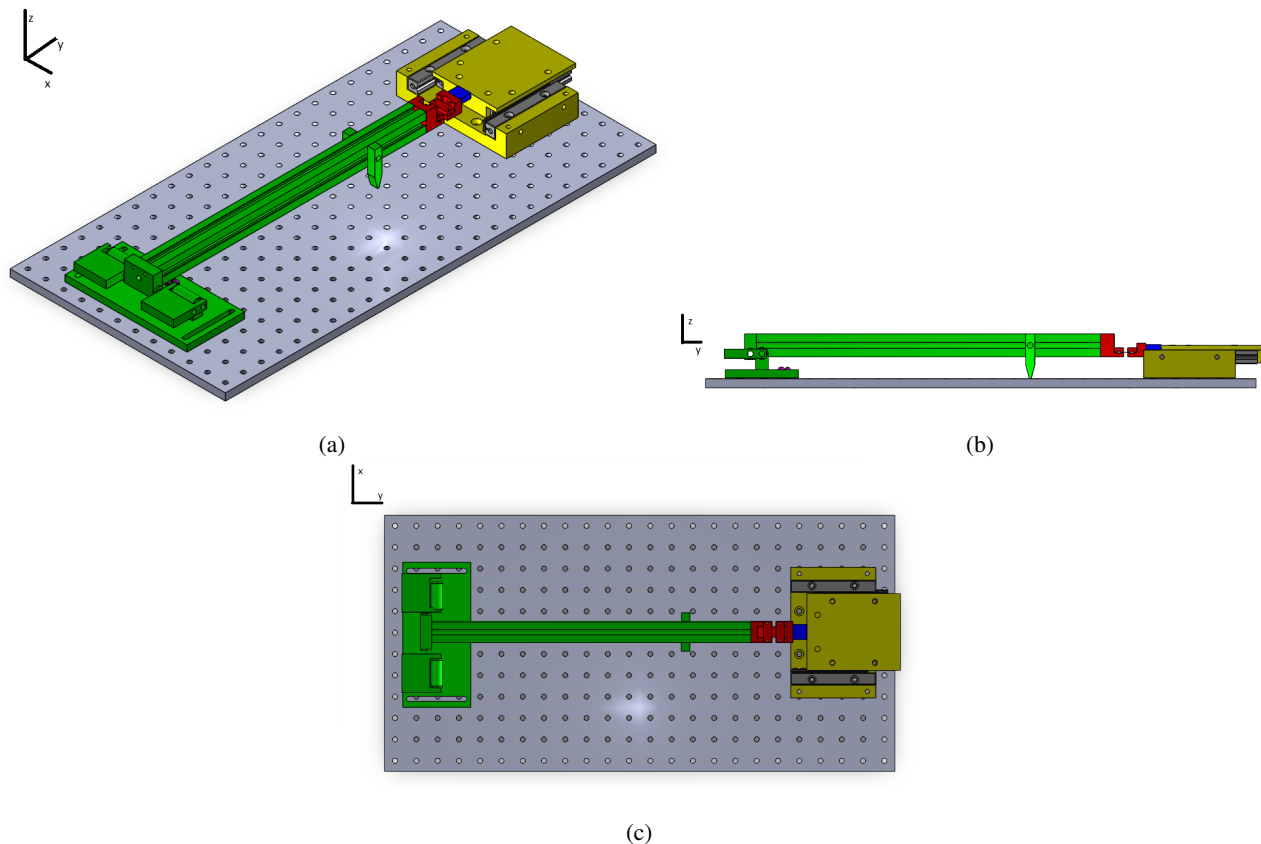


Fig. 1: CAD model of the test setup. The actuation system (green), the kinematic coupling mechanism (purple), the flexural joint (red), the spring mechanism (blue), linear guides (dark gray), and the base plate (yellow).

The preload will be applied uniformly at one side by an adjusting screw, by adding mass on top of the system, and by adjusting only one screw so that the rail is set on a defined angle. These situations will be investigated at three positions on each guide and both longitudinal repeatability and rotational repeatability are measured.

In the second section, the method will be explained. This method is divided into three main subsections. First, the principal design is explained with calculations and simulations. Secondly, the experimental design is described and finally, the measuring procedure is illustrated. In the third section, the results are shown and in the fourth section, we will discuss these results and conclusions. Finally, the fifth section will give a conclusion about the research.

## II. METHOD

In order to investigate the relation between the repeatability and the preload for a linear guide system, a test setup has been designed (Figure 1). This setup should be able to measure the position of the linear guide and there should be a possibility to adjust the applied preload. The external influences should be minimized in order to truly measure the behavior of the linear guide. Therefore, it is essential to know how the parts interact with each other and know their properties, e.g. Young's modulus, stiffness, and dimensions.

There has been chosen to make a position-controlled actuation system to ensure a constant input position of the system. To prescribe this constant input position, a designed end-stop is used. A spring with a known stiffness is placed between this end-stop and the linear guides. The spring acts as a flexible part between the two stiffer mechanisms. The system uses the relation between increased friction (by preload) and flexibility (of the spring) and measures the position change. This change in position is translated to the repeatability.

Figure 2 shows a schematic overview of how the test setup should look like. The system should consist of three parts, the linear guide (red), the spring (gray), and the actuation system with the end-stop (blue).



Fig. 2: Schematic overview of the position-controlled actuation system setup with the linear guide (red), spring (gray), and actuation system with end stop (blue).

The stiffness of the spring should be lower than the stiffness of the actuation system to ensure that the linear guide will not automatically follow the position of the actuation

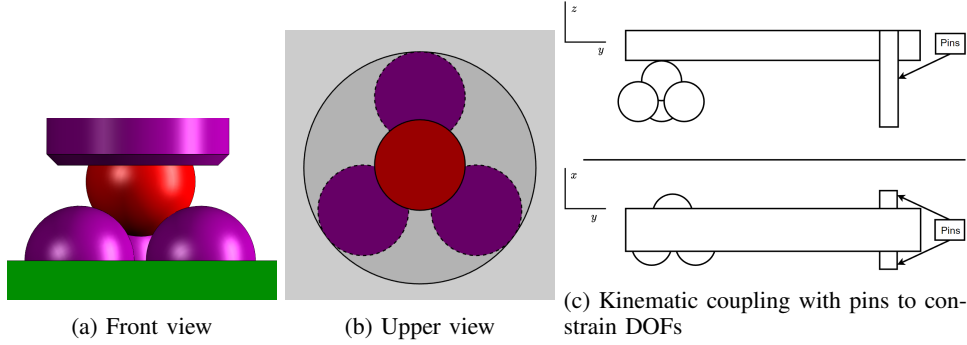


Fig. 3: Kinematic coupling orientation. The bottom three balls are oriented 120 degrees to each other and have a contact angle of 45 degrees with the upper ball. Two additional pins are added at the end of the actuation beam to prevent the beam from rotating around the  $x$ -, and  $y$ -axis.

system. The stiffness of the spring should also not be too low since in that case the position of the actuation system will not have any influence on the linear guide and will only deform the spring. In real-life applications, an actuation mechanism with stiffness of around  $1e5N/m$  and  $1e6N/m$  is used. To simulate that situation in this setup, the same stiffness has been set as a requirement for the spring. In Table I the requirements for the stiffness of the three important part are mentioned. These requirements should be taken into account while designing the test setup.

Part	Stiffness
Linear guide system	$> 1e7N/m$
Spring	$1e5 - 1e6N/m$
Actuation system	$> 1e8N/m$

TABLE I: Stiffness requirements of linear guide, spring, and actuation system.

#### A. Principle Design

In this section, we will discuss the design choices that are made and further elaborate on the aspects of the test setup using some calculations and simulations. The system (Figure 1) consists of five parts. The actuation system, the kinematic coupling mechanism, the flexural joint, the spring mechanism, and the base plate. The actuation system (green part) is in fact a crank slider mechanism that consists of a base plate, two short links, two rotational axes, and one large link. The kinematic coupling mechanism (purple) consists of one ball mounted at the large link of the actuation system and two times three balls at the base plate of the actuation system. The flexural joint (red) has two mounting blocks and a metal strip. For the spring mechanism (blue), a load cell will be used with a given stiffness. The base plate (yellow) consists of a bottom and an upper part to which the linear guides are mounted.

1) *Kinematic coupling mechanism:* For position-controlled systems, it is important that the end position is well-defined. Therefore a kinematic coupling is made that constrains all translational motions. This kinematic coupling mechanism consists of three balls on a plate, oriented 120

degrees to each other, and one ball on top of the three balls Figure 3.

This upper ball makes contact with all three balls with a contact angle of 45 degrees. By realizing this, the load will be equally divided among the balls. Friction forces arise both at the linear guide system when the preload is increased and between the four balls when the balls make contact with each other. To ensure that the ball on top will always make contact with the three other balls, an additional mass is added on top of the actuation beam to overcome these friction forces.

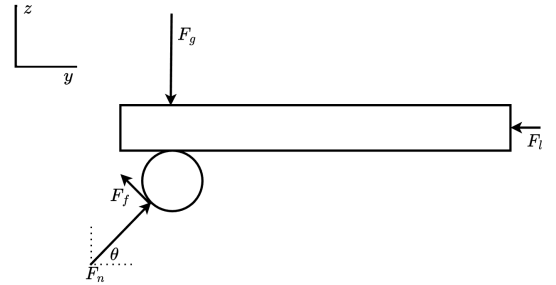


Fig. 4: Forces in kinematic coupling.  $F_g$  gravity force,  $F_l$  force of linear guide,  $F_n$  normal force,  $F_f$  friction force, and  $\theta$  the contact angle

Figure 4 shows the forces that are present when the ball hits one of the balls of the end-stop. The ball should slip, and as a consequence move downwards and touches the other two balls. In Table II, the friction force has been calculated for different gravity forces at different contact angles. Note that the ratio between gravity force and friction force is equal for each contact angle. A ratio of 3.0 (contact angle 45degrees), means that the gravity force should be 3 times larger than the friction force to still allow the upper ball to slip and makes contact with the three balls. A lower ratio means that with a given gravity force a higher friction force can be overcome, which is beneficial for the system. The lowest ratio can be observed at 45 degrees. The gravity force, generated by the additional mass, could be adjusted to match with the friction force. In that way, the right mass can be selected to guarantee that the ball makes contact with all three balls.

		Contact angle ( $\theta$ ) [°]		
		25	45	65
Gravity force ( $F_g$ ) [N]	10	2,1	3,3	3,2
	20	4,2	6,7	6,5
	40	8,4	13,3	13,0
	Ratio	4,8	3,0	3,1

TABLE II: Force of linear guide ( $F_l$ ) for different gravity forces ( $F_g$ ) and contact angles ( $\theta$ ).

To prevent the system from rotating around the x-axis (lateral direction) and y-axis (longitudinal direction) two additional pins are added at the end of the actuation beam (Figure 3c). By adding these constraints the only degree of freedom (DOF) is the rotation around the z-axis (vertical direction).

2) *Actuation system*: The actuation system is similar to a crank slider mechanism. It consists of two parts, one is the actuation link that is connected to the flexural joint and the kinematic coupling mechanism. The other one is the small link that makes the input motion of the system. It is favorable that this second part moves in a sinusoidal motion. This results in a speed in the longitudinal direction of zero meters per second when horizontal. The vibrations in the longitudinal direction will be less due to this concept.

3) *Flexural joint*: To allow the system to make a sinusoidal movement the beam should be able to rotate. Therefore, a flexural joint has been designed that is able to make the required rotation. There has been chosen to use a metal strip that is clamped between two blocks (Figure 5). To ensure that the metal strip is rigidly clamped, two bolts and two nuts connect the two blocks to the flexural joint and make sure the blocks will be in contact with the metal strip. The blocks will exert a force along the whole metal strip to know for sure that the length of the metal strip is as large as the intended length. There is a gap at the place of the bolts so that the forces of the bolts are divided along the surface and do not work only at the place of the bolts. The flexural joint will be connected to the actuation link on one side and to the spring on the other side.

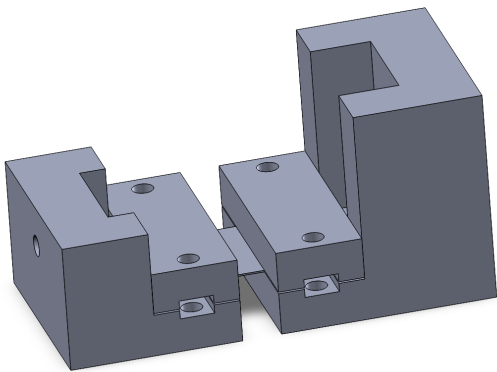


Fig. 5: CAD model of the flexural joint.

This metal strip should not only meet the requirements for stiffness but also buckling and plastic deformation should not

occur. Taking these parameters into account the dimensions of the metal strip could be calculated. The metal strip should have a stiffness of  $1e8N/m$  in the longitudinal direction. This means that the formula for the stiffness of the spring is  $k = AE/L$ . This could be rewritten to calculate the length with a given stiffness (Equation 1) [23].

$$L_s = \frac{w_s h_s E_s}{k_s} \quad (1)$$

In this formula,  $L_s$  is the calculated useful length of the strip,  $w_s$  the width of the strip,  $h_s$  the height of the strip,  $E_s$  the elastic modulus of the strip, and  $k_s$  the stiffness of the strip in the longitudinal direction. The length of the strip is therefore dependent on both the dimensions of the strip and the material choice. To calculate the bending stress on the strip, the bending moment that works on the strip should be calculated using Equation 2 [23].

$$M_s = \frac{\theta E_s I_s}{L_s} \quad (2)$$

In this formula,  $M_s$  is the moment that applies on the strip due to the forced angle and given the calculated dimensions.  $\theta$  is the angle of the actuation link compared to the base plate and is calculated using the arcsin of the length of the actuation link and the length of the short link. The area moment of inertia that is used to calculate the bending moment,  $I_s$ , will be calculated using  $I_s = w_s h_s^3 / 12$ . The calculated moment can be used in Equation 3, to calculate the bending stress [23].

$$\sigma = \frac{6M_s}{w_s h_s^2} \quad (3)$$

$\sigma$  is the bending stress that occurs in the strip due to the moment acting on the strip, given the dimensions of the strip. This bending stress should not exceed the allowable yield stress of the strip, which is defined by the material choice.

The buckling force should also be calculated to verify that it will not be exceeded. The buckling force is calculated using Equation 4 [23].

$$F_{buckling} = \frac{\pi^2 E_s I_s}{4L_s^2} \quad (4)$$

In this formula,  $F_{buckling}$  is the maximum force that could be applied to the strip in the longitudinal direction before the metal strip buckles. This force is generated by the friction of the linear guide system. It is realistic to consider a safety margin since the buckling force will change when the force does not act completely in the longitudinal direction but has a slight offset.

4) *Spring*: Between the flexural joint mechanism shown in Figure 5 and the linear guide system, a spring has been placed. For this spring a load cell has been chosen with the required stiffness. The load cell serves as a substitution for an actuation system in real-life applications of linear guide systems. These systems normally have a stiffness of around  $1e5N/m$  and  $1e6N/m$ , which is therefore the requirement for our load cell.

5) *Base plate*: Two linear guides are mounted on a base plate that is connected to the ground and two are mounted on a moving platform. The base plate has an u-shaped structure with adjustment holes at the side at which the intended preload could be applied. The stiffness of this base plate should be high enough to ensure that deformations caused by the applied preload on the u-shaped structure are minimized. With the maximum intended preload of  $2734N$ , the u-shaped base plate will deform with  $84\mu m$ . In Figure 6, a FEM analysis of the deformations due to the intended preload is illustrated. In this analysis, we assume that the base plate, made of aluminum, is mounted with the three bolts in the middle and will not have contact at other places with the ground. We also assume that the preload is applied uniformly along the rails.

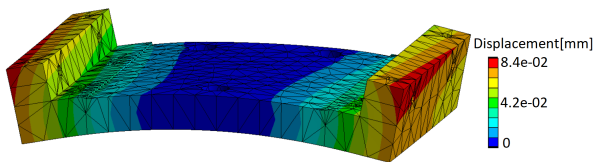


Fig. 6: Deformations base plate with a force of  $2734N$  at each side

Also, the moving platform has two linear guides mounted on it. The structure needs to be able to withstand the forces that will be exerted by the linear guides, and minimize the deformations. In Figure 7, the deformations of the moving platform are shown. In this analysis, we assume that the moving platform, made of aluminum, has a fixed node in the middle of the platform. The preload forces act on both sides of the platform and have a magnitude of  $2734N$ . The calculated stiffness of this part is  $1.77e9N/m$ . The maximum deformation in the x-direction is  $1.5\mu m$ , which is permissible for our measurements.

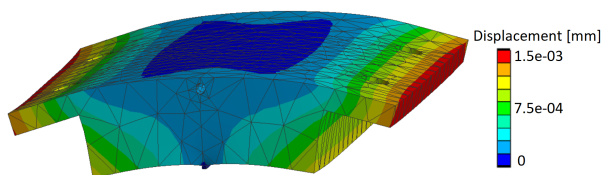


Fig. 7: Deformations moving platform with a force of  $2734N$  at each side

### B. Experimental setup

In this section, the fabrication of the test setup, the material choices that are made, and the chosen measurement tools are discussed. Also, the kinematic coupling mechanism, the actuation system, the flexural joint mechanism, the load cell, and the base plate are highlighted. In Figure 9, the used test setup is shown.

1) *Kinematic coupling mechanism*: As described in the previous section, the kinematic coupling mechanism consists of three balls on a plate, and one ball on top of that. The

balls are made of steel and have a diameter of  $6mm$ . In order to enable the balls to make an angle of  $45$  degrees with each other, a circular box with a diameter of  $14.5mm$  is made. By using a 3D-printed glue tool, the balls are fixed at the right position and could be glued with epoxy. The ball on top is glued to a bolt, which is connected to the actuation link.

2) *Actuation system*: For the actuation beam, as described in the previous section, the aluminum THOR-labs profile XE25 with a length of  $300mm$  has been used. The calculated stiffness of this profile is  $6.9e8N/m$ , which meets the requirements given in Table I. The smaller link, which makes the sinusoidal movement, is made of carbon-reinforced PLA to achieve a higher stiffness (Figure 8). An aluminum  $6mm$  round bar is used that rotates in six slide bearings. These are used to allow the system to make a smooth rotation but still have some play. This play is essential since the kinematic coupling mechanism should prescribe the position and the actuation system should follow this. The base plate of the actuation system has two rectangular-shaped holes to mount the plate at different places on the breadboard.

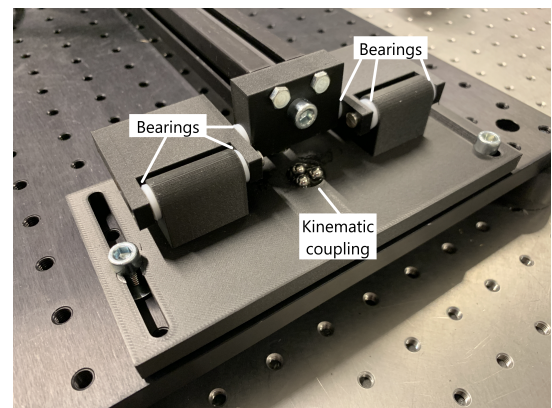
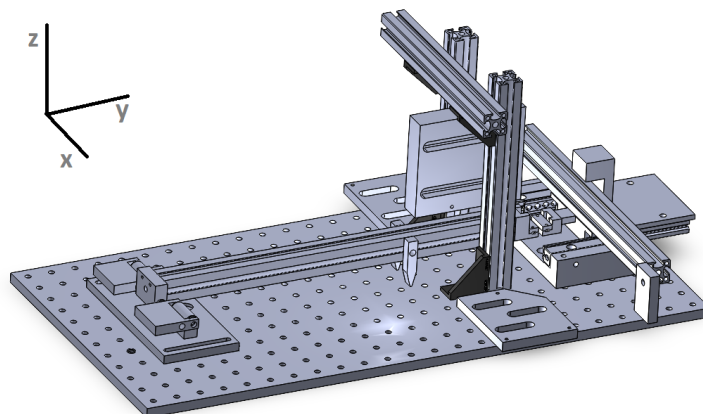


Fig. 8: Actuation mechanism with six slide bearings (white), kinematic coupling (balls), and links (black).

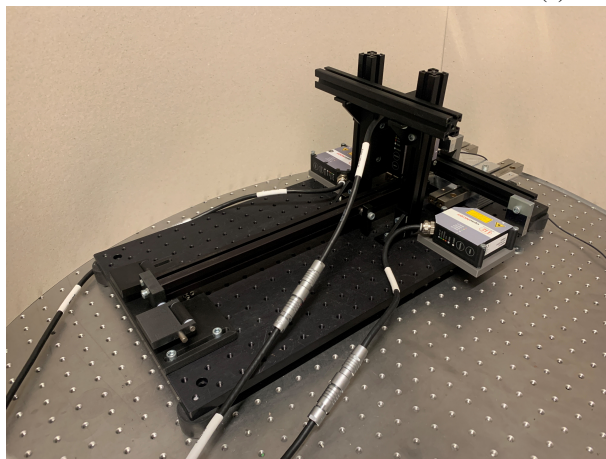
The upper ball of the kinematic coupling mechanism is connected to a bolt that is mounted on the actuation beam. On top of the actuation beam, a mass of  $2kg$  is added as described before. Additional play between the parts is introduced to allow the system to move freely to the position in which it makes contact with the three other balls.

3) *Flexural joint*: The housing of the flexural joint mechanism is made of carbon-reinforced PLA. The metal strip, made of spring steel, has been laser cut with a length, width, and height of  $34.5mm$ ,  $12.5mm$ , and  $0.2mm$  respectively. The effective length of the metal strip is  $4.5mm$  and is, together with the width and height, calculated by Equation 1. The required rotation of the metal strip is  $4.8$  degrees, determined by the ratio of the actuation link and the small link. This rotation does not lead to plastic deformation (factor of almost 3), nor buckling (factor of almost 15) as calculated in Equation 3 and Equation 4. In order to guarantee the right effective length of the metal strip, so-called 'measurement blocks' are clamped between the blocks as a reference during

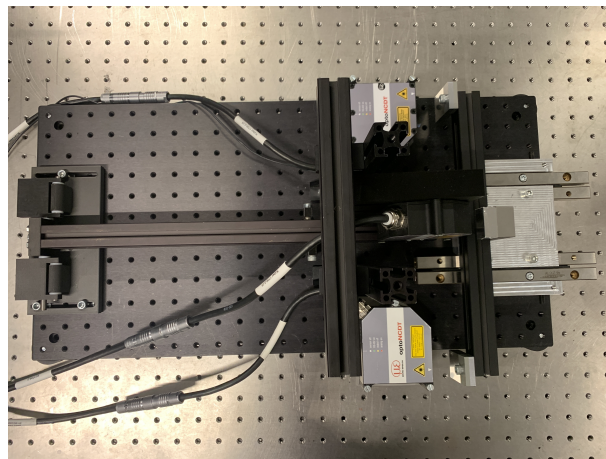




(a) CAD model



(b) Experimental setup: ISO view



(c) Experimental setup: Upper view

Fig. 9: Test setup. Setup is built on a Thorlabs breadboard that is placed on a Nexus Optical Table (T1020CK). Three optoNCDT 1750-2 lasers were used to measure the position and FUTEK model LSB200 miniature s-beam Jr. load cell (FSH03876) as a spring. Lasers and load cell connected to myDAQ and processed in Labview.

assembly (Figure 10). The two blocks are mounted with m3 bolts and nuts.

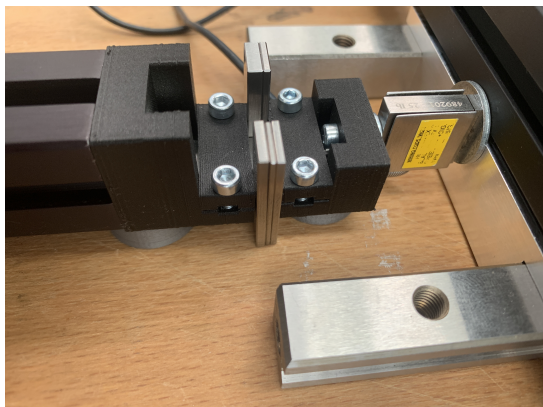


Fig. 10: Reference tool for flexural joint and load cell

4) *Spring*: The load cell that will be used is the FUTEK model LSB200 miniature s-beam Jr. load cell (FSH03876)

[24]. This load cell has a maximum capacity of  $111N$ , a natural frequency of  $2770Hz$ , and stiffness of  $1.09e6N/m$ . This stiffness has been calculated by dividing the maximum force by the deflection and matches with the stiffness requirement given in Table I. The load cell is calibrated and configured to a domain of  $0 - 25N$ . This will increase the resolution of the load cell from  $0.111N$  to  $0.025N$ .

5) *Base plate*: The base plate is made of aluminum and is mounted with three M6 bolts to a Thorlabs breadboard. Three locking rings are placed between the base plate and the breadboard to ensure that the base plate only has three contact points with the ground. The profile of aluminum has been made with the CNC machine using tolerances of  $0.1mm$ . Linear guides are mounted on the base plate with two m5 bolts, while the linear guides on the top plate are connected with m6 bolts. The technique of using m6 bolts is preferred since more powerful fastening is possible due to the larger screw size [19]. However, due to physical space, the linear guides on the base plate could not be mounted by the m6 bolts, so the option of m5 bolts has been chosen.

6) *Position measurement lasers*: For measuring the position three distance measurement lasers are used. The used lasers are the optoNCDT 1750-2 [25]. This laser has a measuring range of  $2mm$  at a distance of  $24 - 26mm$  from the laser itself. It has an analog output value between  $4mA$  and  $20mA$ , leading to an output resolution of  $0.50\mu m$ . Figure 11 shows the used laser. Note that this laser is now in the measuring range which can be seen by the green light. The laser points at an aluminum taped block which acts as a mirror for the laser. The laser is mounted on a 3d-printed block with a rectangular-shaped hole in the middle to mount it at different places.

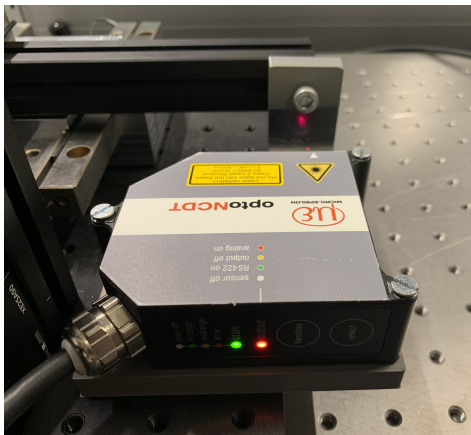


Fig. 11: OptoNCDT 1750-2 [25] laser position system. Green light indicates that the laser is in range.

In Figure 12, the configuration of the lasers is shown. The laser in the middle (laser 2), together with the weighted average of lasers 1 and 3, will be used to get the repeatability in the longitudinal direction. The rotational repeatability is obtained by the average of the angle  $\alpha$  and  $\beta$ , which is the angle between laser 2 and respectively laser 1 and laser 3.

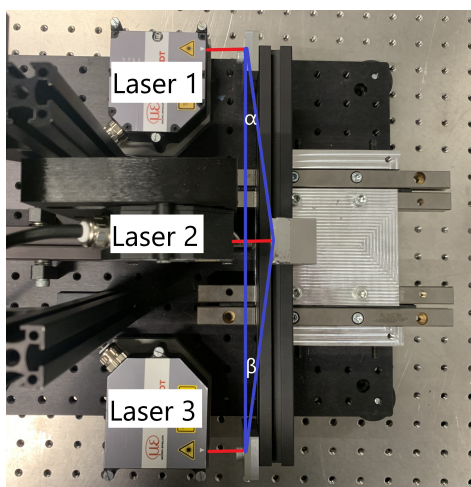


Fig. 12: Configuration lasers. Laser 2 together with the weighted average of laser 1 and 3 for longitudinal repeatability. The average of the angle  $\alpha$  and  $\beta$  for the rotational repeatability.

### C. Measuring procedure

Measurements will be done in the optics lab of the TU Delft. In this room, the temperature is constantly controlled at 20 degrees. The test setup is placed on the Nexus Optical Table (T1020CK) to eliminate vibrations of the surrounding.

All measurements start at the same position, namely at the rear end-stop. The link will be manually rotated ( $\Delta\theta = 180$ ) to the front end-stop and should make contact with that end-stop after 5 seconds. Now it will rest there for another 5 seconds, after which the link will again be manually rotated ( $\Delta\theta = -180$ ) to the rear end-stop. This step will also last 5 seconds. Again at this stage, the system will rest for 5 seconds and a data point is collected. After this step, the process starts over and will be repeated 10 times leading to a total time of 3min and 20 seconds (200 seconds) for one experiment. In Figure 14, the process flow chart is illustrated. A total of 18 experiments are performed in this way for this research (two types of linear guide rails, three different positions, and three different situations).

1) *Type of rail*: The two types of rails are the ball cage linear guide and the cross roller linear guide. The former guide has 16 balls and a maximum load capacity of  $1690N$ . The latter has 16 rollers and a maximum load capacity of  $3651N$ . From theory, we could say that the rollers deform less compared to the balls, withstand more load, and have a higher stiffness [17].

2) *Different position*: The position of the measurement could influence the performance of the rails. Since the moved distance is  $25mm$  each time, the data collected is only about a small piece of the rails. Measuring at three positions allows us to say something about the repeatability at three different locations. The position on the rails could be of interest since the rails stick out partly in some positions and therefore the load is not divided equally along the balls and rollers. There have been chosen to perform experiments from  $0 - 25mm$ ,  $25 - 50mm$ , and  $50 - 75mm$ . Zero represents the position in which both rails are positioned in one line. In Figure 13, the three orientations of the rails are displayed. Note that for illustration purposes the rails are placed at different heights from each other, while in real life this distance between the rails is the same for every position.

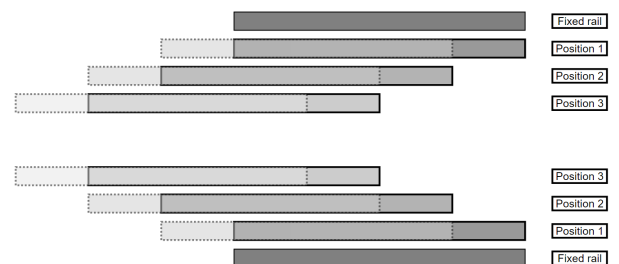
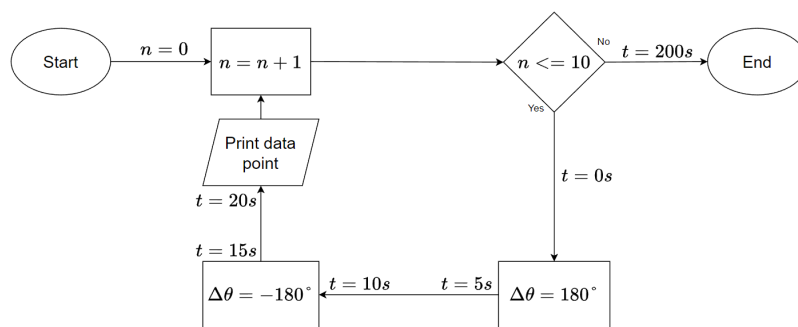
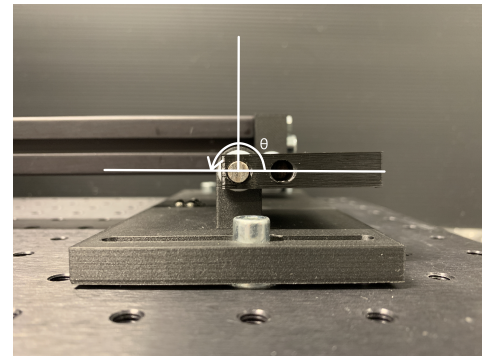


Fig. 13: Three positions of rails. Position 1:  $0 - 25mm$ , position 2:  $25 - 50mm$ , and position 3:  $50 - 75mm$ .



(a) Flow chart



(b) Actuation mechanism

Fig. 14: Measuring procedure. The process starts at  $n=0$  and will be repeated till  $n=10$ . It starts with a rotation of  $-180^\circ$ , which will take 5sec till it reaches the front end-stop. After 5 seconds of standstill, it is rotated  $180^\circ$  back to the rear end-stop. A data point is collected and the process starts over. After 200 seconds the experiment ends.

3) *Different situations*: Preload is exerted in two different manners. In the first and second situations by a position change and in the third situation by adding mass. By exerting the preload as a position change we could assume that the preload exerted on the linear guides is the same in every repetition. In order to measure the position change more easily, the rotation of an adjustment screw is measured instead of the horizontal displacement. This preload will be exerted by a wrench with a dial attached to it.

In the first situation, the preload is applied uniformly along the rails. The applied preload is expressed in the degrees of the dial (0, 10, 20, 30, 40 degrees). This preload will always first be exerted on the left screw and secondly on the right screw. For measurements at position 1, this is done while the system is at the rear end-stop. Due to the construction, it was not possible to do this as well for the second and third positions. Therefore, the preload in this situation is exerted while the system is at the front end-stop.

In the second situation, preload is only applied on the front screw while the rear screw is kept at the neutral position in which it makes contact with the rail but does not exert additional preload. Also in this situation, the preload will be varied by the angle of the wrench. This angle will be divided into 4 steps (0, 10, 20, 30 degrees). This situation is called angular applied preload.

In the third situation, additional mass is added to apply preload on the rails. The rails have one uniform preload while the mass varies between  $0kg$  and  $5kg$  with steps of  $1kg$ . This situation is called external applied preload.

### III. RESULTS

The results section is divided into the following subsections: A) results of uniform applied preload, B) results of angular applied preload, C) results of externally applied preload. These subsections refer to the three different situations as mentioned in section II. For each situation, the two types of rails and the three identified positions are investigated. Both the repeatability in the longitudinal direction and the repeatability of the rotation about the z-axis

are shown. The data shown is the 80% standard deviation of the data that is achieved during the measurements.

#### A. Results uniform applied preload

In Figure 15a, the longitudinal repeatability is plotted against the uniform applied preload. The preload is defined as the rotation of the adjustment screws. This rotation, measured in degrees, will result in a horizontal displacement of the screw. The measurement is performed for 5 rotations of the adjustment screw,  $0^\circ$ ,  $10^\circ$ ,  $20^\circ$ ,  $30^\circ$ , and  $40^\circ$  resulting in a displacement of respectively  $0mm$ ,  $0.03mm$ ,  $0.06mm$ ,  $0.08mm$ ,  $0.11mm$ . The lines represent the combination between the type of rail (R1=ball cage and R2=roller cage) and the position (P1=0 – 25mm, P2=25 – 50mm, P3=50 – 75mm).

Figure 15c shows the repeatability of the rotation about the z-axis with a uniform applied preload. The repeatability is the difference in the angle of the linear guide stage relative to the lasers. The results are the same combination of rail and position as in the longitudinal repeatability case.

In Figure 15b and Figure 15d, the results of the different positions are combined for the ball and the roller guide. Figure 15b shows the results of the longitudinal repeatability and Figure 15d shows the results for the rotational repeatability.

#### B. Results angular applied preload

In Figure 16a, the longitudinal repeatability is plotted against the angular applied preload. The preload is applied at the front adjustment screw and is defined as the angle of rotation of this screw. The measurements are performed for 4 rotations of the adjustment screw,  $0^\circ$ ,  $10^\circ$ ,  $20^\circ$ , and  $30^\circ$  resulting in a calculated angle of the linear guide of respectively  $0^\circ$ ,  $0.0286^\circ$ ,  $0.0573^\circ$ , and  $0.0764^\circ$ . The lines represent the combination between the type of rail (R1=ball cage and R2=roller cage) and the position (P1=0 – 25mm, P2=25 – 50mm, P3=50 – 75mm).

Figure 16c shows the relation between the repeatability of the rotation about the z-axis and the applied angular preload. The results are the same combination of rail and position as in the longitudinal repeatability case (Figure 16a).

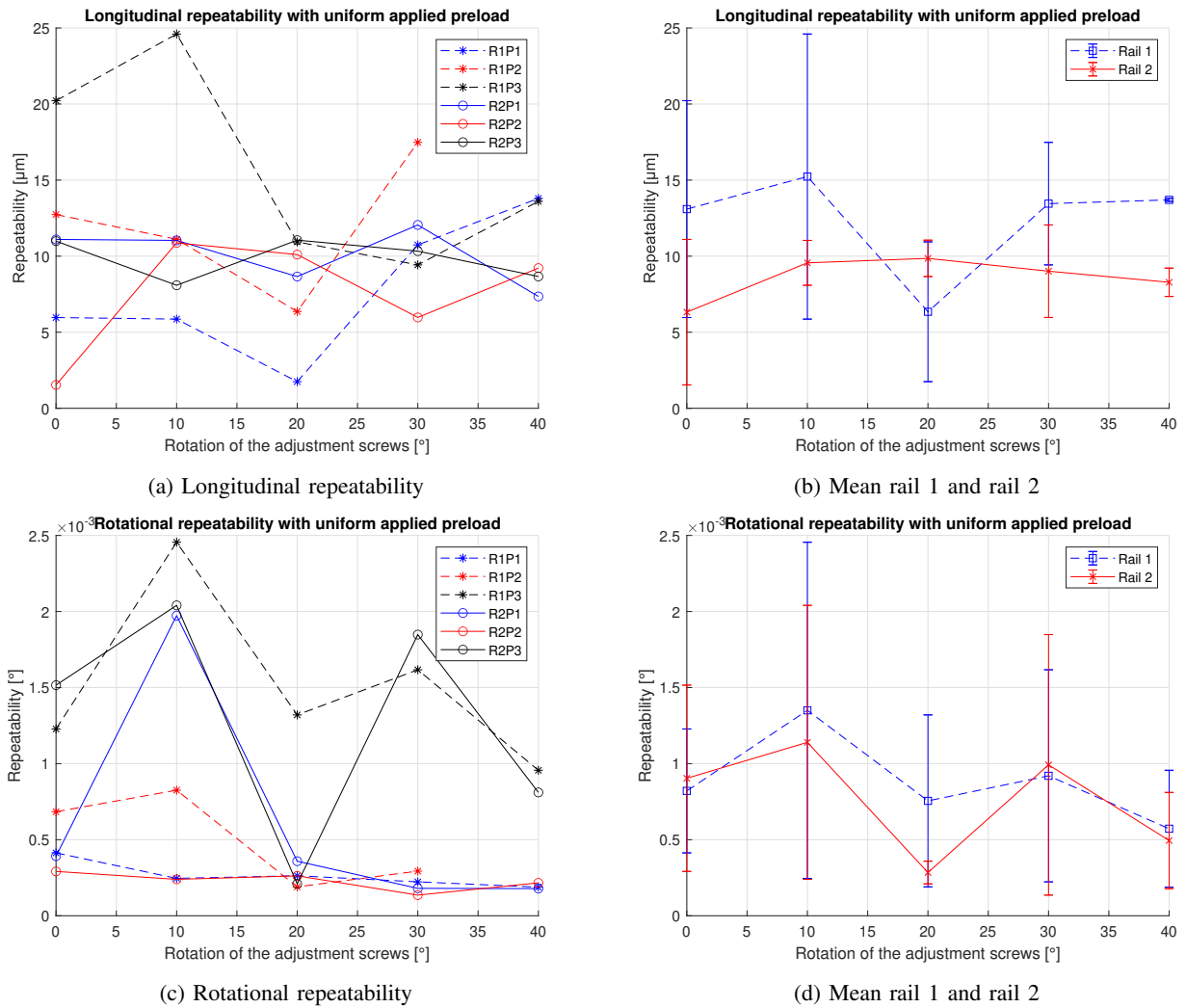


Fig. 15: Uniform applied preload: a,b) Longitudinal repeatability, c,d) Rotational repeatability. The lines represent the combination between the type of rail (R1=ball cage and R2=roller cage) and the position (P1= 0 – 25mm, P2=25 – 50mm, P3=50 – 75mm). b,d) Mean of different positions for the ball guide (rail 1) and roller guide (rail 2). Note that some results are missing since they could not have been measured.

In Figure 16b and Figure 16d, the results of the different positions are combined for the ball and the roller guide. Figure 15b shows the results of the longitudinal repeatability and Figure 15d shows the results for the rotational repeatability.

### C. Results external applied preload

In Figure 17a, the longitudinal repeatability is plotted against the externally applied preload. The externally applied preload is expressed in kilograms, varying from 0kg to 5kg with steps of 1kg. The lines represent the combination between the type of rail (R1=ball cage and R2=roller cage) and the position (P1= 0 – 25mm, P2=25 – 50mm, P3=50 – 75mm).

Figure 17b, shows the mean of the longitudinal repeatability for both the ball and roller guide. This mean is determined by the three positions for one rail type.

In Figure 17c, the relation between the rotational repeatability and the externally applied preload is plotted. The

externally applied preload also varies from 0kg to 5kg with steps of 1kg. The lines represent again the combination between the type of rail and the position.

Figure 17d, shows the mean of the three positions of the rotational repeatability for both the ball and the roller guide.

## IV. DISCUSSION

The results achieved in the experiments, illustrated in section III will be discussed here, together with remarks on the interpretation of the results and recommendations for future work.

### A. Results uniform applied preload

For the ball guide, the longitudinal repeatability has better results (50% lower repeatability) at the point the adjustment screw is rotated 20 degrees. At that point, the backlash in the rails is minimized and slip does not result in higher repeatability. After that optimal point, the slip does play a

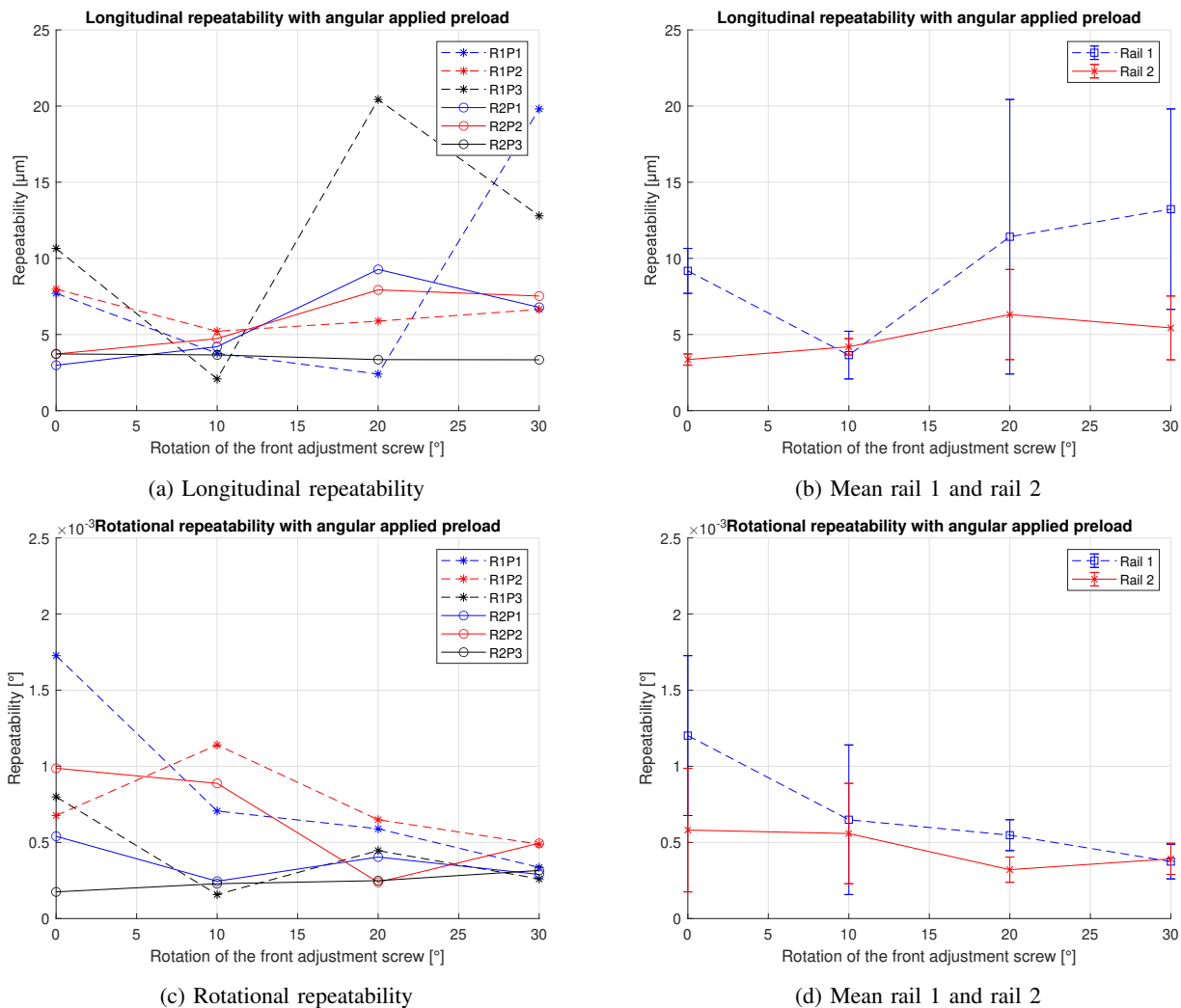


Fig. 16: Angular applied preload: a,b) Longitudinal repeatability, c,d) Rotational repeatability. The lines represent the combination between the type of rail (R1=ball cage and R2=roller cage) and the position (P1= 0 – 25mm, P2=25 – 50mm, P3=50 – 75mm). b,d) Mean of different positions for ball guide (rail 1) and roller guide (rail 2).

role and the repeatability increases. For the roller guide, the longitudinal repeatability slowly decreases with an increase in the uniform applied preload (around 10% per 10° rotation). Backlash in the rails slowly minimizes and due to the shape of the rollers slip does not play a significant role. It could be possible that the optimum point is achieved at an even higher preload. The spread of the ball guide is almost a factor of 2 larger compared to the roller guide. For most of the rotations, the longitudinal repeatability of the roller guide is better than the longitudinal repeatability of the ball guide, with the exception of a rotation of 20 degrees.

The rotational repeatability improves as the uniform applied preload increases (around 50% lower repeatability). This can be seen for both the ball and the roller guide. For positions 1 and 2 this is clearly visible. The backlash decreases as the preload increases which reduces the possibility to rotate. However, position 3 shows other behavior, this is due to the failure of the upper ball to make contact

with the end stop after a rotation of more than 20 degrees of the adjustment screws. Therefore, we could not guarantee a constant input position, resulting in different outputs.

### B. Results angular applied preload

In general, the longitudinal repeatability increases as the rotation of the adjustment screw increases (around 25% higher repeatability). This is a result of the increased stress and deformations due to the misalignment between the rails. For the ball guide, we could see this behavior with an exception for the rotation of 10 degrees (50 % lower repeatability). This could suggest that the rail was not completely parallel at the initial rotation and became more parallel with a rotation of 10 degrees. For the roller guide, the repeatability only slowly increases as the rotation of the adjustment screw increases, suggesting that the roller guide is less sensitive to misalignment in the system. The spread in repeatability for the ball guide is almost a factor of 3 larger than for the roller guide, and the average of the three positions of the

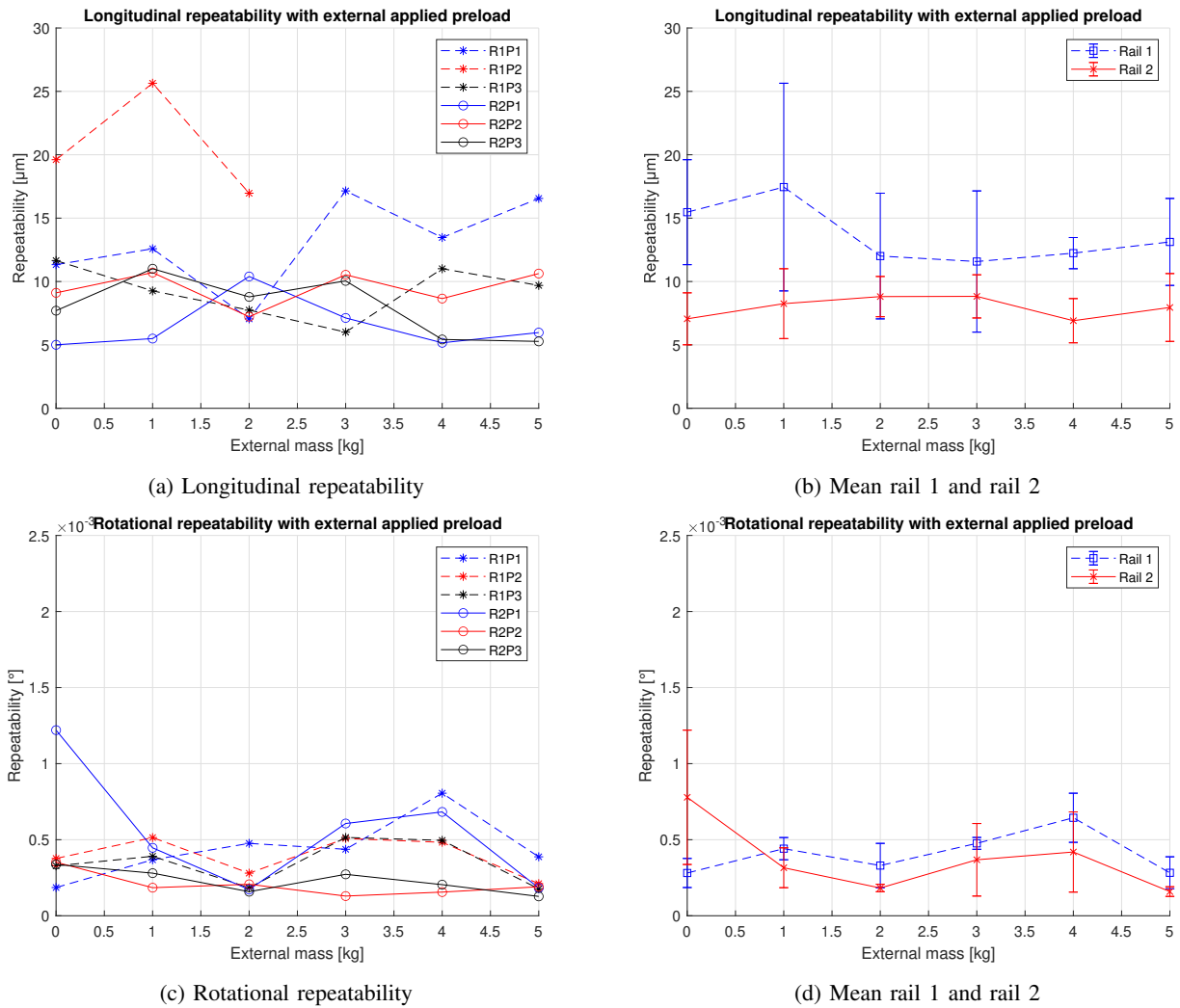


Fig. 17: External applied preload: a,b) Longitudinal repeatability, c,d) Rotational repeatability. The lines represent the combination between the type of rail (R1=ball cage and R2=roller cage) and the position (P1= 0 – 25mm, P2=25 – 50mm, P3=50 – 75mm). b,d) Mean of different positions for ball guide (rail 1) and roller guide (rail 2). Note that some results are missing since they could not have been measured.

roller guide is almost at all times smaller than the average of the ball guide.

The rotational repeatability decreases as the rotation of the adjustment screw increases (around 50% lower repeatability). This behavior can be seen for both the ball and the roller guide. The backlash for both rails decreases with an increase in preload. The possibility to rotate decreases, resulting in a lower repeatability. Especially for R1P3 and R2P3, the rotational repeatability is low compared to the other situations. This is due to the fact that at the third position the change of the angle causes the largest displacement resulting in a larger decrease of the backlash. The average of the three positions of the roller guide is a factor of 2 lower than the average of the ball guide at almost all rotations. The spread of both rails is almost the same magnitude.

### C. Results external applied preload

More externally applied preload does not lead to improvements in the longitudinal repeatability for both the ball and the roller guide. Some fluctuation in performances can be seen but the lines are almost constant at all times. The mean of the roller guide is around a factor of 2 lower than the mean of the ball guide, and the spread of the roller guide is also smaller than the spread of the ball guide.

The rotational repeatability moves slightly up and down. In general, it stays constant for both the ball and the roller guide. The mean of the roller guide is at almost all external loads lower than the mean of the ball guide, although the differences are small in this situation.

### D. General and future work

Looking at the three situations the performances of the ball guide and roller guide differs.

Results of the cross roller guides have a smaller spread at different positions than ball guides (around a factor of 2). Also, the mean of the different positions of the roller guide is generally lower than the mean of the ball guide, suggesting that the performances of the roller guide are better than those of the ball guide. This can be caused since balls are more sensitive to larger deformations. Rollers deform uniformly along the length and therefore only have a larger contact area. The balls deform in a way that the contact point became a line contact at which one point moves one way and the other point in the opposite direction, resulting in slip.

The absolute values of the mean of the ball guide for the longitudinal repeatability at the initial position are between  $9\mu m$  and  $16\mu m$ . For the roller guide this differs between  $4\mu m$  and  $7\mu m$ . This deviation of respectively  $7\mu m$  and  $3\mu m$  could be caused by assembly differences. The rails could have been assembled with a slight angle and the cages that are used were not always exactly at the same position in the rails, which could lead to differences in performances.

Some results are missing in the shown data. This is due to the fact that in some situations it was not possible to get accurate data. The ball connected to the actuation beam could not make contact with the three balls of the kinematic coupling and therefore a constant input position could not be realized. The ratio between friction force and gravity force was not met and as a result, the ball does not slip to the position in which it makes contact with the three balls of the kinematic coupling.

The optimal amount of preload for the best repeatability differs for every situation and could be different when measuring the same situation again. This could be caused by several things like the wear of the bearings, contamination, way of assembling, and drift of the PLA. Therefore, these results should be considered as qualitative results instead of quantitative. Also note that the results depend on the total system, which includes the spring that is used, the end stop, the flexural joint, the actuation beam, and the bearings. Nevertheless, the shape of the graphs would be the same, since it will influence all the measurements. During the measurements, drift occurs in the system which could be caused by the elastic effects of the rollers and balls. By looking at the same moment in time for every measurement, the effect of the drift is minimized in the results.

Note that these results are only valid for these two types of linear guides. To draw a conclusion about the relation between repeatability and preload for different types of linear guides more research should be done to also test these guides. Furthermore, higher load quantities could be used to see if the behavior will keep the same and at what point it will no longer be functional. Besides that, one should try to increase the preload even further. Especially for the roller guide, to see whether a better optimum could be found.

## V. CONCLUSION

The objective of this paper is to investigate the relation between preload and repeatability for both the cross roller guide and the ball guide by performing experimental tests.

Therefore, a method to investigate this relation is proposed. There is found that for the ball guide, the longitudinal repeatability has an optimal point for uniform applied preload. The longitudinal repeatability for the roller guide slowly decreases with the uniform applied preload. Applying angular preload increases the longitudinal repeatability of the roller guide. For the ball guide, better repeatability could be seen at a rotation of 10 degrees of the adjustment screw. The longitudinal repeatability stays constant with the external preload for both rails. Rotational repeatability decreases with both uniform and angular applied preload and remains constant with external preload.

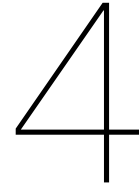
Both the longitudinal and rotational repeatability of the roller guide are generally lower than the ball guides. Also, the spread of the measurement for the roller guide is smaller compared to the ball guide. Furthermore, ball guides are more sensitive to misalignment of the rails than roller guides.

Knowledge about the performances of these two types of guides together with the influence of preload on the performances can be used by companies to help them select the right linear guide for their application. The performances of current high precision machines can be further increased and new machines could be designed with the right type and amount of preload.

## REFERENCES

- [1] X. Y. Wang, H. T. Feng, C. G. Zhou, and K. Q. Ye, "A thermal model for real-time temperature forecast of rolling linear guide considering loading working conditions," *International Journal of Advanced Manufacturing Technology*, vol. 109, no. 7-8, pp. 2249–2271, 2020.
- [2] Z. T. Abdullah, G. S. Sheng, and S. B. Yun, "Conventional Milling Machine into CNC Machine Tool Remanufacturing, Eco-comparison Ratio Based Analysis," *Current Journal of Applied Science and Technology*, vol. 28, no. 6, pp. 1–18, 2018.
- [3] W. Kwintarini, A. Wibowo, B. M. Arthaya, and Y. Y. Martawirya, "Modeling of Geometric Error in Linear Guide Way to Improved the vertical three-axis CNC Milling machine's accuracy," *IOP Conference Series: Materials Science and Engineering*, vol. 319, no. 1, pp. 0–6, 2018.
- [4] M. Figl, C. Ede, J. Hummel, F. Wanschitz, R. Ewers, H. Bergmann, and W. Birkfellner, "A fully automated calibration method for an optical see-through head-mounted operating microscope with variable zoom and focus," *IEEE Transactions on Medical Imaging*, vol. 24, no. 11, pp. 1492–1499, 2005.
- [5] H. Sadeghian, B. Dekker, R. Herfst, J. Winters, A. Eigenraam, R. Rijnbeek, and N. Nulkes, "Demonstration of parallel scanning probe microscope for high throughput metrology and inspection," *Metrology, Inspection, and Process Control for Microlithography XXIX*, vol. 9424, no. March 2015, p. 942400, 2015.
- [6] D. Y. Lee, D. M. Kim, D. G. Gweon, and J. Park, "A calibrated atomic force microscope using an orthogonal scanner and a calibrated laser interferometer," *Applied Surface Science*, vol. 253, no. 8, pp. 3945–3951, 2007.
- [7] D. S. Biggs, "A Practical Guide to Deconvolution of Fluorescence Microscope Imagery," *Microscopy Today*, vol. 18, no. 1, pp. 10–14, 2010.
- [8] L. G. Marques, R. A. Williams, and W. Zhou, "A mobile 3D printer for cooperative 3D printing," *Solid Freeform Fabrication 2017: Proceedings of the 28th Annual International Solid Freeform Fabrication Symposium - An Additive Manufacturing Conference, SFF 2017*, pp. 1645–1660, 2020.
- [9] C. T. Hsieh, "Investigation of Delta Robot 3D Printer for a Good Quality of Printing," *Applied Mechanics and Materials*, vol. 870, pp. 164–169, 2017.
- [10] C. Cajal, J. Santolaria, J. Velazquez, S. Aguado, and J. Albajez, "Volumetric error compensation technique for 3D printers," *Procedia Engineering*, vol. 63, pp. 642–649, 2013. [Online]. Available: <http://dx.doi.org/10.1016/j.proeng.2013.08.276>
- [11] H. H. Huang and J. Wey, "Research on the high-speed pick and place device for die bonders," *2010 8th IEEE International Conference on Control and Automation, ICCA 2010*, pp. 1683–1687, 2010.
- [12] S. Briot and I. A. Bonev, "Pantopteron-4: A new 3T1R decoupled parallel manipulator for pick-and-place applications," *Mechanism and Machine Theory*, vol. 45, no. 5, pp. 707–721, 2010. [Online]. Available: <http://dx.doi.org/10.1016/j.mechmachtheory.2009.07.007>
- [13] E. Amann, "Modeling and motion control of a pick and place machine with air bearings," 2012.
- [14] K. McCarthy, "Accuracy in positioning systems," *Proc. The Motion Control Technology Conf*, 1991. [Online]. Available: <http://fp.optics.arizona.edu/optomech/studentreports/2007/JasonRuhl.doc>
- [15] H. He, M. F. Dyck, R. Horton, M. Li, H. Jin, and B. Si, "Chapter five - distributed temperature sensing for soil physical measurements and its similarity to heat pulse method," ser. *Advances in Agronomy*, D. L. Sparks, Ed. Academic Press, 2018, vol. 148, pp. 173–230. [Online]. Available: <https://www.sciencedirect.com/science/article/pii/S0065211317300883>
- [16] T. Groothuijsen, D. Laro, and T. Ruijl, "Recirculating linear ball bearings and their effect on the accuracy of positioning systems," *European Society for Precision Engineering and Nanotechnology, Conference Proceedings - 19th International Conference and Exhibition, EUSPEN 2019*, no. June, pp. 142–145, 2019.
- [17] G. He, P. Shi, L. Guo, and B. Ding, "A linear model for the machine tool assembly error prediction considering roller guide error and gravity-induced deformation," *Proceedings of the Institution of Mechanical Engineers, Part C: Journal of Mechanical Engineering Science*, vol. 234, no. 15, pp. 2939–2950, 2020.
- [18] D.-H. Cho, H.-C. Kwon, and K.-H. Kim, "Improvement of position repeatability of a linear stage with yaw minimization," *Applied Sciences*, vol. 12, no. 2, 2022. [Online]. Available: <https://www.mdpi.com/2076-3417/12/2/657>
- [19] Schneeberger, "Linear Bearings - Product Catalog," 2021. [Online]. Available: <https://www.schneeberger.com/en/products/linear-bearings-linear-roller-guideways/recirculating-unit-with-long-stroke/recirculating-unit-with-ball/recirculating-unit-with-ball-type-sk/#downloadscatalogue>
- [20] A. Gunduz, J. T. Dreyer, and R. Singh, "Effect of bearing preloads on the modal characteristics of a shaft-bearing assembly: Experiments on double row angular contact ball bearings," *Mechanical Systems and Signal Processing*, vol. 31, pp. 176–195, 2012.
- [21] P. Pawełko, S. Berczyński, and Z. Grzadziel, "Modeling roller guides with preload," *Archives of Civil and Mechanical Engineering*, vol. 14, no. 4, pp. 691–699, 2014.
- [22] T. J. Royston and I. Basdogan, "Vibration transmission through self-aligning (spherical) rolling element bearings: Theory and experiment," *Journal of Sound and Vibration*, vol. 215, no. 5, pp. 997–1014, 1998.
- [23] Mikrocentrum. *Werktuigbouw.nl formuleboekje*. [Online]. Available: <https://www.werktuigbouw.nl/book/formuleboekje.htm>
- [24] F. A. S. Technology. *Miniature s-beam jr. load cell*. [Online]. Available: <https://www.futek.com/store/legacy-sensors-and-instruments/miniature-s-beam-LSB200/FSH03876>
- [25] M. Epsilon. *Operating instructions optoncdt 1750*. [Online]. Available: <https://www.micro-epsilon.com/download/manuals/man--optoNCDT-1750--en.pdf>





## Discussion

The performances of high precision machines are dependent on a lot of variables. One of the variables that has an influence on the repeatability of such systems is the amount of preload that is applied to it. In this thesis, two linear guide systems (non-recirculating ball guide and the non-recirculating cross roller guide) are chosen and the relation with the preload is investigated. Three preload cases (uniform, angular, external) at three positions (0-25mm, 25-50mm, and 50-75mm) are investigated and both longitudinal repeatability and rotational repeatability are measured.

For the ball guide, the longitudinal repeatability has an optimal point for uniform applied preload. This is at a rotation of 20 degrees of the adjustment screws and a lower repeatability of 50%. At that point, the backlash in the rails is minimized and slip does not result in higher repeatability. After that optimal point, the slip does play a role and the repeatability increases. For the roller guide, the longitudinal repeatability slowly decreases while the uniform applied preload increases (around 10% per 10° rotation). Backlash in the rails slowly minimizes and due to the shape of the rollers slip does not play a significant role. The longitudinal repeatability increases with angular applied preload for both rails due to the increased misalignment (around 25% higher repeatability). The parallelism decreases and as a consequence, the balls and rollers slightly deform. For the ball guide, an exception could be seen at a rotation of 10 degrees of the adjustment screw (50 % lower repeatability). From further experiments, we can conclude that at this point the rail was more parallel resulting in better repeatability (section B.5). The longitudinal repeatability stays constant with the external preload, since the added mass does not lead to a significant change in preload.

Rotational repeatability decreases with both uniform and angular applied preload since the backlash in both situations decreases with an increase in preload (around 50% lower repeatability). The possibility to rotate decreases, resulting in a lower repeatability. The rotational repeatability remains constant with external preload, since the additional mass also does not lead to a significant change in preload.

The results of the cross roller guides have a smaller spread at different positions than the ball guides (around a factor of 2). Also, the mean of the roller guide is almost everywhere lower than the mean of the ball guide, suggesting that the performances of the roller guide are better than those of the ball guide. This can be caused since balls are more sensitive to larger deformations. Rollers deform uniformly along the length and therefore only have a larger contact area while the balls deform in a way that the contact point became a line contact at which one point moves one way and the other point in the opposite direction, resulting in slip.

Besides the better performances of cross roller guides, they are also often more expensive than ball linear guides. When selecting the type of linear guides this should also be considered and a trade-off between price and performance based on the application should be made.

The setup does not have contact with the end stop in all situations that are evaluated. Due to the increased friction inside the linear guide system the kinematic coupling was not able to overcome this and could not slip to the position in which it has three contact points. Therefore the position was not fully defined resulting in missing data points. Additional mass could be added to increase the gravity force and more space in the actuation system could be made to allow the system to move more freely.

A different initial starting value can be observed for the three preload cases, while in theory, they are the same. For the ball linear guide, this varies between  $9\mu\text{m}$  and  $16\mu\text{m}$  and for the cross roller linear guide between  $4\mu\text{m}$  and  $7\mu\text{m}$ . This deviation of respectively  $7\mu\text{m}$  and  $3\mu\text{m}$  could be caused by assembly differences. The rails could have been assembled with a slight angle and the cages that are used were not always exactly at the same position in the rails, which could lead to differences in performances.

The absolute values of the performances are however higher than the performances that could be achieved in high precision machines. To achieve these performances the test setup should be further improved. One possibility is by eliminating the PLA parts in the setup. Deformations of PLA could easily occur as well as drift inside the PLA. This negatively influences the results of the measurements.

Drift of the linear guide system could also lead to varying results. There has been chosen to gather the data points 5 seconds after the contact moment of the balls. These data points are however taken manually and there could be a slight difference in the moment the data point is gathered. Taking a range of 1 second in which the data point has been collected the tolerance of the data point is  $0.25\mu\text{m}$  (section B.4). Meaning that this tolerance should be taken into account when evaluating the results.

The results of this paper are only valid for these two linear guides and also for this specific configuration. Since the performances are dependent on the whole system, a minor change in the setup could lead to different results. One main design decision is the spring that has been chosen. Choosing a spring with a different stiffness results in different performances. The spring is the transmitter of the input position to the linear guide system. Choosing a spring that is stiffer would result in a system where the input position fully prescribes the position of the linear guide system. It would therefore only measure the input position without knowing what the effects of the linear guide system are. A spring with a low stiffness damps the motion of the system and could therefore be beneficial for systems with a lot of vibrations. However, the setup is in that case not able to measure the effects of the linear guide since the prescribed input position could not be translated to move the linear guide.

Each part in the system has its own stiffness. The total stiffness is therefore related to all separate stiffness. When designing a measurement system the stiffness of all parts should be considered to guarantee that the repeatability could be measured.

Furthermore, the properties of the frame to which the linear guides are mounted have an influence on the repeatability. The dimensions and material choice determine the stiffness of the frame. Choosing a stiffer base frame leads to higher forces at the linear guide with the same rotation of the adjustment screw(s). This is also true the other way around, resulting in larger deflections with smaller forces. Therefore, a different optimal rotation of the adjusting screw can be found. For a base frame that has a very high stiffness, it is not possible to apply the preload since the force to rotate the screw is simply too high. While on the other hand in a system with a low stiffness of the base frame it is not possible to apply the preload since only the base frame will deform. The base frame is made by a CNC-machine with tolerances of  $0.1\text{mm}$ . Using other tolerances could lead to other results since the parallelism of the rails could be different.

Choosing a system that is force controlled instead of position-controlled will also lead to different results. By choosing a force-controlled system the force that is applied is known. One does on the other hand not know how the force distribution among the different parts is. It could be possible that this distribution is different during different measurements. Therefore, the repeatability of the whole system is measured and not only of the linear guide.

Moreover, a system that is controlled by an actuator or (stepper) motor could be used to actuate the system. One should however know how much force is exerted on the system and if the end stop, if available, is reached. It is also important that the end stop should be in contact at all times when taking the data point.

The used lasers have resolutions of around  $0.5\mu m$ . For this experiment, that resolution was sufficient since the measured values are around a factor of 10 larger. However, when designing a higher-performance setup that could for example achieve repeatability of  $2\mu m$ , different lasers should be selected. One should for example look into the interferometers that have resolutions of around  $100nm$ .



# 5

## Conclusion

A method to investigate the relationship between repeatability and preload is proposed. There is found that for the ball guide, the longitudinal repeatability has an optimal point for uniform applied preload. The longitudinal repeatability for the roller guide slowly decreases with the uniform applied preload. Applying angular preload increases the longitudinal repeatability of the roller guide. For the ball guide, better repeatability could be seen at a rotation of 10 degrees of the adjustment screw. The longitudinal repeatability stays constant with the external preload for both rails. Rotational repeatability decreases with both uniform and angular applied preload and remains constant with external preload.

Both the longitudinal and rotational repeatability of the roller guide are generally lower than the ball guides. Also, the spread of the measurement for the roller guide is smaller compared to the ball guide. Furthermore, ball guides are more sensitive to misalignment of the rails than roller guides.

Knowledge about the performances of these two types of guides together with the influence of preload on the performances can be used by companies to help them select the right linear guide for their application. The performances of current high precision machines can be further increased and new machines could be designed with the right type and amount of preload. A trade-off between costs and performance should be made when selecting the right linear guide for the application.

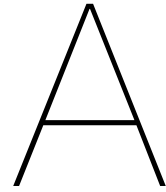


# Bibliography

- [1] Ziyad Tariq Abdullah, Guo Shun Sheng, and Sheng Bu Yun. "Conventional Milling Machine into CNC Machine Tool Remanufacturing, Eco-comparison Ratio Based Analysis". In: *Current Journal of Applied Science and Technology* 28.6 (2018), pp. 1–18. DOI: 10.9734/cjast/2018/42898.
- [2] Elisabeth Amann. "Modeling and motion control of a pick and place machine with air bearings". In: (2012).
- [3] David S.C. Biggs. "A Practical Guide to Deconvolution of Fluorescence Microscope Imagery". In: *Microscopy Today* 18.1 (2010), pp. 10–14. ISSN: 1551-9295. DOI: 10.1017/s1551929510991311.
- [4] Sébastien Briot and Ilian A. Bonev. "Pantopteron-4: A new 3T1R decoupled parallel manipulator for pick-and-place applications". In: *Mechanism and Machine Theory* 45.5 (2010), pp. 707–721. ISSN: 0094114X. DOI: 10.1016/j.mechmachtheory.2009.07.007. URL: <http://dx.doi.org/10.1016/j.mechmachtheory.2009.07.007>.
- [5] C. Cajal et al. "Volumetric error compensation technique for 3D printers". In: *Procedia Engineering* 63 (2013), pp. 642–649. ISSN: 18777058. DOI: 10.1016/j.proeng.2013.08.276. URL: <http://dx.doi.org/10.1016/j.proeng.2013.08.276>.
- [6] Michael Figl et al. "A fully automated calibration method for an optical see-through head-mounted operating microscope with variable zoom and focus". In: *IEEE Transactions on Medical Imaging* 24.11 (2005), pp. 1492–1499. ISSN: 02780062. DOI: 10.1109/TMI.2005.856746.
- [7] Aydin Gunduz, Jason T. Dreyer, and Rajendra Singh. "Effect of bearing preloads on the modal characteristics of a shaft-bearing assembly: Experiments on double row angular contact ball bearings". In: *Mechanical Systems and Signal Processing* 31 (2012), pp. 176–195. ISSN: 10961216. DOI: 10.1016/j.ymsp.2012.03.013.
- [8] Hailong He et al. "Chapter Five - Distributed Temperature Sensing for Soil Physical Measurements and Its Similarity to Heat Pulse Method". In: ed. by Donald L. Sparks. Vol. 148. *Advances in Agronomy*. Academic Press, 2018, pp. 173–230. DOI: <https://doi.org/10.1016/bs.agron.2017.11.003>. URL: <https://www.sciencedirect.com/science/article/pii/S0065211317300883>.
- [9] Cheng Tiao Hsieh. "Investigation of Delta Robot 3D Printer for a Good Quality of Printing". In: *Applied Mechanics and Materials* 870 (2017), pp. 164–169. DOI: 10.4028/www.scientific.net/amm.870.164.
- [10] Hsing Hsin Huang and Jay Wey. "Research on the high-speed pick and place device for die bonders". In: *2010 8th IEEE International Conference on Control and Automation, ICCA 2010* (2010), pp. 1683–1687. DOI: 10.1109/ICCA.2010.5524300.
- [11] Widiyanti Kwintarini et al. "Modeling of Geometric Error in Linear Guide Way to Improved the vertical three-axis CNC Milling machine's accuracy". In: *IOP Conference Series: Materials Science and Engineering* 319.1 (2018), pp. 0–6. ISSN: 1757899X. DOI: 10.1088/1757-899X/319/1/012015.
- [12] Dong Yeon Lee et al. "A calibrated atomic force microscope using an orthogonal scanner and a calibrated laser interferometer". In: *Applied Surface Science* 253.8 (2007), pp. 3945–3951. ISSN: 01694332. DOI: 10.1016/j.apsusc.2006.08.027.
- [13] Lucas Galvan Marques, Robert Austin Williams, and Wenchao Zhou. "A mobile 3D printer for cooperative 3D printing". In: *Solid Freeform Fabrication 2017: Proceedings of the 28th Annual International Solid Freeform Fabrication Symposium - An Additive Manufacturing Conference, SFF 2017* (2020), pp. 1645–1660.
- [14] Kevin McCarthy. "Accuracy in positioning systems". In: *Proc. The Motion Control Technology Conf* (1991). URL: <http://fp.optics.arizona.edu/optomech/student%20reports/2007/Jason%20Ruhl.doc>.

- [15] Newway. "New Way Air Bearings for Translational Motion". In: (2022). URL: <https://www.newwayairbearings.com/solutions/applications/linear-motion/>.
- [16] P. Pawełko, S. Berczyński, and Z. Grzadziel. "Modeling roller guides with preload". In: *Archives of Civil and Mechanical Engineering* 14.4 (2014), pp. 691–699. ISSN: 16449665. DOI: 10.1016/j.acme.2013.12.002.
- [17] Hamed Sadeghian et al. "Demonstration of parallel scanning probe microscope for high throughput metrology and inspection". In: *Metrology, Inspection, and Process Control for Microlithography XXIX* 9424.March 2015 (2015), 942400. ISSN: 1996756X. DOI: 10.1117/12.2085495.
- [18] Schneeberger. "Linear Bearings - Product Catalog". In: (2021). URL: <https://www.schneeberger.com/en/products/linear-bearings-linear-roller-guideways/recirculating-unit-with-long-stroke/recirculating-unit-with-ball/recirculating-unit-with-ball-type-skd/#downloadscatalogue>.
- [19] Xiao Yi Wang et al. "A thermal model for real-time temperature forecast of rolling linear guide considering loading working conditions". In: *International Journal of Advanced Manufacturing Technology* 109.7-8 (2020), pp. 2249–2271. ISSN: 14333015. DOI: 10.1007/s00170-020-05723-x.





# Concept generation

## A.1. Selection of Linear guides

For the system that we are interested in, we need to choose a type of linear guide. As illustrated in the review paper, the types of linear guides that belong to the rolling element linear guides are categorized into the technique used for the movement of the rolling elements and the type of contact of the rolling elements. This categorization is again showed in Figure A.1.



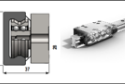

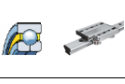






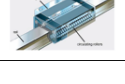


Techniques used for movement of rolling elements				Type of contact of rolling elements
Recirculating	Non-recirculating	Both Recirculating & Non-recirculating		
			2 points	
			3 points	
			4 points	
			2 lines	
			2 x 2 lines	

Figure A.1: Overview of rolling element linear guides

We decided to choose the non-recirculating 4 points contact linear guide and the 2x2lines contact non-recirculating linear guide. By doing that, we could make a comparison between non-recirculating guides that are using balls and linear guides that are using rollers. These types of linear guides are the most promising for high repeatability according to the literature review.

## A.2. Morphological table

To design a system that could measure repeatability some important design choices should be made. Therefore, a morphological table has been composed with different solutions for some key aspects. This table can be found in Table A.1.

	Option 1	Option 2	Option 3	Option 4	Option 5
System	Force controlled	Position controlled			
Actuation	Manual	Step motor	Piezo	Direct drive	
Transmission	Spindle	Linear stage	Direct		
End stop	3 point contact	V-groove	Mechanical stop	Electrical stop	
Spring	Load cell	Leaf spring	Torsion spring		
Rotation	Leaf spring	Notch hinge	Cross strip hinge	Normal cartwheel	Ball joint

Table A.1: Morphological table

### A.3. Trade off

Using this chart, four main concepts are composed.

#### A.3.1. Concept 1

This concept is a position-controlled system that has an electric motor to actuate the system. The motor rotates a spindle which is connected to a spring mechanism. It uses the motor to determine the input position so no end stop is needed.



Figure A.2: Concept 1

#### A.3.2. Concept 2

This concept is a position-controlled system that is actuated manually. It has an actuation beam that is connected to a spring which is in its place connected to the linear guide system. The input position is determined by a mechanical end stop. The actuation beam should be pushed to the end stop to guarantee contact at all times.

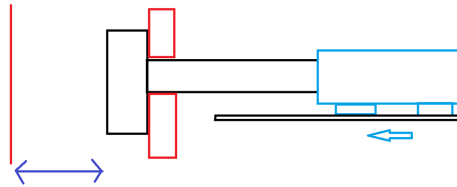


Figure A.3: Concept 2

#### A.3.3. Concept 3

This concept is a position-controlled system that is actuated manually by rotating a link. It is based on a crank slider mechanism and uses a 3-point contact mechanism to regulate the input position. The crank is connected to a spring and a load cell that is in its place connected to the linear guide system.

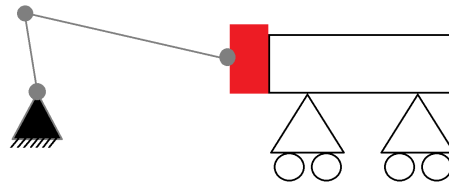


Figure A.4: Concept 3

### A.3.4. Concept 4

This concept is a force-controlled system that is actuated by a moving mass. The mass is connected to the linear guide and the linear guide is connected to a spring that is connected to the ground. No end stop is needed in this concept since the system stops moving when the equilibrium position is found between the spring and the mass.

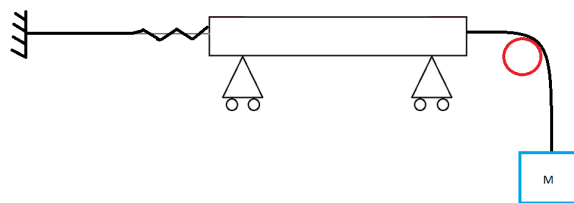


Figure A.5: Concept 4

### A.3.5. Selection

A trade-off between the concepts has been made to come up with the final decision on which concept should work the best. This trade-off is displayed in Figure A.6.

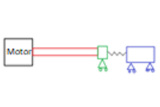
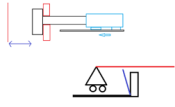
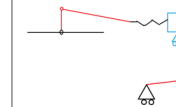
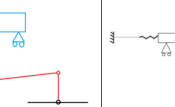
					
	Weight	Concept 1	Concept 2	Concept 3	Concept 4
Ease of measuring	4	2	1	2	-1
Ease of manufacturing	5	-1	2	2	0
Size	3	1	1	1	0
Feasibility	5	0	2	2	0
costs	2	-1	1	1	1
Vibrations	3	0	0	1	2
Total		4	29	36	4

Figure A.6: Trade off concepts

The concept that has been chosen is concept 3.

## A.4. Final Design

The system consists of 4 main parts; actuation mechanism, rotational mechanism, spring mechanism, linear guide system

### A.4.1. Actuation

Actuation will be done manually by rotating the link clockwise and counterclockwise till it hits the end stop. This is done so that the velocity in the horizontal direction reaches zero at the moment the end stop is reached, resulting in fewer vibrations in that direction.

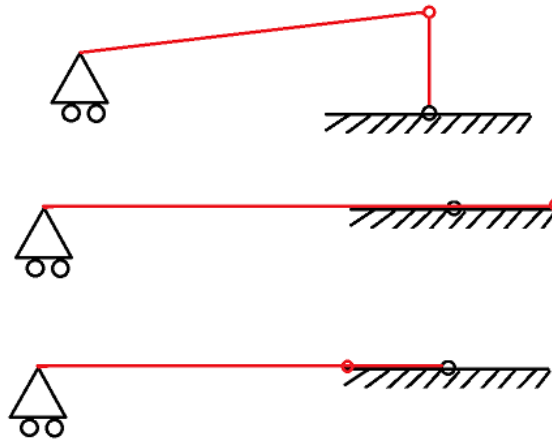


Figure A.7: Schematic illustration of actuation

### A.4.2. Rotational mechanism

To allow the actuation system to make this rotational movement and maintain a horizontal movement of the linear guide system a rotational mechanism should be made between the actuation beam and the spring. Multiple kinds of hinges are investigated. Especially the complexity, ease of manufacturing, and costs let us decide to choose the leaf spring.

### A.4.3. Spring mechanism

A load cell with a given stiffness has been selected to act as the spring mechanism. By using a load cell we could also analyze the forces that act in the system. Multiple load cells are investigated based on range, ability to handle off-center loads, price, and ability to measure both tension and compression. The S Beam load cell has been chosen to be used for this setup.

	Compression	Tension	off-center loading	price	Range
Thru Hole Load Cell	x		-		-
In Line Load Cell	x	x	+		-
Pancake Load Cell	x		+	low	50 lbs to 1 million lbs
Column Load Cell	x		+		2,000 to 30,000 lbs
S Beam Load Cell	x	x	-	low	10 grams to 100 lbs.
Load Button Load Cell	x		-		1lb to 100,000 lbs
Single Point Load Cell	x	x	+	high	1 gram to 500 lbs
Multi Axis Load Cell	x	x	+	high	-

Table A.2: Load cell comparison

### A.4.4. End stop

The end stop has the goal to make sure that the system stops at a certain position and will keep at that position. The stiffness of the mechanism should be high so that the deformations of the end stop are minimized.

### A.4.5. Linear guide system

The construction of the linear guide system should be made in a way that we could vary the construction so that we can do all the measurements. There has been chosen to make a u-shaped base frame to allow the possibility to apply preload from both sides. The moving platform in the middle has a maximum height so that the deformations are minimized.

# B

## Additional results

### B.1. Results external preload rail 1 and rail 2

The external preload has been tested with 3 different uniform preloads. In the research papers one of them is shown. In this appendix the other two cases are illustrated.

#### B.1.1. V1

The results of the first preload class of the external applied preload is illustrated in Figure B.1.

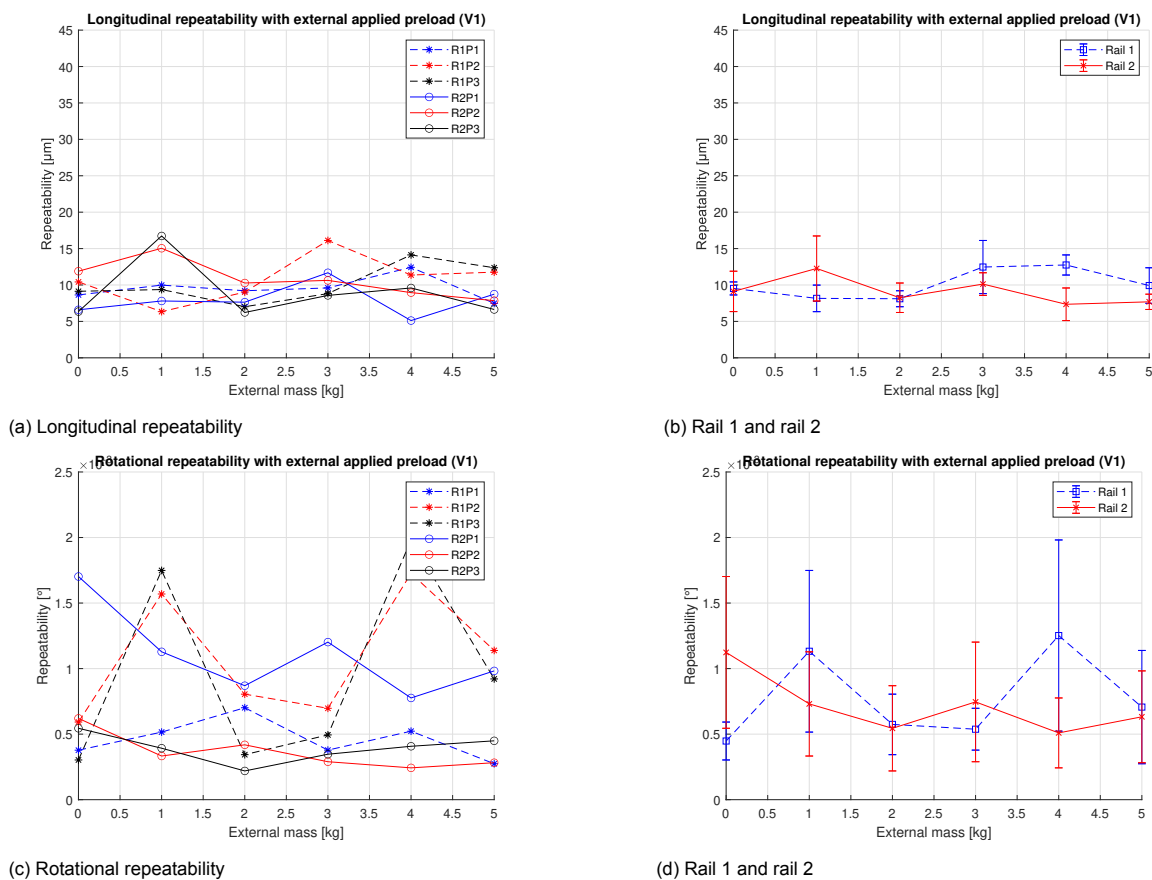


Figure B.1: External applied preload class 1: a,b) Longitudinal repeatability, c,d) Rotational repeatability

**B.1.2. V3**

The results of the third preload class of the external applied preload is illustrated in Figure B.2

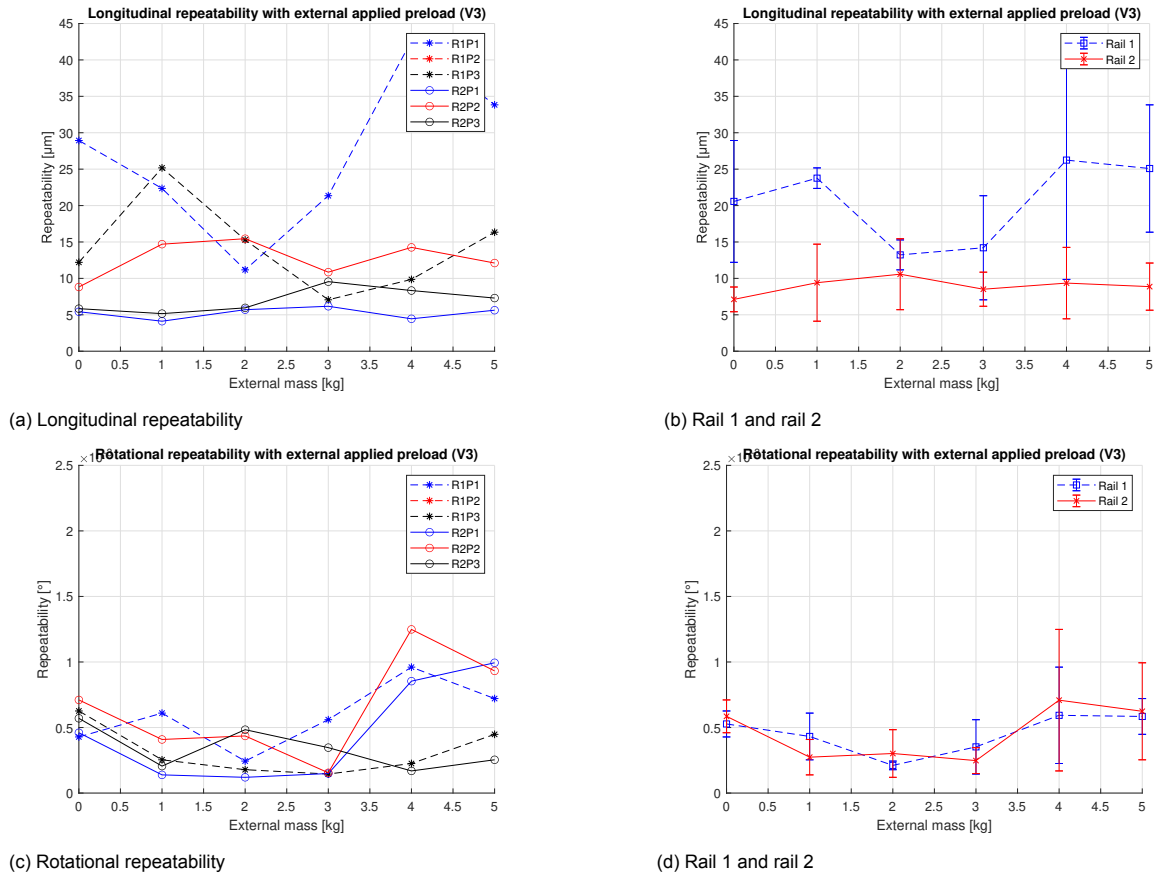
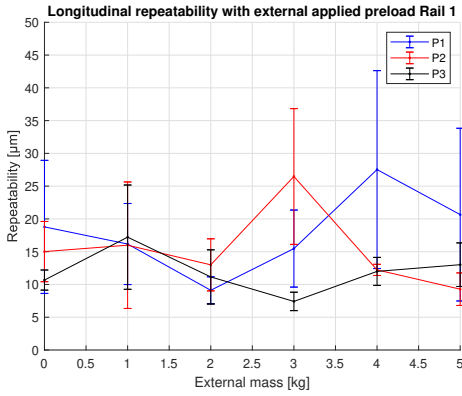


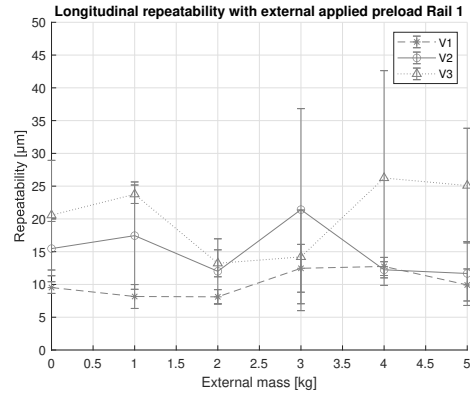
Figure B.2: External applied preload class 3: a, b) Longitudinal repeatability, c, d) Rotational repeatability

**B.1.3. Longitudinal repeatability position and preload class**

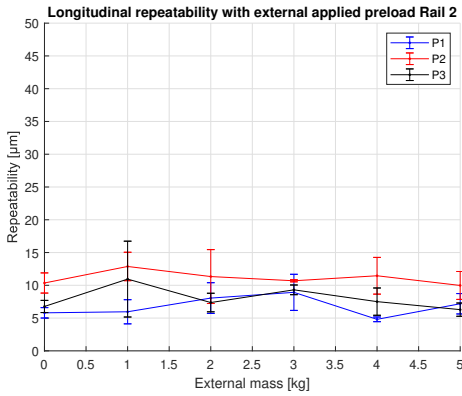
The longitudinal repeatability is plotted against the applied external preload. This has been done for each position in Figure B.3a for rail 1 and in Figure B.3c for rail 2. Also the comparison of each uniform preload class has been made in Figure B.3b for rail 1 and in Figure B.3d for rail 2.



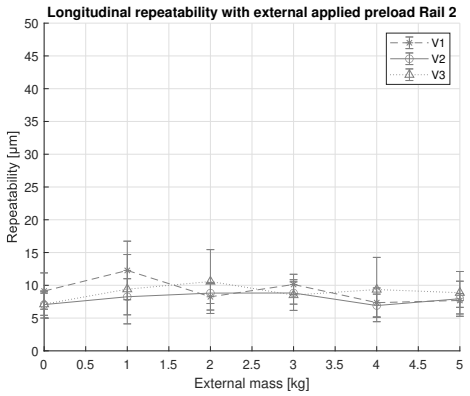
(a) Rail 1 longitudinal by position



(b) Rail 1 longitudinal by preload



(c) Rail 2 longitudinal by position

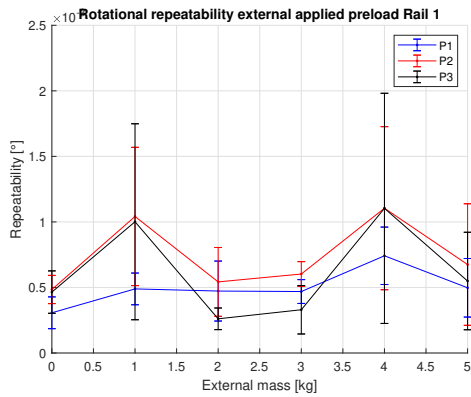


(d) Rail 2 longitudinal by preload

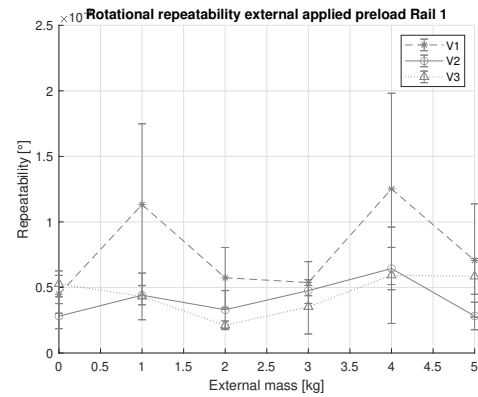
Figure B.3: External applied preload longitudinal repeatability by: a,c) position, c,d) preload

### B.1.4. Rotational repeatability position and preload class

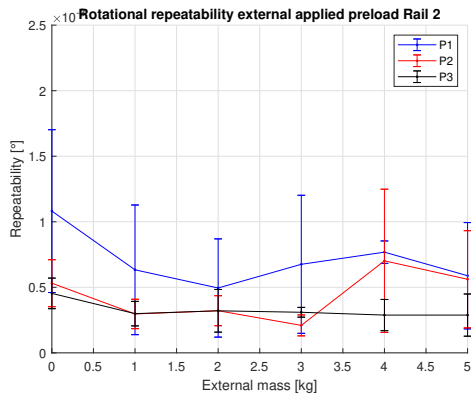
The rotational repeatability is plotted against the applied external preload. This has been done for each position in Figure B.4a for rail 1 and in Figure B.4c for rail 2. Also the comparison of each uniform preload class has been made in Figure B.4b for rail 1 and in Figure B.4d for rail 2.



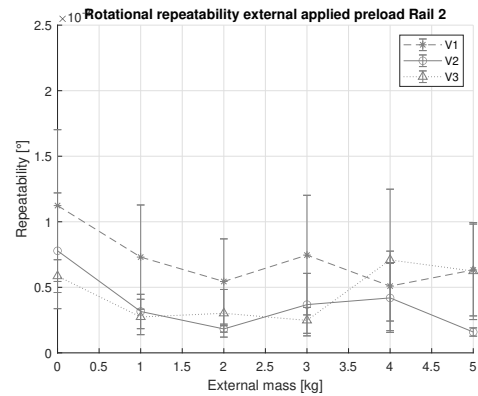
(a) Rail 1 rotational by position



(b) Rail 1 rotational by preload



(c) Rail 2 rotational by position



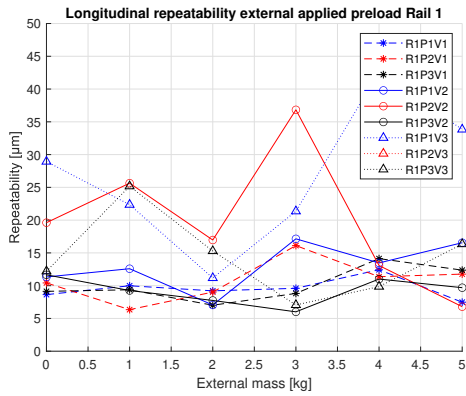
(d) Rail 2 rotational by preload

Figure B.4: External applied preload rotational repeatability by: a,c) position, c,d) preload

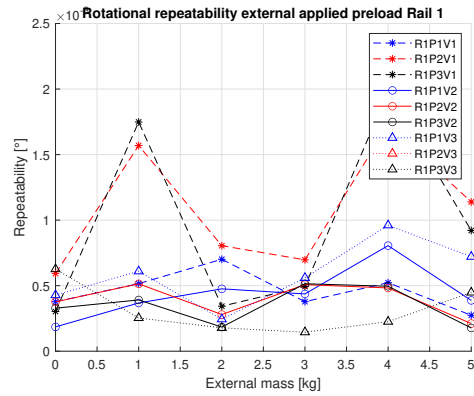


**B.1.5. All preload classes combined**

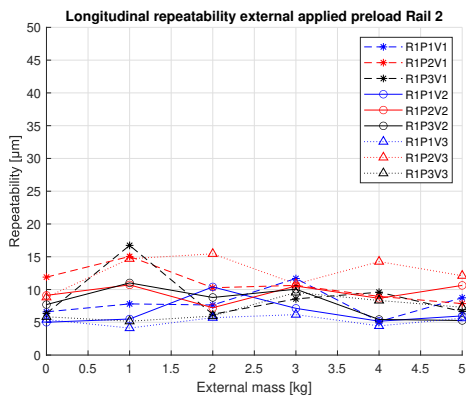
The combined results of all 3 preload classes are shown in figure Figure B.5



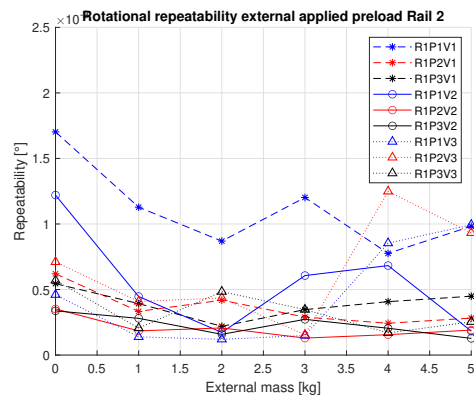
(a) Rail 1 longitudinal



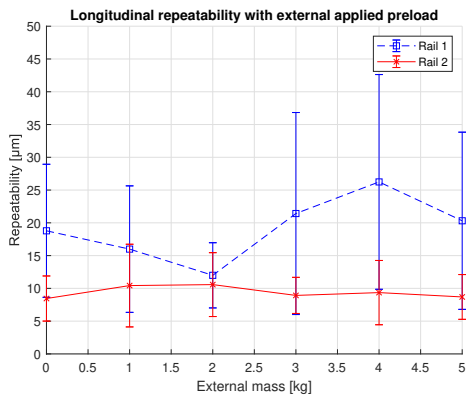
(b) Rail 1 rotational



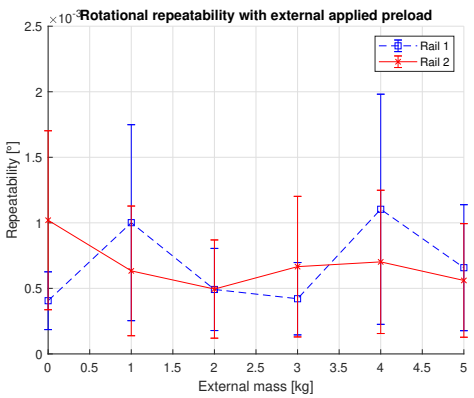
(c) Rail 2 longitudinal



(d) Rail 2 rotational



(e) Rail 1 and rail 2



(f) Rail 1 and rail 2

Figure B.5: External applied preload: a,c,e) Longitudinal repeatability, b,d,f) Rotational repeatability

## B.2. Forces & Moments in system

### B.2.1. Forces

The forces acting on the linear guide system are monitored by the load cell. In Figure B.6a, the forces in the case of uniform applied preload can be seen. The mean of the three positions for both rail 1 and rail 2 is illustrated in Figure B.6b. The forces of rail 1 are significantly larger than the forces of rail 2. The forces in the case of angular applied preload are shown in Figure B.6c and the mean of the three positions for both rails are illustrated in Figure B.6d. Also here, the forces of rail 1 are higher compared to rail 2. Comparing the case of uniform applied preload with the angular applied preload one could see that the force of the uniform applied preload case are almost a factor 2 higher.

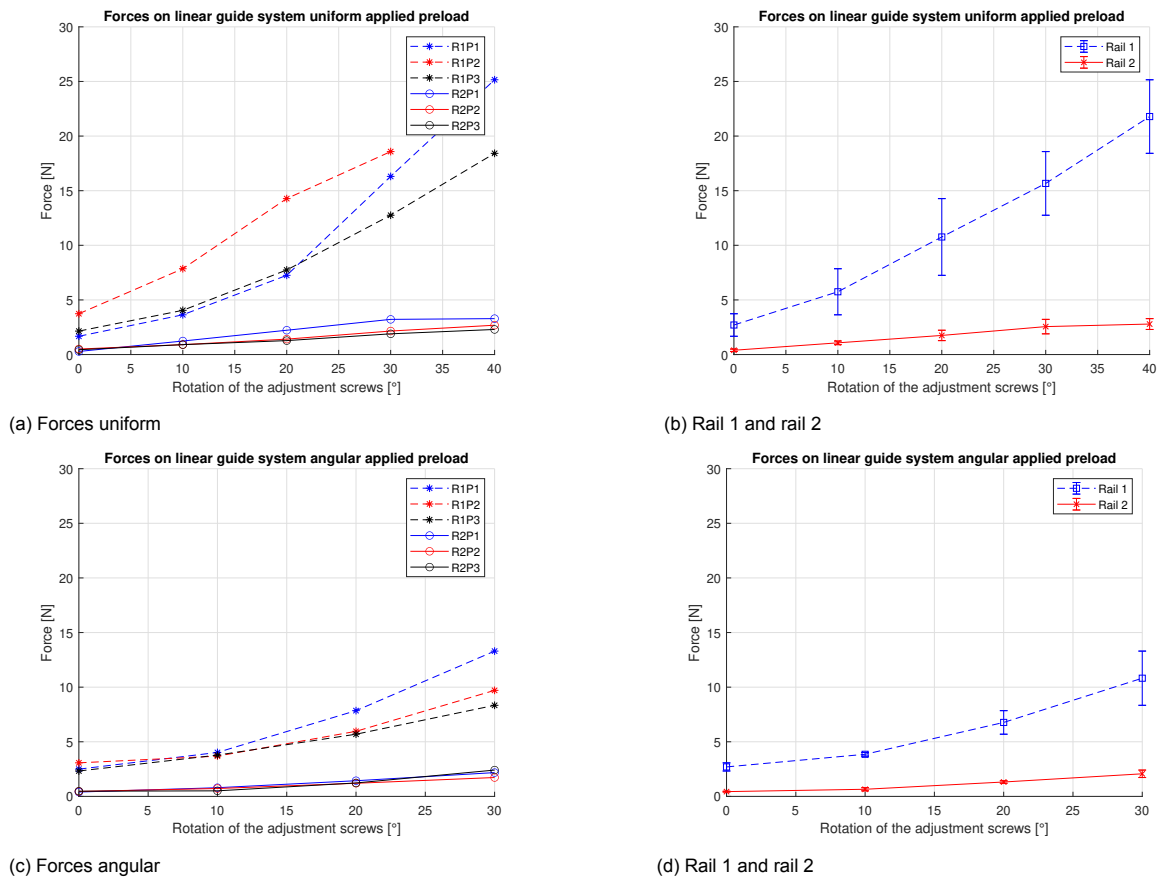
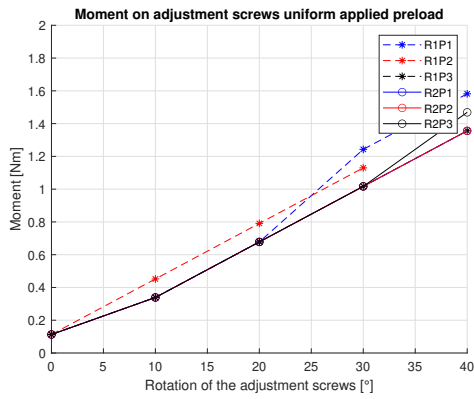


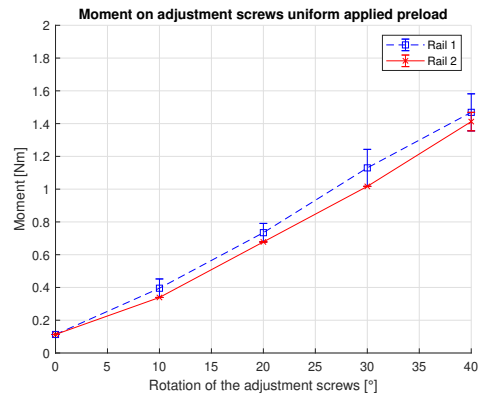
Figure B.6: Forces on linear guide system: a,b) uniform, c,d) angular

### B.2.2. Moments

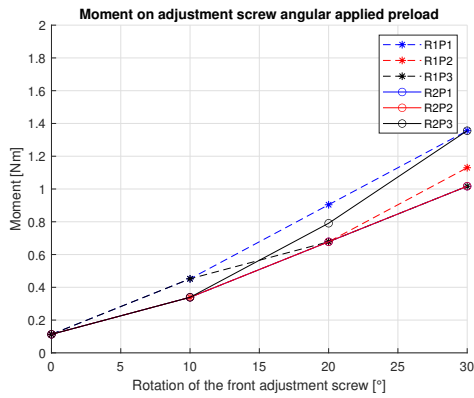
The rotational moments at which the adjustment screw has been rotated are also monitored. These are shown in Figure B.7. The moments of rail 1 are slightly higher than the moments of rail 2 for both the uniform and the angular applied preload case.



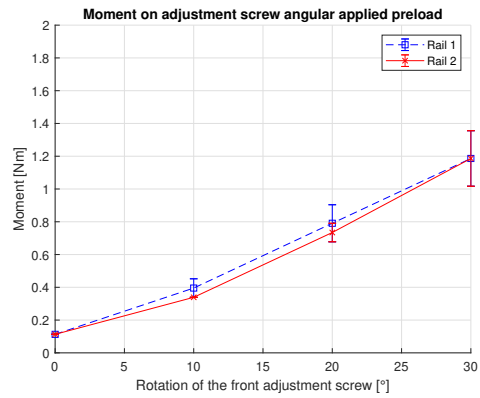
(a) Moment uniform



(b) Rail 1 and rail 2



(c) Moment angular

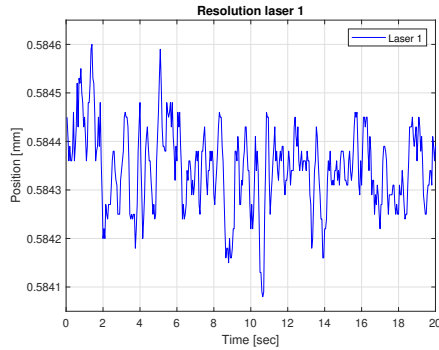


(d) Rail 1 and rail 2

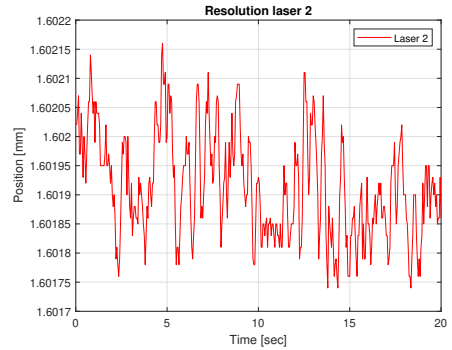
Figure B.7: Moment on adjustment screw(s): a,b) uniform, c,d) angular

### B.3. Resolution lasers

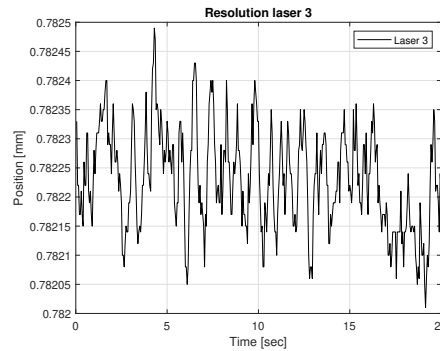
The resolution of the lasers is measured to know the accuracy of the measurements. The measurement, in which the laser was pointing toward an object that was not in motion, took 20 seconds. The results of the measurement are shown in Figure B.9. The corresponding resolutions are displayed in Table B.1.



(a) Resolution laser 1



(b) Resolution laser 2



(c) Resolution laser 3

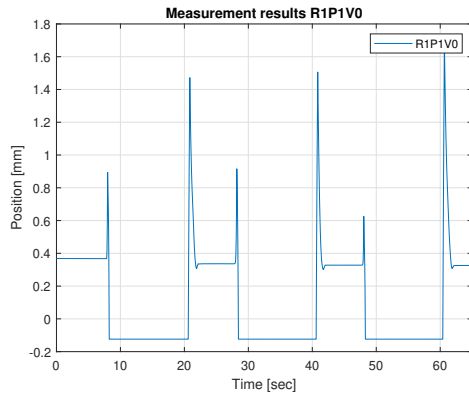
Figure B.8: Resolution of used lasers

	Resolution 20s	Resolution 10s	Resolution 5s	Resolution 2s	Resolution 1s
Laser 1	0.52 $\mu\text{m}$	0.45 $\mu\text{m}$	0.42 $\mu\text{m}$	0.40 $\mu\text{m}$	0.19 $\mu\text{m}$
Laser 2	0.42 $\mu\text{m}$	0.40 $\mu\text{m}$	0.40 $\mu\text{m}$	0.24 $\mu\text{m}$	0.22 $\mu\text{m}$
Laser 3	0.48 $\mu\text{m}$	0.44 $\mu\text{m}$	0.41 $\mu\text{m}$	0.25 $\mu\text{m}$	0.18 $\mu\text{m}$

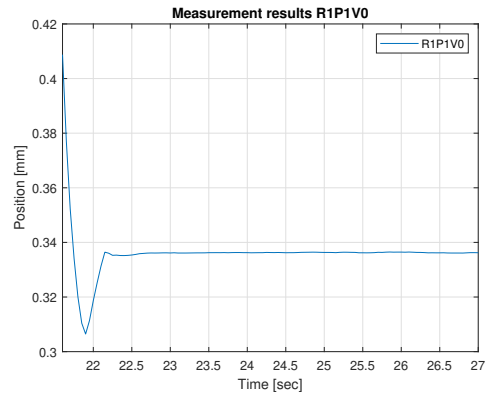
Table B.1: Resolution lasers for different time intervals

### B.4. Drift linear guides

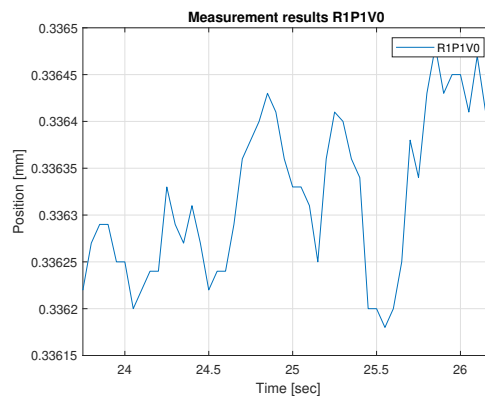
Drift could occur in the linear guides that influence the results of the measurements. Since the data is achieved manually the moment of data collection is not always exactly the same. In Figure B.9a, a part of a measurement is displayed. Figure B.9b, shows a more detailed view of the moment that the kinematic coupling makes contact. In Figure B.9c, an interval of 2,5 seconds is illustrated at which the data collection takes place. The resolution, defined as the difference between the maximum value and the minimum value, of this interval of 2.5 seconds is  $0.30\mu\text{m}$ . This is almost similar to the resolution of the lasers explained in section B.3.



(a) Measurement data 3 cycles



(b) Moment kinematic coupling makes contact



(c) Data point collection

Figure B.9: Measurement results R1P1V0

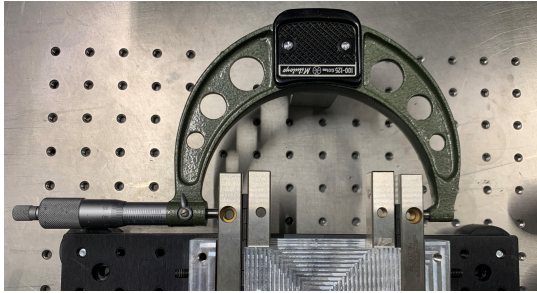
For different measurements, the resolution of the measurements is given in Table B.2. This has been done for different time intervals to show that the more accurate one collects its data, the better the resolution is.

	Interval 0.5s	Interval 1s	Interval 1.5s	Interval 2s	Interval 2.5s
R1P1V0	0.09 $\mu\text{m}$	0.16 $\mu\text{m}$	0.23 $\mu\text{m}$	0.25 $\mu\text{m}$	0.30 $\mu\text{m}$
R1P1V1	0.14 $\mu\text{m}$	0.25 $\mu\text{m}$	0.27 $\mu\text{m}$	0.27 $\mu\text{m}$	0.27 $\mu\text{m}$
R1P1V2	0.12 $\mu\text{m}$	0.14 $\mu\text{m}$	0.23 $\mu\text{m}$	0.25 $\mu\text{m}$	0.25 $\mu\text{m}$
R2P1V0	0.32 $\mu\text{m}$	0.32 $\mu\text{m}$	0.37 $\mu\text{m}$	0.48 $\mu\text{m}$	0.57 $\mu\text{m}$
R2P1V1	0.10 $\mu\text{m}$	0.17 $\mu\text{m}$	0.21 $\mu\text{m}$	0.28 $\mu\text{m}$	0.28 $\mu\text{m}$
R2P1V2	0.16 $\mu\text{m}$	0.16 $\mu\text{m}$	0.22 $\mu\text{m}$	0.22 $\mu\text{m}$	0.22 $\mu\text{m}$

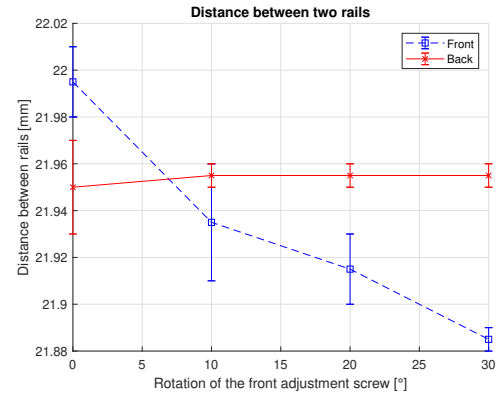
Table B.2: Drift of measurements along different intervals

## B.5. Parallelism rails

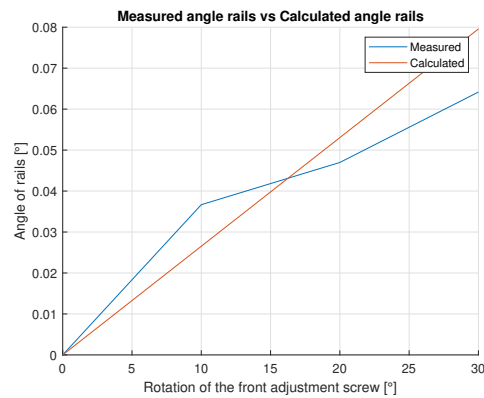
The parallelism of the rails has been measured to verify that the rotation of the front adjustment screw results in a rotation of the rails. This has been done by using a micrometer (Figure B.10a). In Figure B.10b, the measured distance between the two rails is shown for the front and the back side of the rails. It shows that the back side of the rails does not rotate equally with the front side, but stays somewhat constant. From this graph, we can conclude that the rails were in a parallel configuration at the moment the adjustment screw was between a rotation of 5 and 10 degrees.



(a) Micrometer

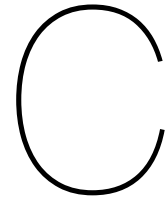


(b) Results measurement front and back side rails



(c) Angle measured value vs angle calculated value

Figure B.10: Measurement of parallelism of rails



## Kinematic coupling

To calculate whether the ball at the actuator beam makes contact with the three other balls, the relation of the friction force with the normal force has been calculated. In order to do this the following FBD has been used.

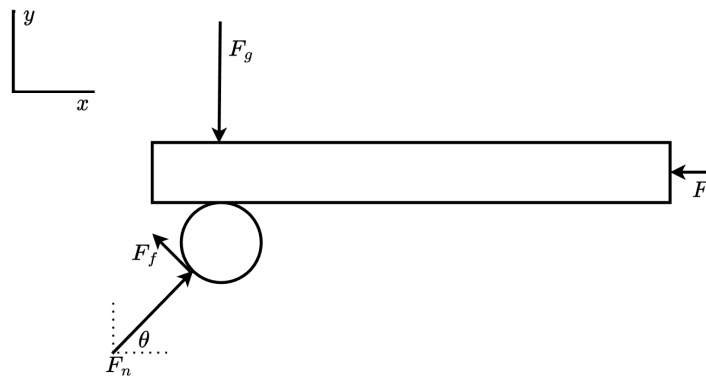


Figure C.1: Forces in kinematic coupling

The equilibrium equations of x and y have been composed which results in the following equations:

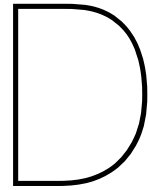
$$\sum F_x = -F_l + \cos(\theta)F_n + \mu F_n \cos(90 - \theta) = 0 \quad (\text{C.1})$$

$$\sum F_y = -F_g + \sin(\theta)F_n - \mu F_n \sin(90 - \theta) = 0 \quad (\text{C.2})$$

In this equation,  $\theta$  is the contact angle of the upper ball with the other balls.  $F_n$  is the normal force perpendicular to the ball in contact and  $F_f$  is the friction force tangential to the contact point.  $F_l$  is the resistance force due to the friction in the linear guide and  $F_g$  is the gravity force due to the additional load.

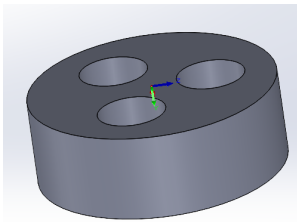




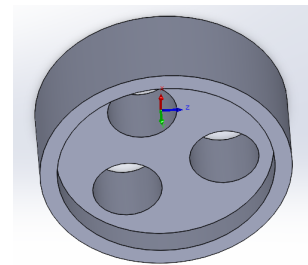


## Glue process kinematic coupling

In order to ensure that the balls in the kinematic coupling are oriented 120 degrees to each other, a glue tool has been designed. This glue tool is a kind of capsule that should be placed on top of the balls. Epoxy glue is used to fixate the balls. The gluing process is as follows:



(a) Glue tool top

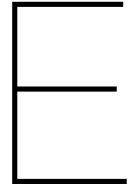


(b) Glue tool bottom

Figure D.1: Glue tool

- Step 1: Combine the two parts of the epoxy glue on the cardboard and mix it till it becomes one whole.
- Step 2: Dose enough glue onto the actuation base plate.
- Step 3: Insert the balls in the glue in an almost 120-degree orientation. It does not matter if it is not exactly 120 degrees because the glue tool will correct this.
- Step 4: Place the glue tool on top of the balls and make sure it will not move anymore.
- Step 5: Place a mass on top of the glue tool and wait for at least 12 hours to guarantee that the glue has hardened.





## SAM analysis

An analysis of the motion of the actuator beam has been done to verify that the velocity in x direction reaches zero at the moment the ball connected at the actuation beam makes contact with the kinematic coupling mechanism. As can be seen in Figure E.1, the actuation beam makes a sinusoidal motion.

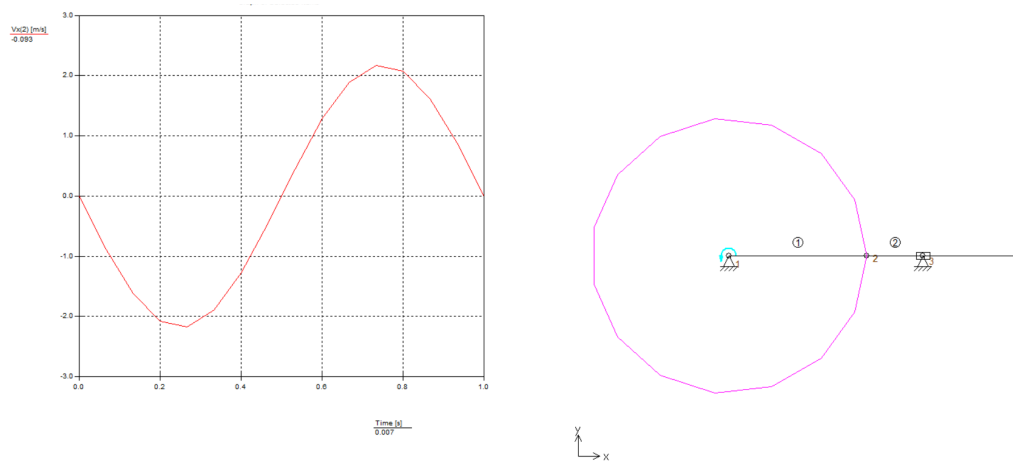
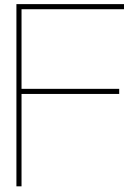


Figure E.1: SAM analyses

The velocity has a sinusoidal profile as well (Figure E.1). The graphs show that the velocity in x direction is zero at the moment the beam is horizontal, representing the case in which the ball hits the end-stop.





# Data processing

## F.1. Data analyses experiments

The data from the experiments is achieved by using Labview. The output of this program was an excel file with all the data points. This data has been used in excel to calculate the 80% standard deviation. The output of this calculation is a matrix that has been implemented into MATLAB. With this software, the mean values have been calculated and the results have been plotted. The code used to do this is displayed below. Note that for all other situations the code looks similar but uses other data and titles.

```
1 % Plot of longitudinal repeatability with uniform applied preload
2 %Laurens van Driessen
3
4 close all
5 clear all
6
7 xas = [0, 10, 20, 30, 40];
8 R = [ 0.005726032, 0.005748811, 0.001648185, 0.01086429, 0.013980613;
9       0.01214456, 0.010317923, 0.006441158, 0.017664057, missing;
10      0.020624521, 0.024387612, 0.010371765, 0.009174107, 0.013734115;
11      0.010787867, 0.010533136, 0.008952554, 0.012048608, 0.007232903;
12      0.001559791, 0.010876172, 0.010063582, 0.005978827, 0.00913471;
13      0.010676072, 0.009057019, 0.010949297, 0.011412567, 0.007754694;
14 ];
15
16 R= R*1000;
17 M1=mean(R);
18 M1_R1=mean(R(1:3,:));
19 M1_R2=mean(R(4:6,:));
20
21 ymin1 = min(R(1:3,:), [], 1);
22 ymax1 = max(R(1:3,:), [], 1);
23
24 ymin2 = min(R(4:6,:), [], 1);
25 ymax2 = max(R(4:6,:), [], 1);
26
27 figure
28 hold on
29
30 plot(xas, R(1,:), '*--', 'Color', '#0000FF')
31 plot(xas, R(2,:), '*--', 'Color', '#0072BD')
32 plot(xas, R(3,:), '*--', 'Color', '#4DBEEE')
33 plot(xas, R(4,:), 'o-', 'Color', '#FF0000')
34 plot(xas, R(5,:), 'o-', 'Color', '#D95319')
35 plot(xas, R(6,:), 'o-', 'Color', '#A2142F')
36
37
38 xlabel('Rotation of the adjustment screws [°]');
39 ylabel('Repeatability [m]');
40 labels = {'R1P1', 'R1P2', 'R1P3', 'R2P1', 'R2P2', 'R2P3'};
```

```

41     legend(labels);
42     title('Longitudinal repeatability with uniform applied preload')
43     ylim([0 25])
44
45     grid on
46     hold off
47
48     figure
49     hold on
50     errorbar(xas,(ymin1+ymax1)/2,(ymax1-ymin1)/2, '*--')
51     errorbar(xas,(ymin2+ymax2)/2,(ymax2-ymin2)/2, 'o-')
52     legend('Rail 1', 'Rail 2')
53     title('Longitudinal repeatability with uniform applied preload')
54     xlabel('Rotation of the adjustment screws [°]');
55     ylabel('Repeatability [m]');
56     ylim([0 25])
57     grid on
58     hold off

```

## F.2. Calculations resolution

```

1  % Resolution lasers
2  %Laurens van Driessen
3
4  close all
5  clear all
6
7
8  reso = readcell('resolutie_lasers.xlsx');
9
10 A = cell2mat(reso);
11 x1 = [1:length(A)]*0.05;
12
13
14 Reso1=(max(A(:,1))-min(A(:,1)))*1000;
15 Reso2=(max(A(:,2))-min(A(:,2)))*1000;
16 Reso3=(max(A(:,3))-min(A(:,3)))*1000;
17
18 Reso4=(max(A(1:400,1))-min(A(1:400,1)))*1000;
19 Reso5=(max(A(1:400,2))-min(A(1:400,2)))*1000;
20 Reso6=(max(A(1:400,3))-min(A(1:400,3)))*1000;
21
22
23 Reso7=(max(A(1:200,1))-min(A(1:200,1)))*1000;
24 Reso8=(max(A(1:200,2))-min(A(1:200,2)))*1000;
25 Reso9=(max(A(1:200,3))-min(A(1:200,3)))*1000;
26
27 Reso10=(max(A(1:100,1))-min(A(1:100,1)))*1000;
28 Reso11=(max(A(1:100,2))-min(A(1:100,2)))*1000;
29 Reso12=(max(A(1:100,3))-min(A(1:100,3)))*1000;
30
31 Reso13=(max(A(1:40,1))-min(A(1:40,1)))*1000;
32 Reso14=(max(A(1:40,2))-min(A(1:40,2)))*1000;
33 Reso15=(max(A(1:40,3))-min(A(1:40,3)))*1000;
34
35
36 Reso16=(max(A(1:20,1))-min(A(1:20,1)))*1000;
37 Reso17=(max(A(1:20,2))-min(A(1:20,2)))*1000;
38 Reso18=(max(A(1:20,3))-min(A(1:20,3)))*1000;
39
40
41 Reso_total= [ Reso4, Reso7, Reso10, Reso13, Reso16;
42              Reso5, Reso8, Reso11, Reso14, Reso17;
43              Reso6, Reso9, Reso12, Reso15, Reso18;];
44
45 RESO_round= round(Reso_total,4, 'significant');
46
47

```

```

48 %% plot
49 figure
50 plot(x1,A(:,1), 'Color', '#0000FF')
51 legend('Laser 1')
52 title('Resolution laser 1')
53 xlabel('Time [sec]');
54 ylabel('Position [mm]');
55 xlim([0 20])
56 ylim([0.58405 0.58465])
57 grid on
58
59 figure
60 plot(x1,A(:,2), 'Color', '#FF0000')
61 legend('Laser 2')
62 title('Resolution laser 2')
63 xlabel('Time [sec]');
64 ylabel('Position [mm]');
65 xlim([0 20])
66 ylim([1.6017 1.6022])
67 grid on
68
69 figure
70 plot(x1,A(:,3), 'Color', '#000000')
71 legend('Laser 3')
72 title('Resolution laser 3')
73 xlabel('Time [sec]');
74 ylabel('Position [mm]');
75 xlim([0 20])
76 ylim([0.782 0.7825])
77 grid on

```

### F.3. Calculations drift

```

1 % Calculations drift
2 %Laurens van Driessen
3
4 close all
5 clear all
6
7
8 R1P1V0 = readcell('drift1.xls');
9 R1P1V1 = readcell('drift2.xls');
10 R1P1V2 = readcell('drift3.xls');
11 R2P1V0 = readcell('drift4.xls');
12 R2P1V1 = readcell('drift5.xls');
13 R2P1V2 = readcell('drift6.xls');
14
15 A = cell2mat(R1P1V0);
16 B = cell2mat(R1P1V1);
17 C = cell2mat(R1P1V2);
18 D = cell2mat(R2P1V0);
19 E = cell2mat(R2P1V1);
20 F = cell2mat(R2P1V2);
21
22 x1 = [0:length(A)-1]*0.05;
23 x2 = [1:length(B)]*0.05;
24 x3 = [1:length(C)]*0.05;
25 x4 = [1:length(D)]*0.05;
26 x5 = [1:length(E)]*0.05;
27 x6 = [1:length(F)]*0.05;
28
29 A = cell2mat(R1P1V0);
30 B = cell2mat(R1P1V1);
31 C = cell2mat(R1P1V2);
32 D = cell2mat(R2P1V0);
33 E = cell2mat(R2P1V1);
34 F = cell2mat(R2P1V2);
35

```

```

36 adrift0_5s=(max(A(475:485,1))-min(A(475:485,1)))*1000;
37 adrift1s=(max(A(475:495,1))-min(A(475:495,1)))*1000;
38 adrift1_5s=(max(A(475:505,1))-min(A(475:505,1)))*1000;
39 adrift2s=(max(A(475:515,1))-min(A(475:515,1)))*1000;
40 adrift2_5s=(max(A(475:525,1))-min(A(475:525,1)))*1000;
41
42 bdrift0_5s=(max(B(475:485,1))-min(B(475:485,1)))*1000;
43 bdrift1s=(max(B(475:495,1))-min(B(475:495,1)))*1000;
44 bdrift1_5s=(max(B(475:505,1))-min(B(475:505,1)))*1000;
45 bdrift2s=(max(B(475:515,1))-min(B(475:515,1)))*1000;
46 bdrift2_5s=(max(B(475:525,1))-min(B(475:525,1)))*1000;
47
48 Cdrift0_5s=(max(C(475:485,1))-min(C(475:485,1)))*1000;
49 Cdrift1s=(max(C(475:495,1))-min(C(475:495,1)))*1000;
50 Cdrift1_5s=(max(C(475:505,1))-min(C(475:505,1)))*1000;
51 Cdrift2s=(max(C(475:515,1))-min(C(475:515,1)))*1000;
52 Cdrift2_5s=(max(C(475:525,1))-min(C(475:525,1)))*1000;
53
54 Ddrift0_5s=(max(D(475:485,1))-min(D(475:485,1)))*1000;
55 Ddrift1s=(max(D(475:495,1))-min(D(475:495,1)))*1000;
56 Ddrift1_5s=(max(D(475:505,1))-min(D(475:505,1)))*1000;
57 Ddrift2s=(max(D(475:515,1))-min(D(475:515,1)))*1000;
58 Ddrift2_5s=(max(D(475:525,1))-min(D(475:525,1)))*1000;
59
60 Edrift0_5s=(max(E(475:485,1))-min(E(475:485,1)))*1000;
61 Edrift1s=(max(E(475:495,1))-min(E(475:495,1)))*1000;
62 Edrift1_5s=(max(E(475:505,1))-min(E(475:505,1)))*1000;
63 Edrift2s=(max(E(475:515,1))-min(E(475:515,1)))*1000;
64 Edrift2_5s=(max(E(475:525,1))-min(E(475:525,1)))*1000;
65
66 Fdrift0_5s=(max(F(475:485,1))-min(F(475:485,1)))*1000;
67 Fdrift1s=(max(F(475:495,1))-min(F(475:495,1)))*1000;
68 Fdrift1_5s=(max(F(475:505,1))-min(F(475:505,1)))*1000;
69 Fdrift2s=(max(F(475:515,1))-min(F(475:515,1)))*1000;
70 Fdrift2_5s=(max(F(475:525,1))-min(F(475:525,1)))*1000;
71
72
73 Drift_table= round([ adrift0_5s, adrift1s, adrift1_5s, adrift2s, adrift2_5s;
74                      bdrift0_5s, bdrift1s, bdrift1_5s, bdrift2s, bdrift2_5s;
75                      Cdrift0_5s, Cdrift1s, Cdrift1_5s, Cdrift2s, Cdrift2_5s;
76                      Ddrift0_5s, Ddrift1s, Ddrift1_5s, Ddrift2s, Ddrift2_5s;
77                      Edrift0_5s, Edrift1s, Edrift1_5s, Edrift2s, Edrift2_5s;
78                      Fdrift0_5s, Fdrift1s, Fdrift1_5s, Fdrift2s, Fdrift2_5s;
79
80                      ],3);
81
82
83 % R1PIV0 (plot drift for R1PIV0, note that for other situations the code ...
84 %       looks the same but with other data and titles)
85
86
87 figure
88 plot(x1,A)
89 legend('R1PIV0')
90 title('Measurement results R1PIV0')
91 xlabel('Time [sec]');
92 ylabel('Position [mm]');
93 xlim([0 65])
94 grid on
95
96 figure
97 plot(x1(1,433:555), A(433:555,1))
98 legend('R1PIV0')
99 title('Measurement results R1PIV0')
100 xlabel('Time [sec]');
101 ylabel('Position [mm]');
102 xlim([21.6 27])
103 grid on
104
105 figure
106 plot(x1(1,475:525), A(475:525,1))

```



```

107 legend('R1P1V0')
108 title('Measurement results R1P1V0 ');
109 xlabel('Time [sec]');
110 ylabel('Position [mm]');
111 xlim([23.75 26.2])
112 grid on

```

## F.4. Calculations kinematic coupling

```

1 %Calculations kinematic coupling
2 %Laurens van Driessen
3
4 clear all
5 close all
6 clc
7
8 %
9 syms F_n F_r F_t
10 mu = 0.5
11 g = 9.81
12 m = 15
13 F_g = m*g
14 theta = linspace(1,80, 80)
15
16 for i = 1:length(theta)
17     thetaN = theta(i);
18
19     SumFx = -F_r + cosd(thetaN)*F_n + mu*F_n*cosd(180-90-thetaN) == 0 ;
20     SumFy = -F_g + sind(thetaN)*F_n - mu*F_n*sind(180-90-thetaN) == 0;
21
22     [F_rsolve, F_nsolve] = solve([SumFx, SumFy], [F_r, F_n]);
23
24     Ratio(i) = F_rsolve/F_nsolve;
25     Ratio2(i) = F_rsolve/F_g;
26 end
27 % end
28
29
30 figure
31 plot(theta, Ratio)
32 xlabel('Angle [degrees]');
33 ylabel('Ratio [-]');
34 title('Ratio between Fr and Fn for different contact angles')
35 legend('Ratio Fr / Fn');
36 grid on
37
38 figure
39 plot(theta, Ratio2)
40 xlabel('Angle [degrees]');
41 ylabel('Ratio [-]');
42 title('Ratio between Fr and Fg for different contact angles')
43 legend('Ratio Fr / Fg');
44 grid on

```

## F.5. Calculations dimensions

```

1 %Calculations dimensions
2 %Laurens van Driessen
3
4 close all
5 clear all
6
7 E_a=69*10^9; %e_modulus Aluminum
8 E_b=210*10^9; %e_modulus Steel
9

```

```

10 rho_a=2755; %kg/m^3 aluminum
11 rho_b=7850; %kg/m^3 staal
12
13 L_a=25/10^3; %length short link
14 L_b=300/10^3; %Length long link
15
16 thetad= asind(L_a/L_b); % Required angle of rotation degrees
17 theta= asin(L_a/L_b); % Required angle of rotation rad
18
19 %Thorlabs profile
20 A_thor=3.13*10^-4; %cross sectional area in m^2 of thorlabs profile
21 E_thor=67*10^9; %e-modus aluminium alloy 6000 series minimum (67-140GPa)
22 k_thor=A_thor*E_thor/L_b; %4.6E8; --> ...
    https://www.thorlabs.com/newgrouppage9.cfm?objectgroup_id=194
23
24 % m_a=A_a*L_a*rho_a;
25 % m_b=A_b*L_b*rho_b;
26
27 k_kop=1e8; %required stiffness metal strip [N/m]
28 E_v=180*10^9; %e_modulus metal strip [N/mm^2]
29 b_v=12.5/10^3; %width of metal strip [m]
30 h_v=0.2/10^3; %height of metal strip [m]
31 I_v=(b_v*h_v^3)/12; %Area moment of inertia metal strip [m^4]
32
33 %Effective length spring
34 L_v=b_v*h_v*E_v/(k_kop);
35
36 F_v=theta*2*E_v*I_v/(L_v^2); %Force to generate rotation
37 M_v=theta*E_v*I_v/L_v; %Moment to generate rotation
38
39 Eg_rvs=965; %MPa
40 sig=6*M_v/(b_v*h_v^2)/10^6; %bending stress of metal strip [MPa]
41 Fk=pi^2*E_v*I_v/(L_v^2); %Buckling force
42
43 safety_margin_bending=Eg_rvs/sig; %safety margin bending
44 safety_margin_buckling=Fk/F_v; %safety margin buckling
45
46
47 %% Deformation Base plate
48
49 Fr=430; %Force on cross roller
50 ur=17.3*10^-6; %Displacement of cross roller
51 k_crg=Fr/ur; %Stiffness cross roller
52 us=0.11*10^-3; %Maximum displacement by adjustment screw
53
54 F_cross=k_crg*us; %Force generated by displacement of cross roller
55
56 b_up=145/10^3; %width base frame
57 d_up=7.5/10^3; %middle line base frame
58 h_up=6/10^3; %Height base frame
59 L_up=100/10^3; %Length base frame
60 E_up=69*10^9; %e-modulus aluminum
61
62 A_up= b_up*h_up; %Area base frame
63 I_up_front=1/12*b_up*h_up^3; %area moment of inertia front
64 I_up_side=1/12*L_up*h_up^3; %area moment of inertia side
65 M_bending=F_cross*d_up; %bending moment
66
67 phi_up=M_bending*(b_up/2)/(E_up*I_up_side); %rotation of base frame
68 u_side=sin(phi_up)*d_up; %motion to the side due to force

```